Nagra
Nationale
Genossenschaft
für die Lagerung
radioaktiver Abfälle

Cédra
Société coopérative
nationale
pour l'entreposage
de déchets radioactifs

Cisra
Società cooperativa
nazionale
per l'immagazzinamento
di scorie radioattive

TECHNICAL REPORT 85-54

Thermal loading in the near field of repositories for high and intermediate level nuclear waste

R. J. Hopkirk
W. H. Wagner

July 1986

POLYDYNAMICS Ltd, Zürich

Parkstrasse 23 5401 Baden/Schweiz Telephon 056/20 55 11

Nagra
Nationale
Genossenschaft
für die Lagerung
radioaktiver Abfälle

Cédra
Société coopérative
nationale
pour l'entreposage
de déchets radioactifs

Cisra
Società cooperativa
nazionale
per l'immagazzinamento
di scorie radioattive

TECHNICAL REPORT 85-54

Thermal loading in the near field of repositories for high and intermediate level nuclear waste

R. J. Hopkirk
W. H. Wagner

July 1986

POLYDYNAMICS Ltd, Zürich

Parkstrasse 23 5401 Baden/Schweiz Telephon 056/20 55 11

Der vorliegende Bericht wurde im Auftrag der Nagra erstellt. Die Autoren haben ihre eigenen Ansichten und Schlussfolgerungen dargestellt. Diese müssen nicht unbedingt mit denjenigen der Nagra übereinstimmen.

Le présent rapport a été préparé sur demande de la Cédra. Les opinions et conclusions présentées sont celles des auteurs et ne correspondent pas nécessairement à celles de la Cédra.

This report was prepared as an account of work sponsored by Nagra. The viewpoints presented and conclusions reached are those of the author(s) and do not necessarily represent those of Nagra.

A B S T R A C T

The feasibility, the principal features and operational aspects of the two underground nuclear waste repositories Type B and Type C have been analysed in the NAGRA "Project Gewähr 1985" study.

The near-field thermal calculations performed for this study are described in detail in this report. The calculations, which have been made to ensure that there is at no time a risk of excessive temperatures being reached, account for heat transfer by conduction, convection and radiation. All these mechanisms may be relevant during the first few years after disposal.

The high-level wastes considered are reprocessing waste and spent fuel. The heat generating intermediate level wastes comprise hulls and end-caps, co-precipitation sludges from reprocessing and certain decommissioning wastes. Disposal of heat-generating wastes has been analysed both for the Type B and the Type C repository. Within the present repository concepts, acceptable temperature distributions can be achieved by appropriate disposal plans and configurations.

Z U S A M M E N F A S S U N G

Die Machbarkeit, Auslegung und betrieblichen Aspekte der zwei Endlager Typ B und Typ C wurden im Projekt Gewähr 1985 untersucht.

Im vorliegenden Bericht werden die dazu durchgeführten thermischen Berechnungen im Detail beschrieben. Diese wurden durchgeführt, um nachzuweisen, dass zu keiner Zeit ein Risiko übermässiger Temperaturen besteht. Die Wärmetransportberechnungen berücksichtigen Wärmeleitung, konvektiven Wärmetransport und Wärmetransport durch Strahlung. Alle diese Mechanismen sind während der ersten paar Jahre nach der Einlagerung von Bedeutung.

Die betrachteten hochaktiven Abfälle sind widerauffgearbeitete Abfälle sowie abgebrannte Brennelemente. Die für die Wärmetransportberechnungen berücksichtigten mittelaktiven Abfälle bestehen aus Hülsen und Endstükken, Fällungen und Konzentraten aus der Wiederaufarbeitung und aus einem Teil der Stillegungsabfälle. Für einen Teil der Abfälle wurde die alternative Einlagerung entweder in einem Endlager Typ B oder Typ C untersucht. Die Berechnungen zeigen, dass die gewählten Endlagerkonzepte vom thermischen Standpunkt aus für alle Abfälle eine akzeptable Lösung darstellen.

R E S U M E

La faisabilité, la conception et les aspects d'exploitation des deux dépôts finals de types B et C ont été analysés dans le projet Garantie 1985.

Les calculs thermiques qui ont été réalisés pour cela sont décrits en détail dans ce rapport. Ils ont été effectués pour prouver qu'un risque de températures excessives n'existe à aucun moment. Les calculs de transport thermique tiennent compte de la conduction thermique, du rayonnement et de la convection. Tous ces mécanisms sont importants pendant quelques années suivant l'emmagasinage des déchets.

Les déchets hautement radioactifs considérés sont des déchets retraités ainsi que des éléments combustibles usés. Les déchets moyennement radioactif considérés pour les calculs de transport thermique sont constitués de coques et embouts, précipitations et concentrats provenant du retraitement et d'une partie des déchets de démantèlement. On a étudié l'emmagasinage alternatif d'une partie de ces déchets dans un dépôt final de type B ou de type C. Les calculs montrent que les concepts de dépôt final sélectionnés offrent, du point de vue thermique, une solution acceptable pour tous les déchets.

LIST OF CONTENTS

1. INTRODUCTORY REMARKS

For the characterisation of the near field of a repository for high-level nuclear waste, it is essential to take into account the evolution with time during the first few hundred years of the temperature distribution resulting from the heat produced by the radioactive waste packages.

The calculations described in the present report have been carried out in order to check maximum temperatures and the exposure to elevated temperature of both waste packages and backfill materials.

Calculations have been carried out for a number of different packages, both of high level and of intermediate level wastes. Two high level waste packages have been treated, one containing vitrified fuel reprocessing waste in an iron overpack and the other containing spent fuel (unreprocessed fuel) in a copper overpack. Heat generating intermediate level waste comprises fuel hulls and end caps and the co-precipitation sludges from reprocessing, both in steel drums and decommissioning wastes stabilised in concrete blocks.

The situation modelled for the high level wastes is NAGRA's type C repository, hypothetically sited at approximately 1200 m below ground level in a crystalline host rock whose natural temperature at that depth, typical for the rocks beneath the northern Swiss lowland plateau, is 55 °C. It is proposed to emplace high-level waste along the axes of backfilled tunnels in this repository 40 years after its removal from a reactor core. Hulls and end caps and possibly co-precipitation sludges may also be disposed of in this repository, the waste drums being stored layer-by-layer in cylindrical, concrete-walled silos.

The type B repository for intermediate and low level wastes is to be installed in a formation at considerably smaller depth. Host rock temperatures are not expected to exceed 30 °C. Storage is to be in horizontal caverns.

That portion of the potential waste inventory with non-negligible heat output is expected to consist of certain plant decommissioning wastes and possibly also the co-precipitation sludges from the fuel reprocessing. For disposal of this latter waste type, the type B repository is considered as an alternative to the silos of the type C repository. All waste is filled into standardised concrete containers designed for convenient stacking in the concrete-lined caverns which are finally backfilled with a special cement mixture.

Within the present report the disposal in the type C repository is treated first, commencing in Chapter 2 with the tunnel storage of the high level wastes and continuing in Chapter 3 with silos for intermediate level waste disposal. Chapter 4 treats the disposal in the type B repository.

The sub-models for the various heat transfer mechanisms are described briefly in Chapters 2, 3 and 4. Algebraic symbols are explained both locally and in the global nomenclature list in Chapter 7.

The criteria for acceptability of thermal loading are engineering design targets, based on conservative estimates of damaging mechanisms in each of the materials used.

2. HIGH LEVEL WASTE

2.1 Geometry of the Storage Tunnels

The basis of all of the calculations described in this chapter is a repository designed with the high-level waste packages spaced at regular intervals along the axes of parallel tunnels of 3.7 m diameter. The tunnels are backfilled with precompacted bentonite blocks, which swell and produce an integral, low permeability barrier ([1], [2], [3] and [4]) when wetted by infiltrating groundwater.

Figure 2.1 is a perspective cut away sketch of a length of storage tunnel showing two reprocessing waste packages separated by bentonite blocks from the host rock. The design axial pitch for the reprocessed waste has been fixed from previous thermal considerations [5] at 5 m. In the present report axial pitches of 7 m and 10 m for the spent fuel disposal have been examined.

The distance between the axes of neighbouring tunnels is 40 m.

2.2 Repository Materials

2.2.1 Bentonite Backfill

The variation of thermal conductivity of sodium bentonite with temperature and water content may be fitted (in W m^{-1} K^{-1}) by the following formula [6]:

$$k_b = 0.6(\rho_b - \rho_w) + 0.004\ \phi\rho_b^3 + 0.01\ \sqrt{T} \qquad (2.1)$$

where:

ρ	Density [Mg m^{-3}]
ϕ	Water content [Mg water per Mg solid]
T	Temperature [°C]

and the suffices imply:

b Bulk property of wet bentonite
d Property of the equivalent dry material
w Property of the pore water

so that the total density:

$$\rho_b = \rho_d(1 + \phi)$$

The dry density has been taken to be 1.635 Mg m^{-3} (see [1] for the degree of precompression considered in the repository design analysed).

The volumetric heat capacity of the bentonite is expressed as (See [1]):

$$(\rho C)_b = \rho_b \left(\frac{1}{(1 + \phi)} C_d + \frac{\phi}{(1 + \phi)} C_w\right) = \rho_d (C_d + \phi C_w) \qquad (2.2)$$

where now:

C Specific heat [J kg^{-1} K^{-1}]

It is to be expected that the inner region of the backfill will tend to dry out as its temperature increases, causing water:

a) to evaporate off into the ventilated repository mine workings,
b) to migrate outwards towards the tunnel walls.

As groundwater from the surrounding host rock gains access to the bentonite the wetting process will counteract the drying out ([7], [8]) and eventually reverse it. The rates of drying and wetting will be dependent on the availability of escape paths for water vapour, on the local availability of groundwater and upon absolute levels of temperature as well as temperature gradients. Since it has not yet been possible to study either experimentally or theoretically in detail the interaction of all these processes on the water migration rates a simplified approach has been taken.

The design water content of the bentonite blocks at the time of insertion is 7 % by weight. A direct dependence of the water content on temperature has been assumed as shown in Figure 2.2 whereby the piecewise linear variation from the design level at 30 °C to 2 % at 100 °C and to zero at 150 °C has been assumed. This assumption has been based upon the laboratory-drying experiments on small unconfined samples performed in Sweden [7]. The rewetting of the bentonite by the groundwater and the resulting recovery of the thermal conductivity have been neglected. Thus, the conductivity can only decrease from its initial value.

The dependence of thermal conductivity, k_b, upon temperature resulting from the elimination of water content from equation (2.1) with the help of the relation in Figure 2.2 has been modelled as a 4th order polynomial function.

The volumetric heat capacity resulting from a similar elimination in (2.2) is dependent upon temperature as a piecewise linear function. Table 2-1 gives an overview of the variations of both conductivity and heat capacity with temperature.

Table 2-1: Temperature dependence of the thermal properties of the precompressed bentonite prior to wetting by groundwater

Temperature [°C]	k_b [W m^{-1} K^{-1}]	$(\rho C)_b$ [MJ m^{-3} K^{-1}]
35	0.646	2.091
50	0.621	
75	0.578	
100	0.542	1.772
125	0.518	
150	0.511	1.635

2.2.2 Host Rock

The thermal conductivity of the granite host rock has been assumed to take the value [1]:

$$k_r = 2.5 \text{ W m}^{-1} \text{ K}^{-1}$$

Measurements have been made on samples from the Böttstein borehole, which has provided reference data for the design and safety studies of which the present work forms a part. A high quartz content in the granite has tended to yield conductivities higher than the above value. The lower value has been selected to provide some conservatism in the temperature predictions within the repository tunnels (see [5] for the effects).

The volumetric thermal capacity for granite used was [1]:

$$(\rho C)_r = 2.3 \times 10^6 \text{ J m}^{-3} \text{ K}^{-1}$$

2.3 The Waste Packages

2.3.1 Vitrified Reprocessing Waste

The reprocessed waste package which has been examined is illustrated in Figure 2.3. The stainless steel bottle into which the vitrified waste is cast is inserted into an essentially cylindrical cast steel overpack. This is of 0.94 m diameter and its cylindrical wall is 2 m long. The wall thickness is 0.25 m and that of the end caps 0.15 m.

Values of the material thermal properties over the relevant temperature range are listed in Table 2-2 (see also [1]). The conductivity of the vitrified waste has been modelled approximately within this range by a linear function of temperature (in Celsius):

$$k = 0.95 + 0.001 \text{ T } [\text{W m}^{-1} \text{ K}^{-1}] \qquad (2.3)$$

It is apparent in Table 2-2 that over the expected temperature range (35° to 200°) a 15 % variation occurs in the thermal conductivity of the vitrified waste. The variation in the cast overpack material over the same range is only 7 %. This has, therefore, been ignored and a constant value used:

$$k = 50 \ [W \ m^{-1} \ K^{-1}] \tag{2.4}$$

The volumetric heat capacities were also assumed to be constant in both cases.

Table 2-2: Thermal properties of the materials used in the reprocessing waste package (cf. [1])

Properties	Vitrified waste	Cast steel overpack
Thermal conductivity $[W \ m^{-1} \ K^{-1}]$ at 35 °C	0.99	53.01
at 100 °C	1.05	52.00
at 200 °C	1.15	49.33
Thermal capacity $[MJ \ m^{-3} \ K^{-1}]$	3.00	3.05

Table 2-3 contains a list of heat generation rates per waste package at times from forty up to one thousand years after unloading from the reactor core. These values result from calculations with the ORIGEN-2 code [9]. Figure 2.4 shows the tabulated points superposed on a plot of a third order polynomial function which was fitted to them and which has been used to model the time-varying heat source strength of a waste package. The period covered corresponds approximately to that following emplacement in the repository until the heat release rate has declined by two orders of magnitude.

Table 2-3: Residual heat production of the vitrified reprocessing waste, per package

Time from unloading [yrs]	Heat generation rate per package [W]
40	582
50	464
80	235
100	164
200	60
400	25.0
600	15.4
800	11.0
1'000	8.6

2.3.2 Spent Fuel

A spent fuel package is approximately cylindrical, 4.8 m long and has a diameter of 0.812 m. The circumferential wall of its copper overpack is 0.1 m thick, the thickness of the end caps has been assumed to be 0.2 m.

Alternative fillings [9, 10] are considered for these packages. The present study treats that fuel loading yielding the highest thermal load. It contains a mixture of UO_2, zircaloy and steel, and is filled up with sintered copper of 1 % porosity.

In the calculations the package content has been modelled as a homogeneous mixture of the materials listed above, an approximation which seems well justified by the fact that the bundles consist of comparatively thin structures surrounded by highly conductive copper. Conductivity has therefore been expressed as a geometric mean of the conductivities of the materials involved, with their relative volumes as exponents. The volumetric heat capacity of this mixture has been calculated as the weighted arithmetic mean of the volumetric heat capacities of the individual components.

Values of the material properties in the range of interest for the calculations can be found in Table 2-4 below. The data are derived from the properties given in [13] and [14].

Table 2-4: Thermal properties of the proposed spent fuel package

Material property [units]	Temp. [°C]	Fuel elements in pressed Cu. powder	Copper overpack
Thermal cond.	35	192	384
[W m^{-1} K^{-1}]	100	189	382
	150	188	381
Thermal capacity	35	3.31	3.45
[MJ m^{-3} K^{-1}]	100	3.39	3.51
	150	3.46	3.56

Because of the extremely small variations of the thermal properties with temperature the underlined values for 100 °C were input to the computations and treated as constants.

The heat released by a spent fuel package as a function of time has been represented by a log-log polynomial of 3rd order. This function, as for the reprocessing waste, has been fitted to heat release data derived from inventory decay via ORIGEN computations in the fuel bundles (see Table 2-5). Figure 2.5 compares tabulated points with the fitted function.

As for the high level waste, disposal 40 years after removal from the reactor has been assumed in the calculations.

Table 2-5: Residual heat production of the spent fuel package

Time from unloading [yrs]	Heat generation rate per package [W]
40	808
50	660
80	470
100	407
200	240
400	149
600	112
800	92
1000	78

2.4 Method of Calculation

2.4.1 The Geometry of the Domain

Though, obviously, the problem is basically a 3-dimensional one, a method of solution based on two linked 2-dimensional calculations has been developed and used. This technique, which makes use of the repository's geometry and of the times during which high temperatures persist in the near field, has brought about a substantial reduction in computing effort.

The temperature distribution in the host rock, in spite of the inhomogeneous distribution of the heat source from the waste, spaced at regular intervals along the tunnel axes, is essentially axially invariant, even at fairly small distances from the tunnel wall. This has been indicated by preliminary calculations and confirmed by a verification study, described in detail in Appendix 1.

At any radius within the backfill material the temperature fluctuates with axial position. Owing to the slowness of the temperature change at

the tunnel wall and the relatively high conductivity of the host rock compared with that of the bentonite backfill, the temperature equalisation by conduction within the rock is sufficiently fast to damp out the axial fluctuations almost completely by a radius of only a few metres in the host rock. Here the situation is effectively indistinguishable from that to which an axially continuous heat source of the same average strength would give rise.

This means that a calculation of the temperature evolution in a plane perpendicular to the tunnel axes with an axially averaged heat source yields, for that part of the host rock outside the immediate region of the tunnel, the same result as a fully detailed three-dimensional computation.

Figure 2.6, represents such a plane perpendicular to the axes of two neighbouring tunnels. Two vertical planes of symmetry are shown. One of these bisects one of the tunnels and the other is situated midway between tunnels. In addition, the horizontal line joining the axes of the tunnels is shown also as a symmetry plane. Strictly speaking the temperature field is not symmetrical about a horizontal line on account of the geothermal temperature gradient (in Northern Switzerland typically about 4 °C per 100 m). The temperature gradient was included in the results reported in [1]. However, comparative calculations have shown that the geothermal gradient may be disregarded (cf. [5]). There are two reasons for this. On one hand, the host rock in the overall model concept is assumed to behave in a purely linear manner. On the other hand, the perturbed zone in and around a repository tunnel is dominated by the essentially axisymmetric heat source within it. It is the perturbed zone which is of interest and within its limited extent (see later and also Figure 2.7) a peak deviation from the symmetrical situation of less than 0.2 °C may be expected. Thus, the initial two-dimensional calculations may be made in the hatched domain in Figure 2.6 bounded by these three planes of symmetry. The initial temperature of the host rock has been assumed to be uniform throughout at 55 °C. A more detailed discussion of initial conditions is included in Section 2.4.3.

The three symmetry planes constitute zero-flux boundaries to the domain, whereas the 300 metre distant lower horizontal boundary is assumed to remain unperturbed and is hence fixed at the initial rock temperature. This set-up, in a field defined in cartesian coordinates, will be referred to henceforth as the coarse scale model.

The results of calculations with this coarse scale model indicate an almost perfect rotational invariance of the temperature distribution in the tunnel and its surroundings with respect to the axis of the tunnel's circular cross-section. The region of rotational invariance, stretching out to a radial distance of several metres from the tunnel wall overlaps the inner boundary of the region of axial invariance. There exists therefore a hollow cylindrical zone of rock where the 3-dimensional temperature distribution remains in effect both axially and rotationally invariant at all times. Within this zone a surface with radius R_1 may be chosen to serve as an interface for linking the coarse scale model calculation assuming axial invariance to a second 2-dimensional calculation based on the rotational symmetry of the temperature distribution within the tunnel and its immediate surroundings. Calculations of the second kind require a fine scale model.

A cylindrical domain comprising a section of storage tunnel and that portion of the rock within the interface radius R_1 forms the basis of the fine scale model. It extends axially from a first plane perpendicular to the tunnel axis and bisecting a waste package to a second plane, parallel to the first one and situated exactly halfway between the waste package and one of its immediate neighbours (see Figure 2.7). The two parallel planes constitute zero heat flux boundaries, whereas at the circumferential surface the temperature time history at radius R_1 obtained from the coarse scale calculations are applied as a (time-dependent) boundary condition. Thus, the fine scale calculations, whereby the waste package is modelled in detail, are effectively embedded into the initial coarse scale ones, which take into account the overall geometric situation.

Since the bentonite is inserted into place in the tunnel in the form of prefabricated blocks, the occurrence of constructional gaps in the resulting backfill seems inevitable. This situation has been accounted for in that, in the model geometries, there are three circumferential gaps, each 1 cm wide, a first one immediately at the outer surface of the waste package, a second one at the tunnel wall and a third one almost halfway between them at a radius of 1.1 m. As gaps will occur in construction preferentially in the upper half of the tunnel due to settlement, the assumption of gaps existing all around the cylinder is certainly conservative with respect to peak temperatures and high temperature exposure of the central region of the storage tunnel.

2.4.2 The Equations

With the exception of the gaps, heat transfer has been assumed to be solely by conduction. For both the coarse and fine model calculations, versions of the Fourier heat conduction equation in cartesian and cylindrical coordinates have been employed:

$$\frac{\partial}{\partial t}(C_v T) = \frac{\partial}{\partial x}\left(K_{xx}\frac{\partial T}{\partial x}\right) + \frac{\partial}{\partial z}\left(K_{zz}\frac{\partial T}{\partial z}\right) + S \qquad (2.5a)$$

$$\frac{\partial}{\partial t}(C_v T) = \frac{1}{r}\frac{\partial}{\partial r}\left(rK_{rr}\frac{\partial T}{\partial r}\right) + \frac{\partial}{\partial z}\left(K_{zz}\frac{\partial T}{\partial z}\right) + S \qquad (2.5b)$$

where:

C_v	Volumetric heat capacity [J m^{-3} K^{-1}]
K_{ii}	Diagonal tensor coefficient of heat conductivity [W m^{-1} K^{-1}]
T	Temperature [K]
S	Heat production per volume element [W m^{-3}]
x,z	Components of the position vector in cartesian coordinates [m]
r,z	Components of the position vector in cylindrical coordinates [m]

The assumed axisymmetric nature of the construction joints remaining between the blocks of backfill material means that heat can only be transmitted across them by convection, conduction and radiation. The convective contribution has been ignored since pre-calculations indicate its minor importance at the temperature levels experienced in these small annular gaps during the early years after waste disposal. Instead, a simple formulation for radiative exchange between a pair of long, concentric, cylindrical grey bodies of identical material and surface quality has been used. This formulation (see for example [11]) permits the radial heat flux across a gap, inner radius r_i, outer radius r_o to be expressed per unit distance along the axis as:

$$\dot{q}'_{i\to o} = \frac{2\pi r_i \sigma \varepsilon}{1 + \frac{r_i}{r_o}(1-\varepsilon)} (T_i^4 - T_o^4) \qquad [W\ m^{-1}] \tag{2.6}$$

where:

ε	Surface emissivity ($\sim$ absorptivity) [-]
$\dot{q}'$	Radial heat flux per unit length of the whole cylinder
r	Radius [m]
σ	Stefan Boltzmann constant [$W\ m^{-2}\ K^{-4}$]
T	Surface temperature [K]
i	Inner surface of annular gap
o	Outer surface of annular gap

Across the air gap then, radiation heat exchange is superposed upon conductive exchange. At the temperature levels experienced during the first fifty years after disposal, radiation transmits approximately 80 % of the energy. This is achieved in the numerical calculations by the addition of an extra non-linear component to the coefficients linking node pairs which experience radiative exchange.

Since small temperature differences are experienced across the gaps (see results in Section 2.5) the assumption of equal emissivities and absorptivities leading to the formulation of (2.6) is an acceptable simplification. No definite information being available concerning emissivities of compressed bentonite blocks, a value of 1.0 has been used. The ratio r_i/r_o is approximately unity. Experimental calculations (see for example Appendix 2) show that in general the heat flux across a gap and thus the temperature profiles in the adjacent solids are very insensitive to the properties of the radiating surfaces due to the fourth power dependence of radiative flux on surface temperature.

2.4.3 Initial Conditions

The following initial temperatures have been assumed to hold:

Bentonite:	35 °C
Rock:	55 °C
Waste package:	65 °C

During the operating phase of the repository, whilst excavation and disposal are proceeding, the air in the excavations has to be kept below a maximum of 35 °C to maintain tolerable working conditions. The bentonite blocks are assumed to have reached this temperature by the time that disposal occurs.

Cooled air circulating in the excavated tunnels over long periods will also cool down the host rock in the neighbourhood of the exposed surfaces. This effect has been ignored, the rock being assumed initially to be at a uniform 55 °C.

The initial temperature of the waste packages has been established by the use of simple, free-convection heat exchange calculations. For these calculations two assumptions were made:

- That the high level waste packages are maintained in a horizontal attitude in the repository up to the point of being manipulated into their final resting place.

- That before being encapsulated in backfill material, each fuel package is present long enough in the underground excavations for a steady heat transfer rate between it and the surrounding air to become established.

The use of the empirical expression for average heat exchange on the curved surface of a horizontal cylinder developed and tested by Churchill and Chu [12] enables the rate of heat exchange to be calculated for a given surface/air temperature difference:

$$Nu_D^{1/2} = 0.60 + \frac{0.387(Ra_D)^{1/6}}{\left[1 + \left(\frac{0.559}{Pr}\right)^{9/16}\right]^{8/27}} \qquad (2.7)$$

where:

Nu_D	Diameter-based Nusselt Number for air = $\bar{h}D/k$
Ra_D	Diameter-based Rayleigh Number = $\beta g C_p \rho^2 D^3 \Delta T/\mu k$
Pr	Prandtl Number for air = $C_p\mu/k$
β	Air coefficient of thermal expansion [K^{-1}]
C_p	Air specific heat at constant pressure [$J\ kg^{-1}\ K^{-1}$]
D	Diameter of the cylindrical waste package [m]
g	Gravitational acceleration [$m\ s^{-2}$]
$\bar{h}$	Average heat transfer coefficient [$W\ m^{-2}\ K^{-1}$]
μ	Air viscosity [$kg\ m^{-1}\ s^{-1}$]
k	Air thermal conductivity [$W\ m^{-1}\ K^{-1}$]
ΔT	Temperature difference between surface layer and bulk fluid [K]

Properties for air have been taken from the abbreviated tables presented by Eckert & Drake [13], package dimensions from 2.3.1 and 2.3.2 and a temperature difference has been assumed between cylindrical surface and bulk surrounding air of 30 °K. Use of (2.7) indicates that 650 W can be removed by free convection from the reprocessed fuel package (initial load 582 W) by free convection and 1535 W from the spent fuel (initial load 808 W).

Although no credit has been taken for the (small) radiative heat exchange nor for the contributions of the end caps, the 30 degree temperature difference provides more than sufficient heat removal capacity in both cases. This figure has been taken therefore in conjunction with the already conservative level of 35 °C for the air temperature to give initial temperatures of 65 ° both for the packages of reprocessing waste and for those of unreprocessed, spent fuel.

2.5 Results

2.5.1 Vitrified Reprocessing Waste

The evolution of the temperature distribution around a tunnel with packages of high level reprocessing waste disposed on an axial pitch of 5 m has been calculated up to 650 years.

The results are presented in Figures 2.8 to 2.11 and Table 2-6. Figure 2.8 shows radial temperature profiles on the plane intersecting the package centre at various times. The vertical lines indicate the positions of the gaps. Peak values at various positions inside the tunnel and the times of their occurrence are listed in Table 2-6.

High temperature exposure at various positions can be seen in the temperature time history plots in Figures 2.9 to 2.11. Figure 2.9 shows the temperature evolution at the package centre, Figure 2.10 the temperature time histories of the hottest and the coldest point in the iron overpack. In this and the subsequent cases studied (2.5.2 and

2.5.3) the hottest point is, as expected, on the overpack's inner radius on the transverse plane through the package centre, whilst the coldest point is on the overpack's outer radius at its axial extremity. The difference between these extremes is never greater than 4.1 °C, because of the high conductivity of the iron. Figure 2.11 contains the temperature time histories at various positions in the bentonite: near the container wall (r = 0.532 m), at a radius just less than that of the middle one of the three annular gaps (r = 1.036 m), at a radius just greater than that of the middle gap (r = 1.173 m) and near the tunnel wall (r = 1.765 m).

It will be noted that the transient peaks everywhere within the storage tunnel have passed in less than 20 years.

Table 2-6: Vitrified Reprocessing waste, maximum temperatures in the very near field

Location	Max. Temp. [° C]	Time of occurrence [years]
Package centre R = 0.000 m	195.3	1.02
Iron overpack R = 0.262 m	152.7	1.51
Bentonite:		
a) R = 0.532 m	139.9	1.51
b) R = 1.036 m	101.2	3.16
c) R = 1.173 m	92.8	3.48
d) R = 1.765 m	73.7	15.70

2.5.2 Spent Fuel

For spent fuel packages two different sets of calculations have been carried out. A first one for which an axial pitch between storage loca-

tions of 10 m was assumed, extending to 650 years and a second one with 7 m pitch extending to 50.2 years.

a) 10 m Pitch

The results of these calculations are presented in Figures 2.12 to 2.15 and Table 2-7 in a similar manner to those for the high level reprocessing waste.

It will be noted that the peak temperature at the package centre is fairly low, partly because of the equalisation effected by the very high conductivities of the package materials. For the same reason temperature differences remain very small in the overpack (less than 1 °C).

In the bentonite, even immediately inside the middle gap, temperatures only just exceed 90 °C. Further outside they remain at very moderate values. Peak temperatures are reached everywhere with this spacing in the storage tunnel in less than 35 years.

b) 7 m Pitch

The results presented in Figures 2.16 to 2.19 and Table 2-8 show that peak temperatures are about 5 °C higher and time evolution is somewhat retarded by comparison with the previous case with 10 m axial pitch. Consequently, in addition to the higher temperatures attained, exposure times tend to be longer.

Table 2-7: Spent fuel, axial pitch 10 m, maximum temperatures in the very near field

Location	Max. Temp. [° C]	Time of Occurrence [years]
Package centre R = 0.000 m	129.9	2.03
Copper overpack R = 0.329 m	129.2	2.03
Bentonite:		
a) R = 0.462 m	120.5	2.35
b) R = 1.042 m	90.4	5.96
c) R = 1.174 m	84.9	7.99
d) R = 1.766 m	73.8	31.20

Table 2-8: Spent fuel, axial pitch 7 m, maximum temperatures in the very near field

Location	Max. Temp. [° C]	Time of Occurrence [years]
Package centre R = 0.000 m	134.1	2.72
Copper overpack R = 0.329 m	134.0	2.59
Bentonite:		
a) R = 0.462 m	125.3	3.16
b) R = 1.042 m	95.4	9.25
c) R = 1.174 m	90.3	15.20
d) R = 1.766 m	80.0	50.20 *

* still slowly increasing at the end of the 50 year calculation

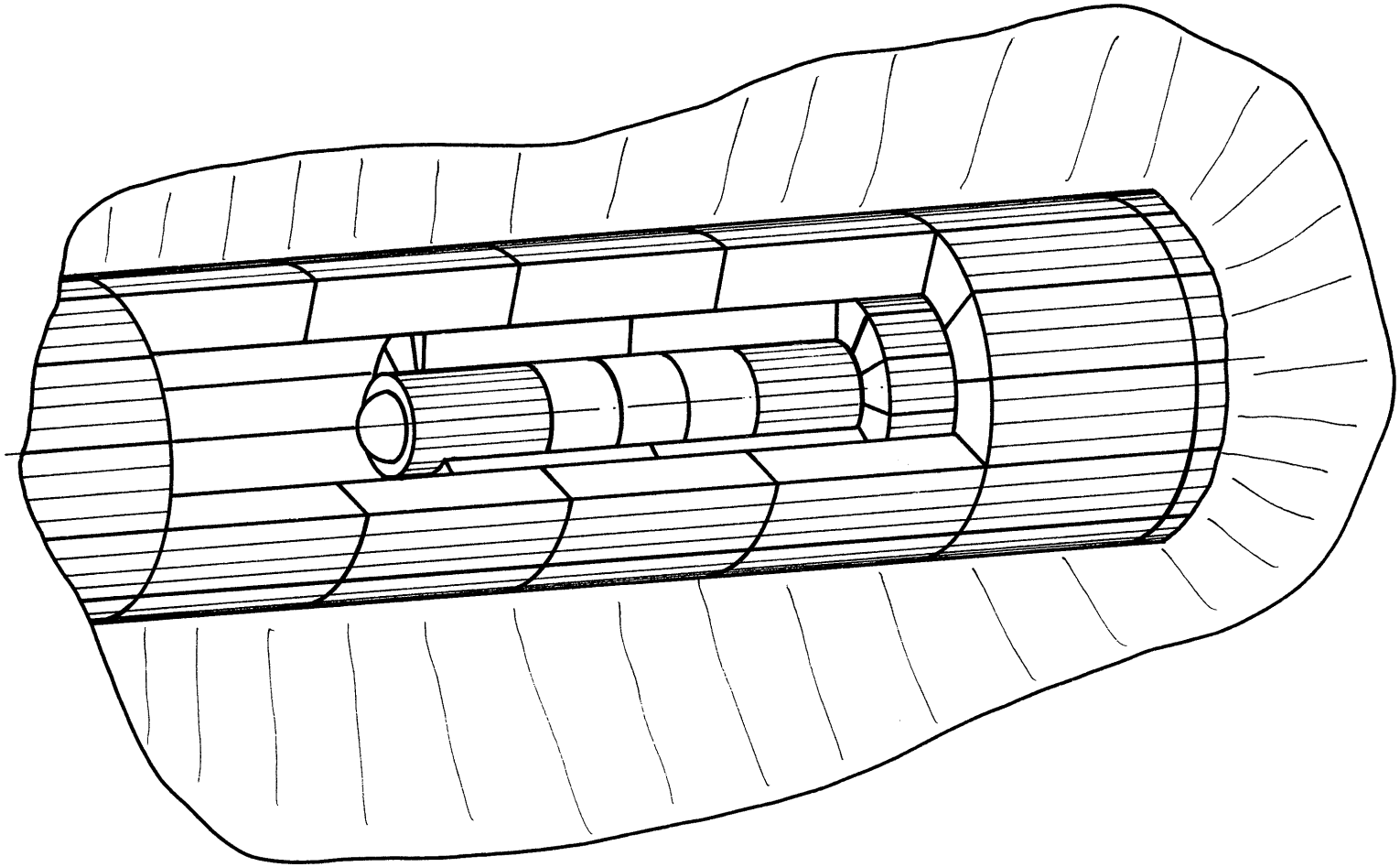

FIGURE 2.1: PERSPECTIVE CUTAWAY VIEW INTO A STORAGE TUNNEL IN THE HIGH LEVEL WASTE REPOSITORY

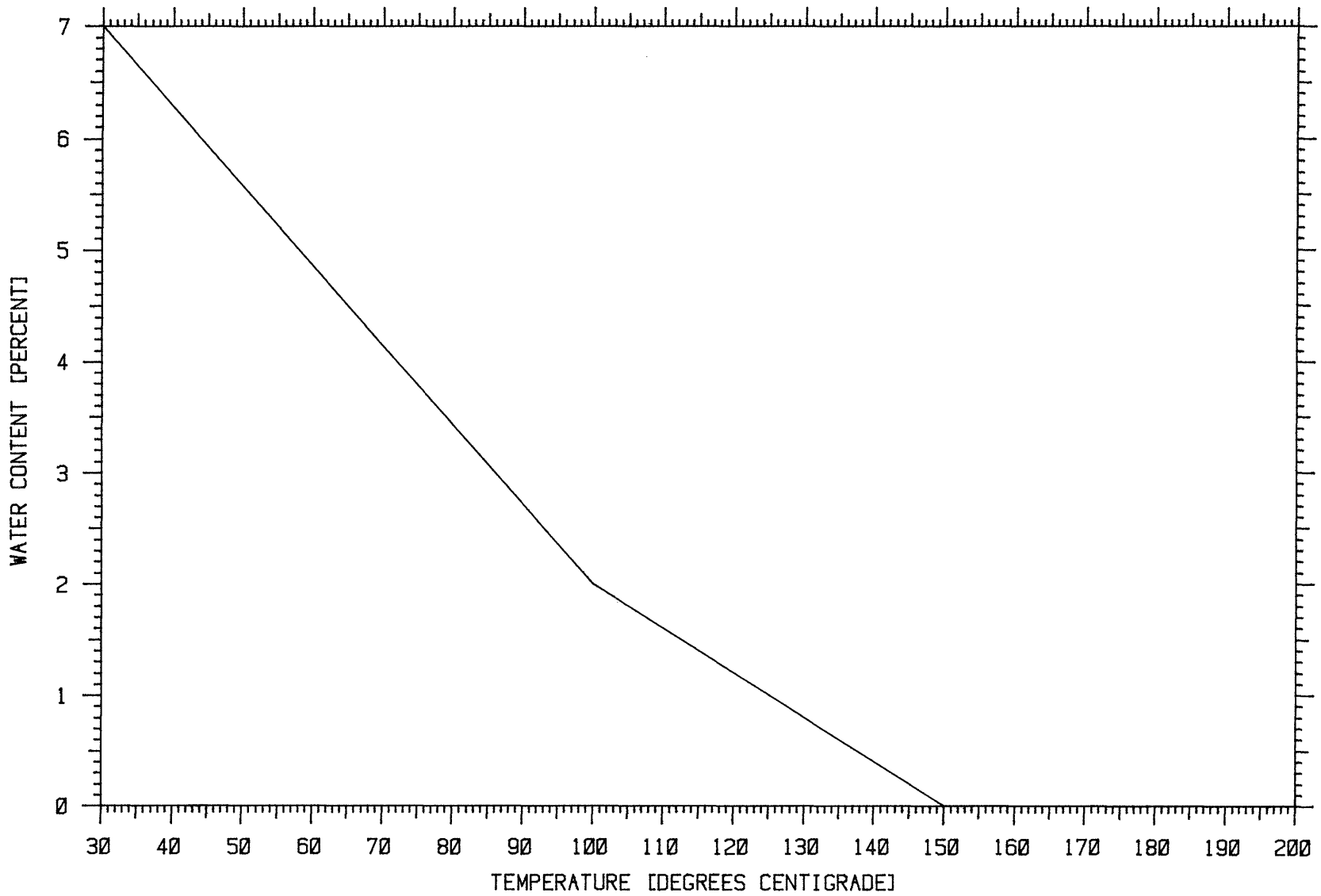

FIGURE 2.2: VARIATION OF WATER CONTENT IN BENTONITE BACKFILL AS A FUNCTION OF TEMPERATURE

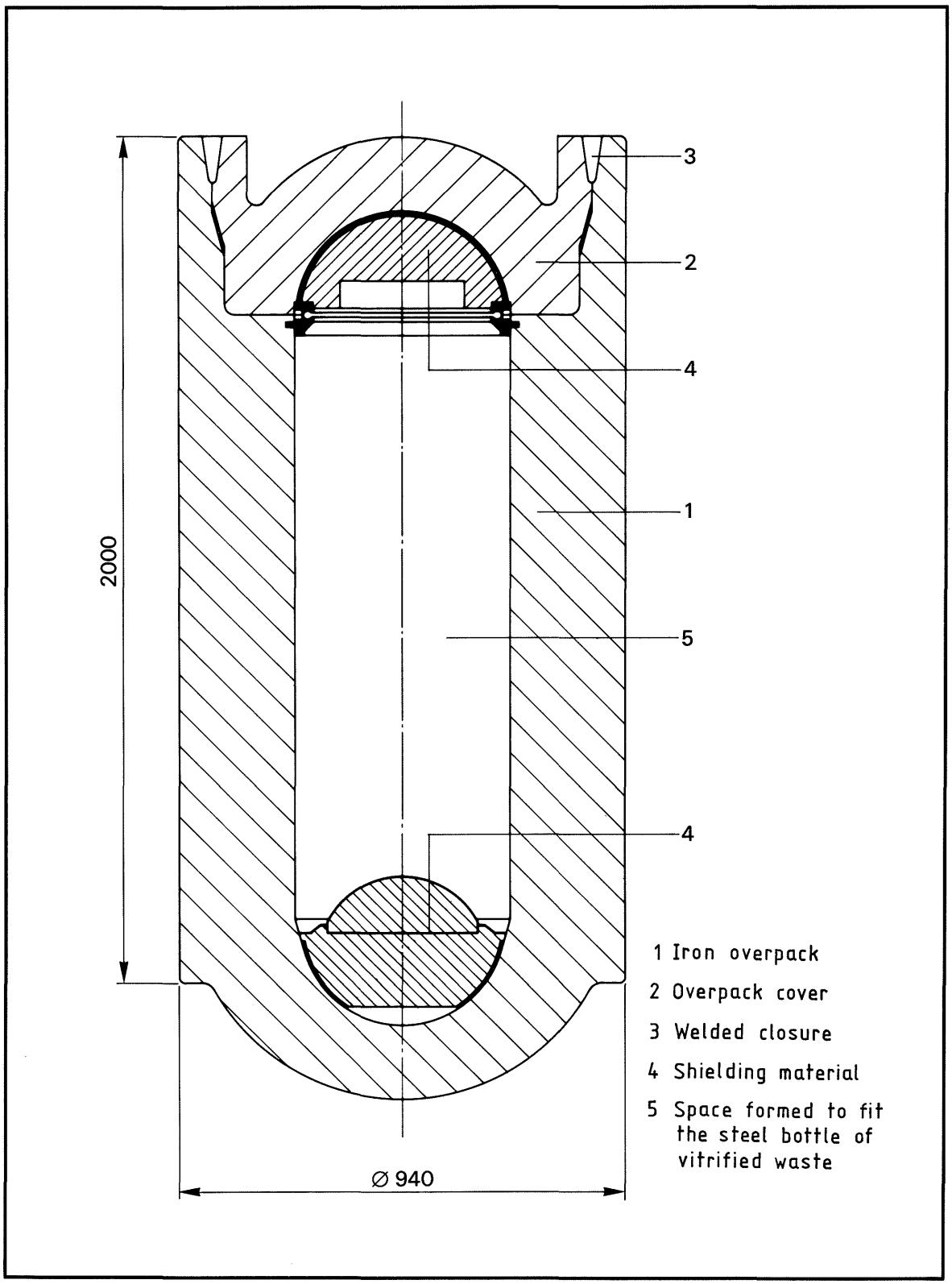

FIGURE 2.3: THE HIGH LEVEL REPROCESSING WASTE PACKAGE (SEE NTB 84-32)

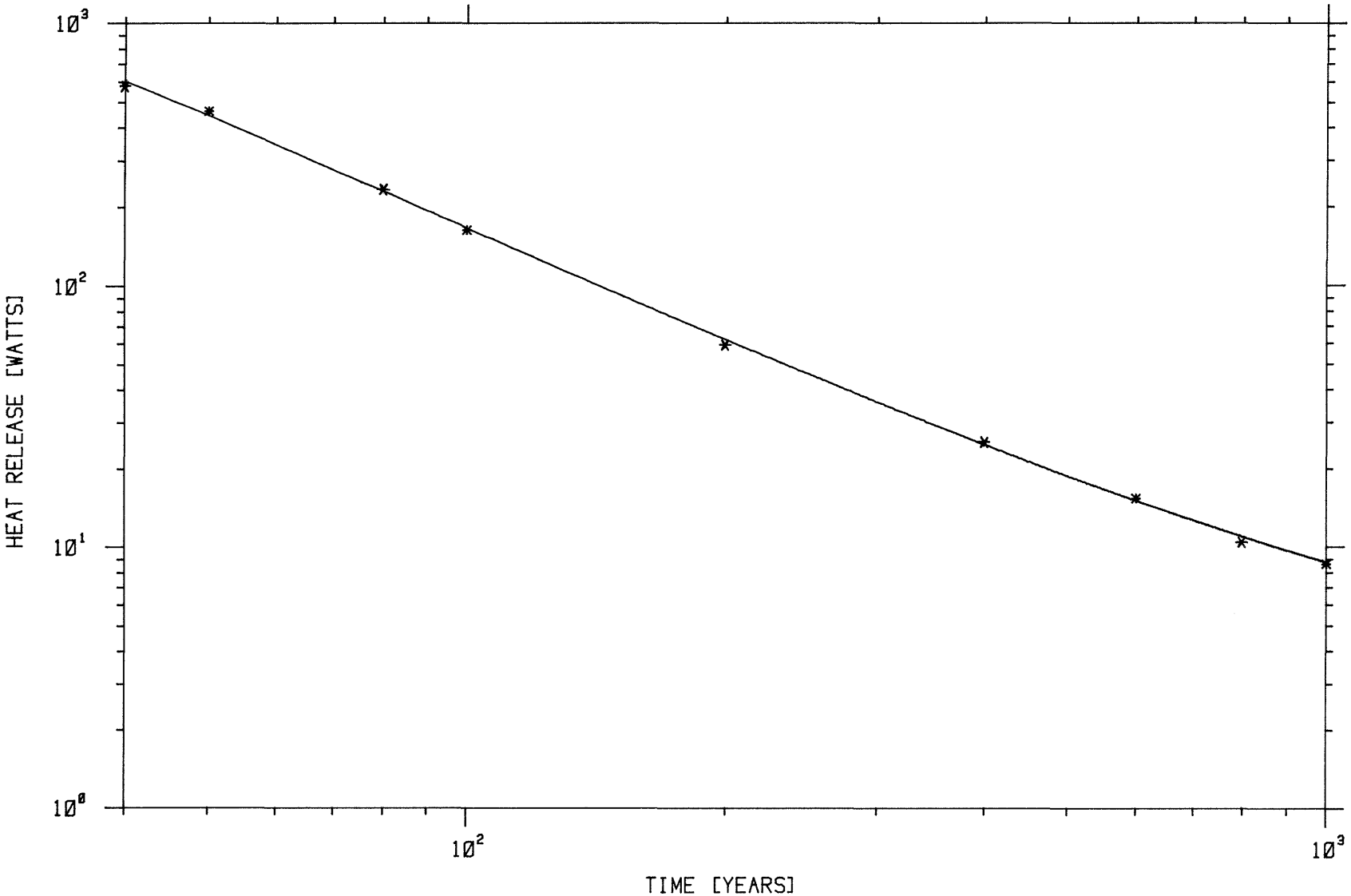

FIGURE 2.4: HEAT RELEASE RATES FROM HIGH LEVEL REPROCESSING WASTE PACKAGES AT DISCRETE TIMES AFTER UNLOADING FROM THE REACTOR COMPARED WITH THE FITTED FUNCTION USED IN THE ANALYSIS

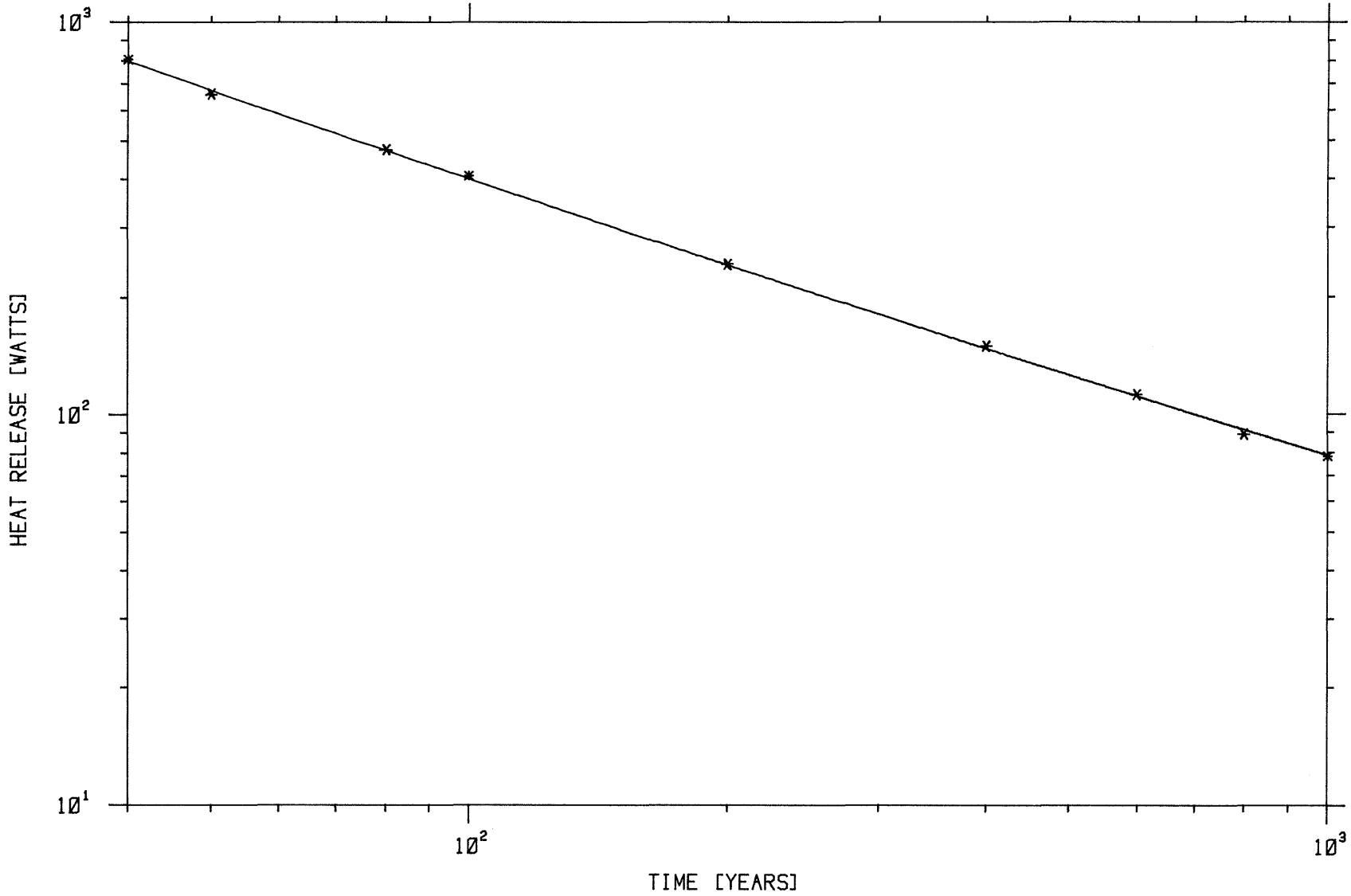

FIGURE 2.5: HEAT RELEASE RATES FROM SPENT FUEL PACKAGES AT DISCRETE TIMES AFTER UNLOADING FROM THE REACTOR COMPARED WITH THE FITTED FUNCTION USED IN THE ANALYSIS

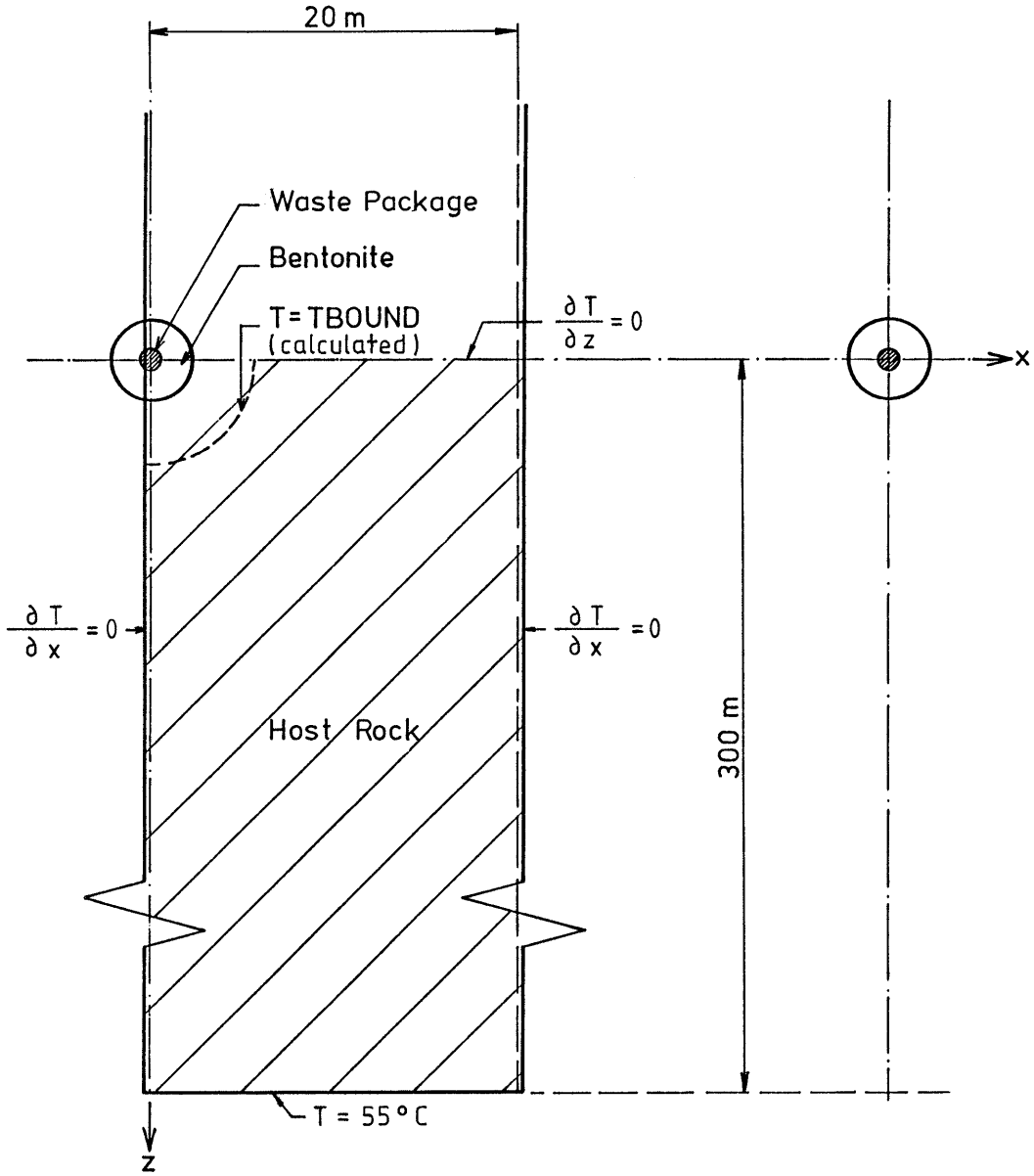

FIGURE 2.6: PLANE PERPENDICULAR TO STORAGE TUNNEL AXES SHOWING (HATCHED) THE DOMAIN OF THE COARSE SCALE (CARTESIAN) MODEL

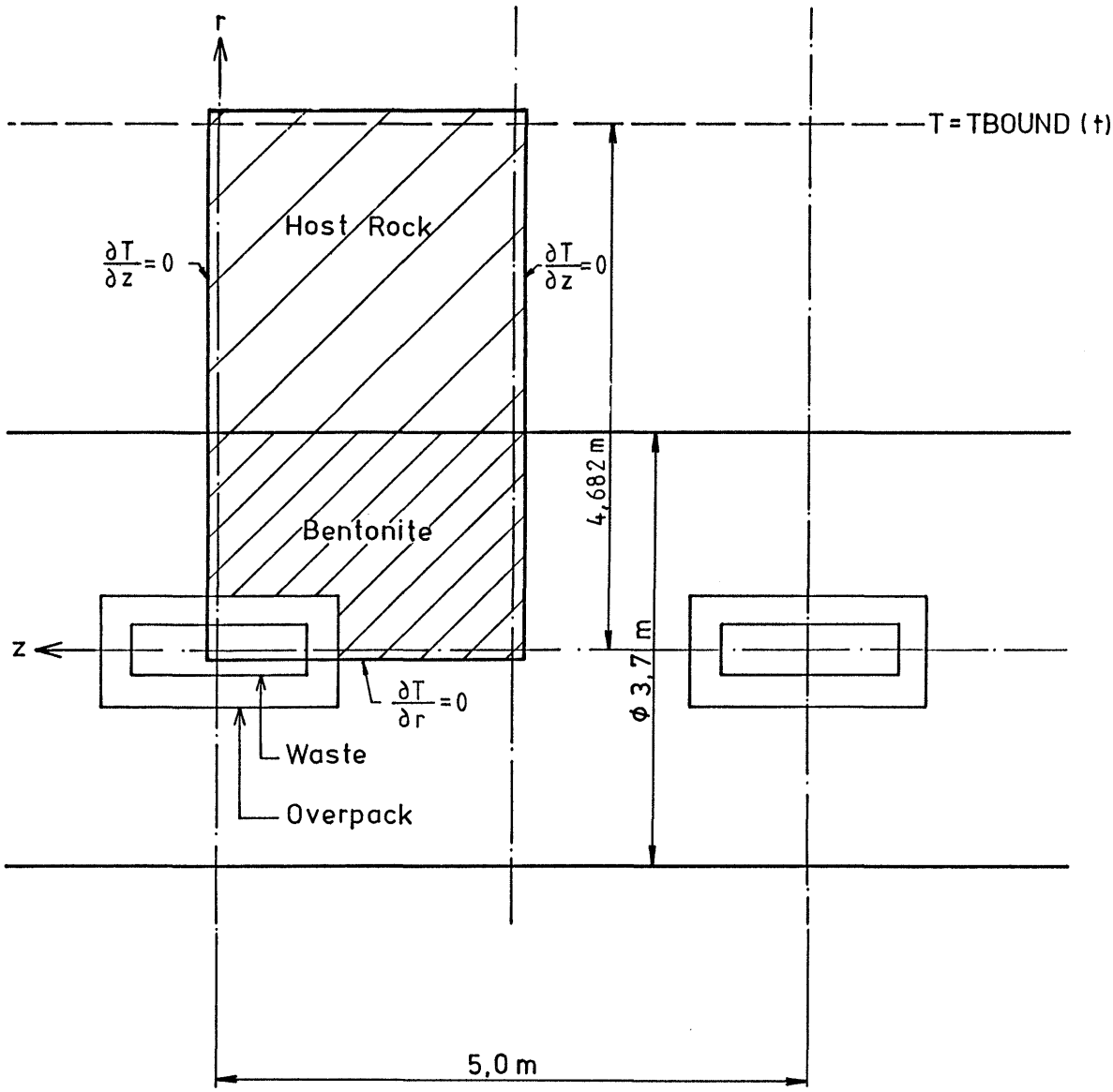

FIGURE 2.7: DIAMETRAL PLANE THROUGH THE AXIS OF A STORAGE TUNNEL SHOWING (HATCHED) THE DOMAIN OF THE FINE SCALE (CYLINDRICAL) MODEL

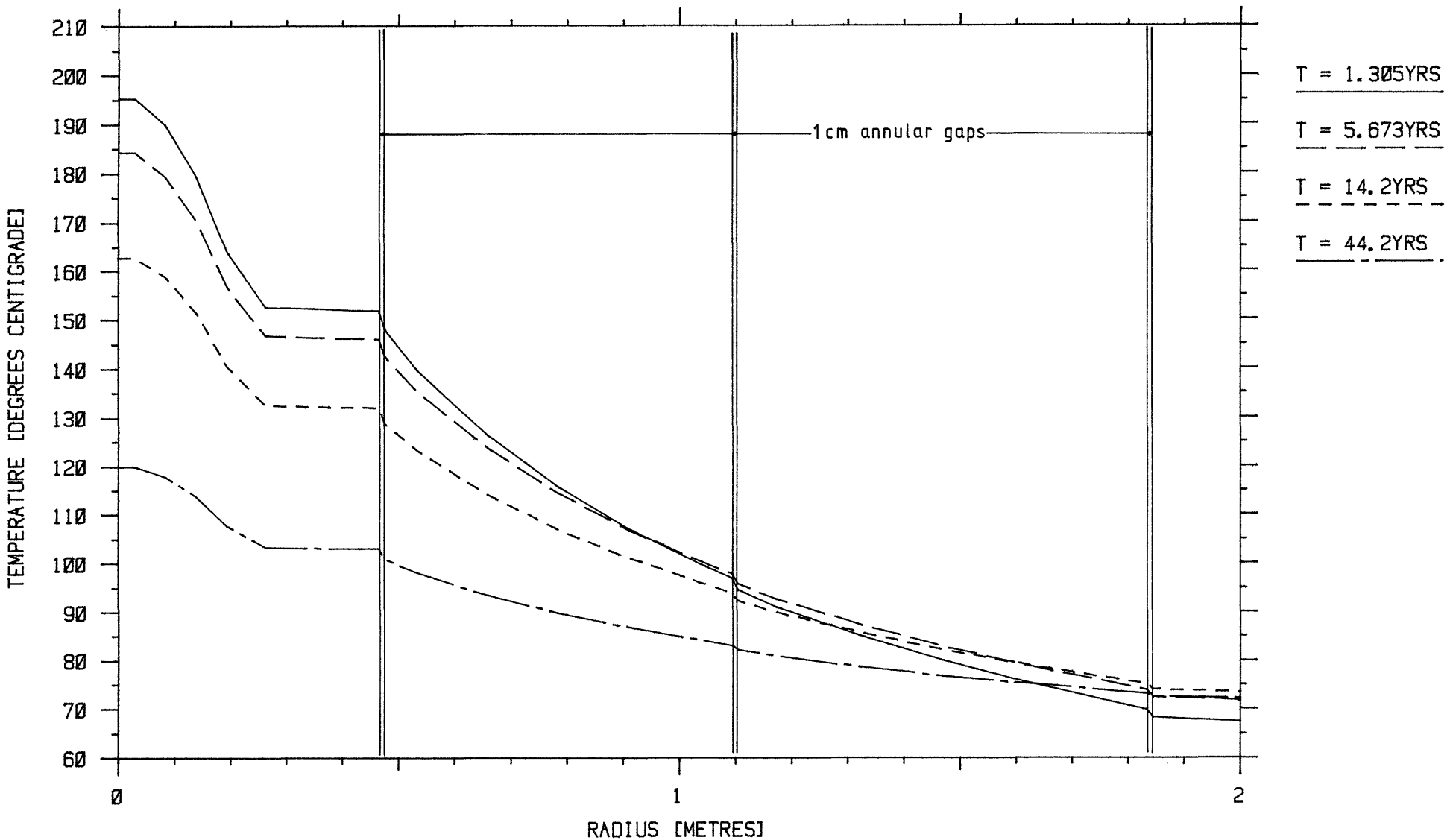

FIGURE 2.8: RADIAL TEMPERATURE PROFILES ON A TRANSVERSE PLANE THROUGH THE CENTRE OF A PACKAGE OF VITRIFIED HIGH LEVEL REPROCESSING WASTE

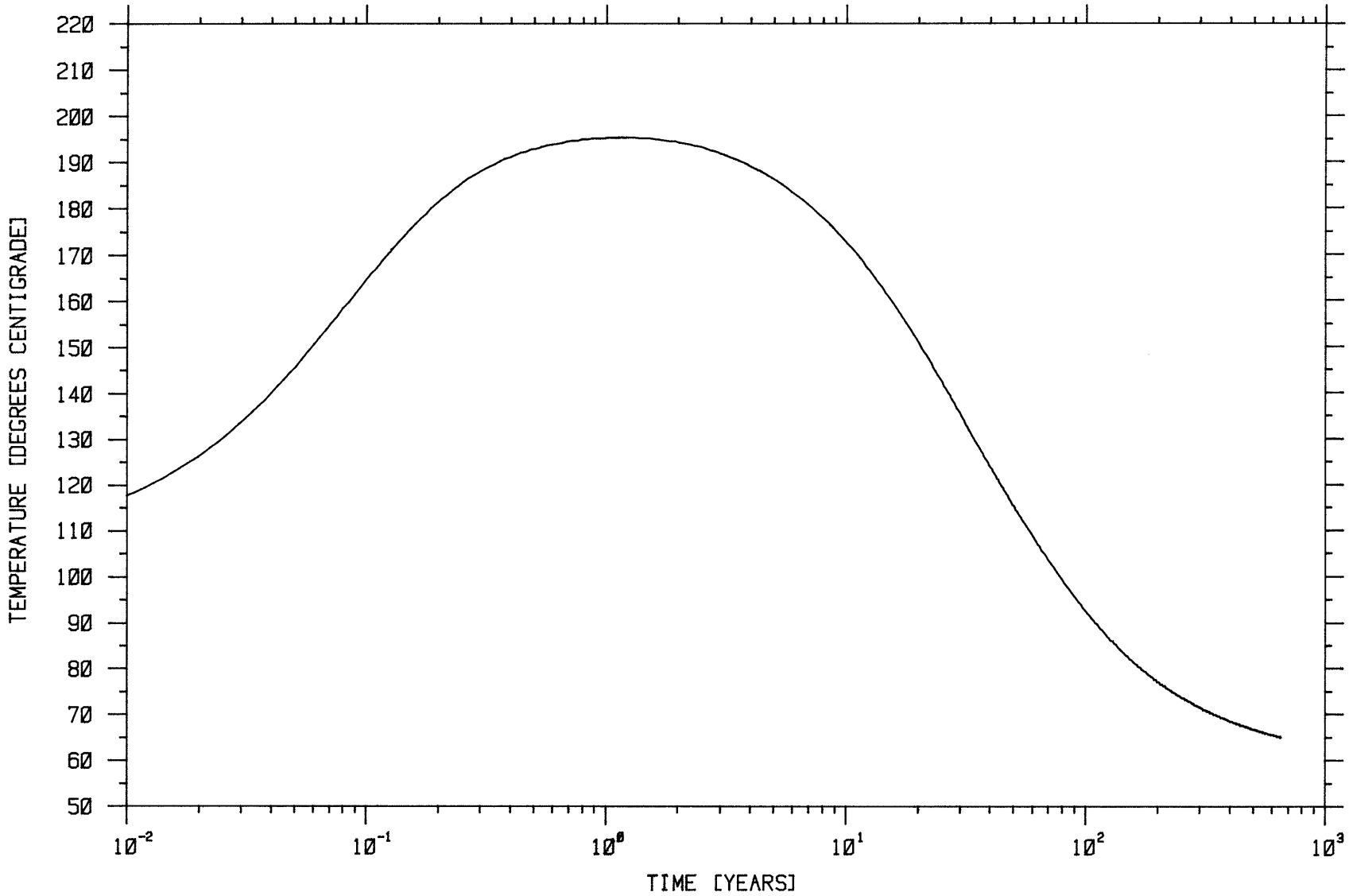

FIGURE 2.9: TEMPERATURE TIME HISTORY: CENTRE OF VITRIFIED REPROCESSING WASTE PACKAGE

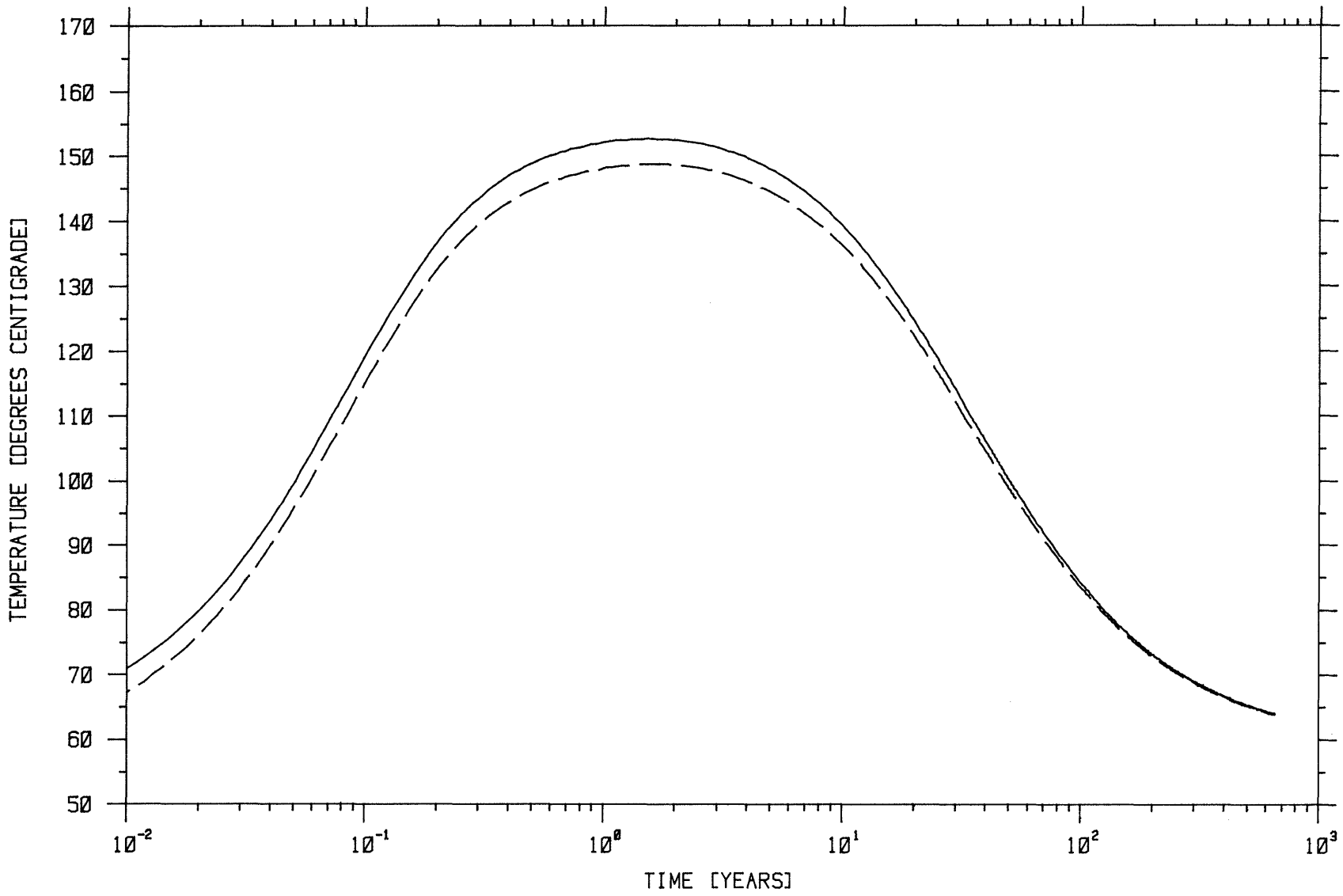

FIGURE 2.10: TEMPERATURE TIME HISTORIES: HOTTEST AND COLDEST POINTS IN THE IRON OVERPACK

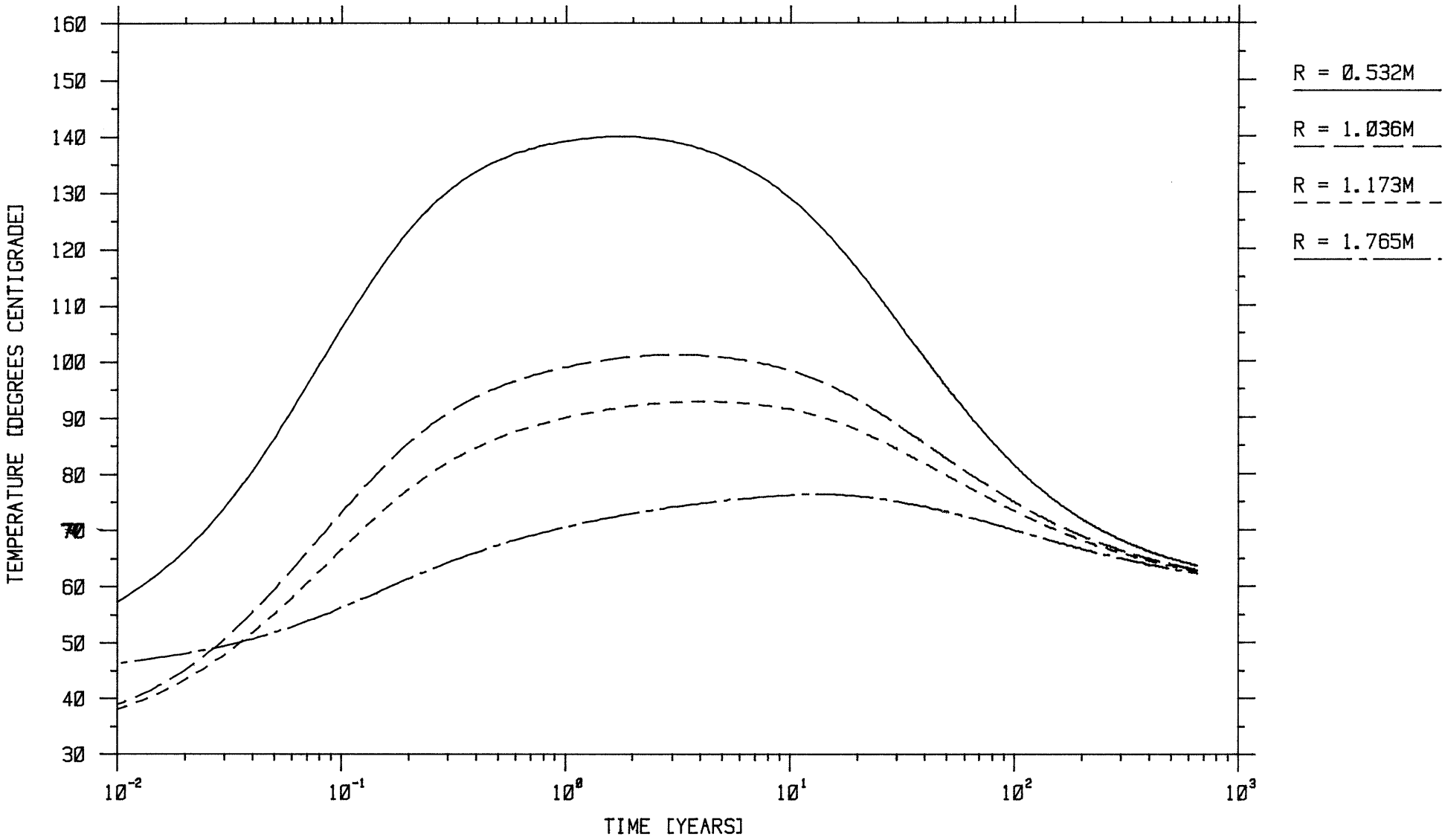

FIGURE 2.11: TEMPERATURE TIME HISTORIES: AT VARIOUS RADII IN THE BACKFILL ON A TRANSVERSE PLANE THROUGH THE CENTRE OF A VITRIFIED REPROCESSING WASTE PACKAGE

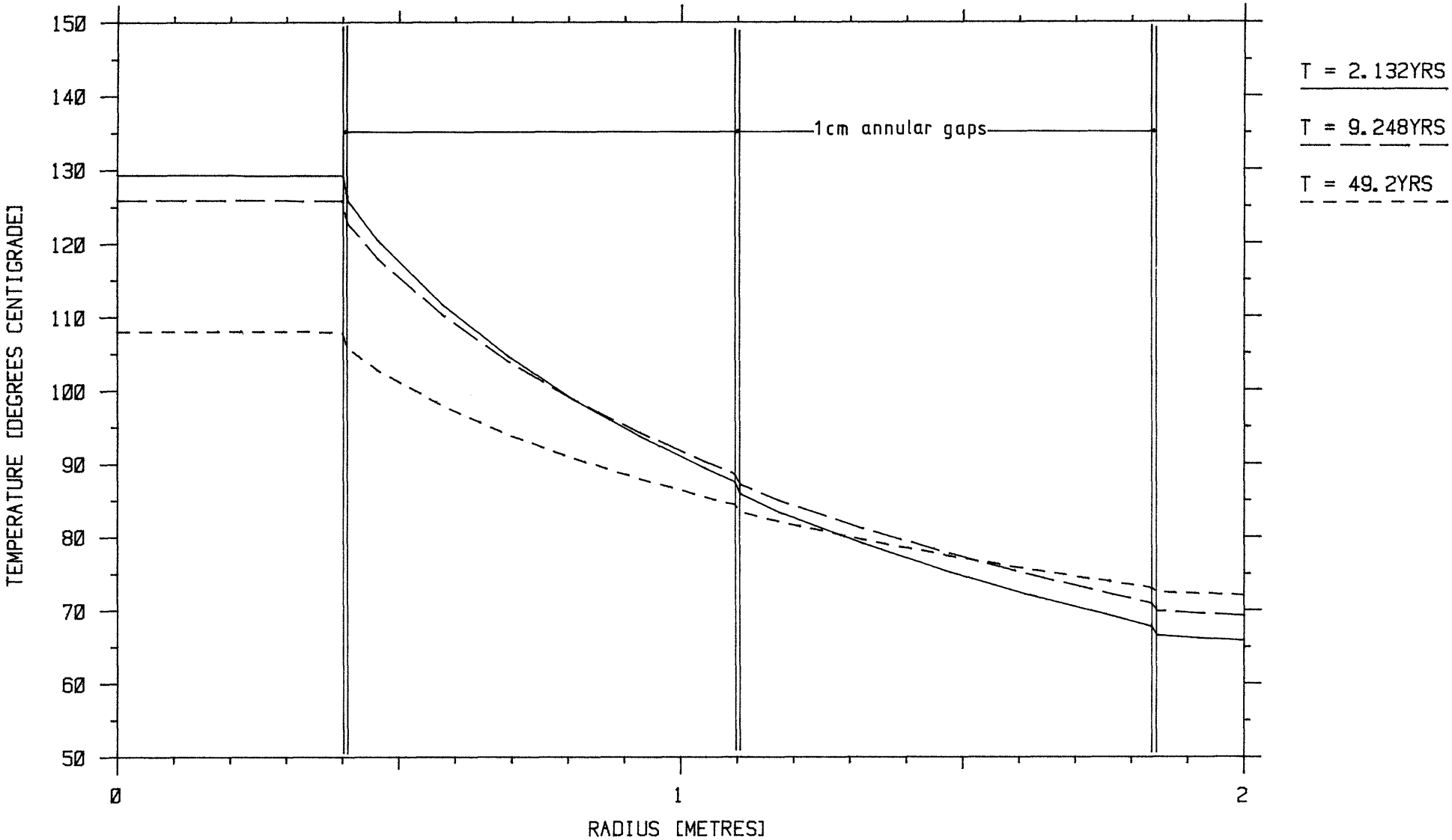

FIGURE 2.12: RADIAL TEMPERATURE PROFILES ON A TRANSVERSE PLANE THROUGH THE CENTRE OF A PACKAGE OF SPENT FUEL ELEMENTS - 10M AXIAL STORAGE PITCH

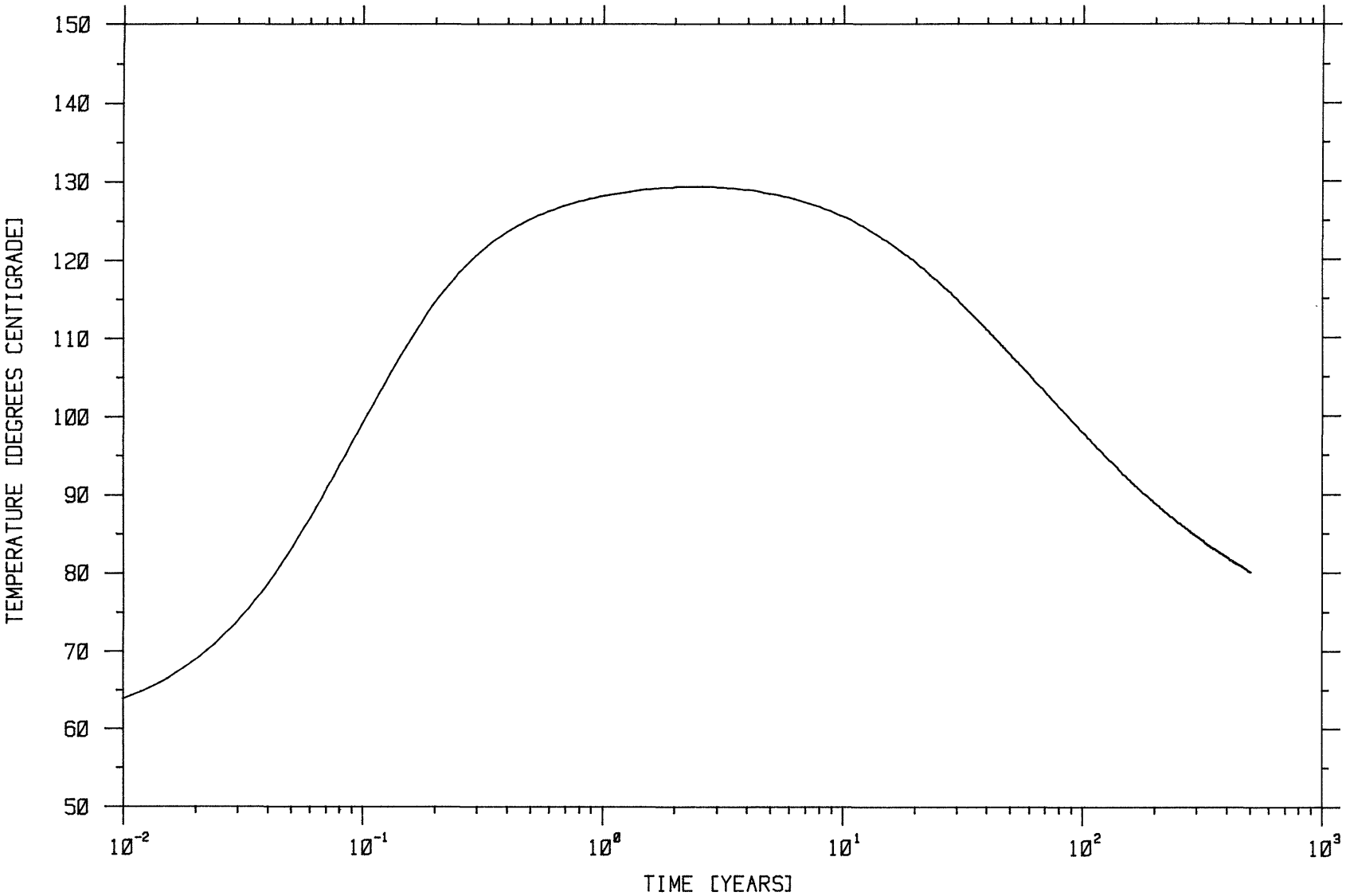

FIGURE 2.13: TEMPERATURE TIME HISTORY: CENTRE OF SPENT FUEL ELEMENT PACKAGE AT 10M AXIAL STORAGE SITE PITCH

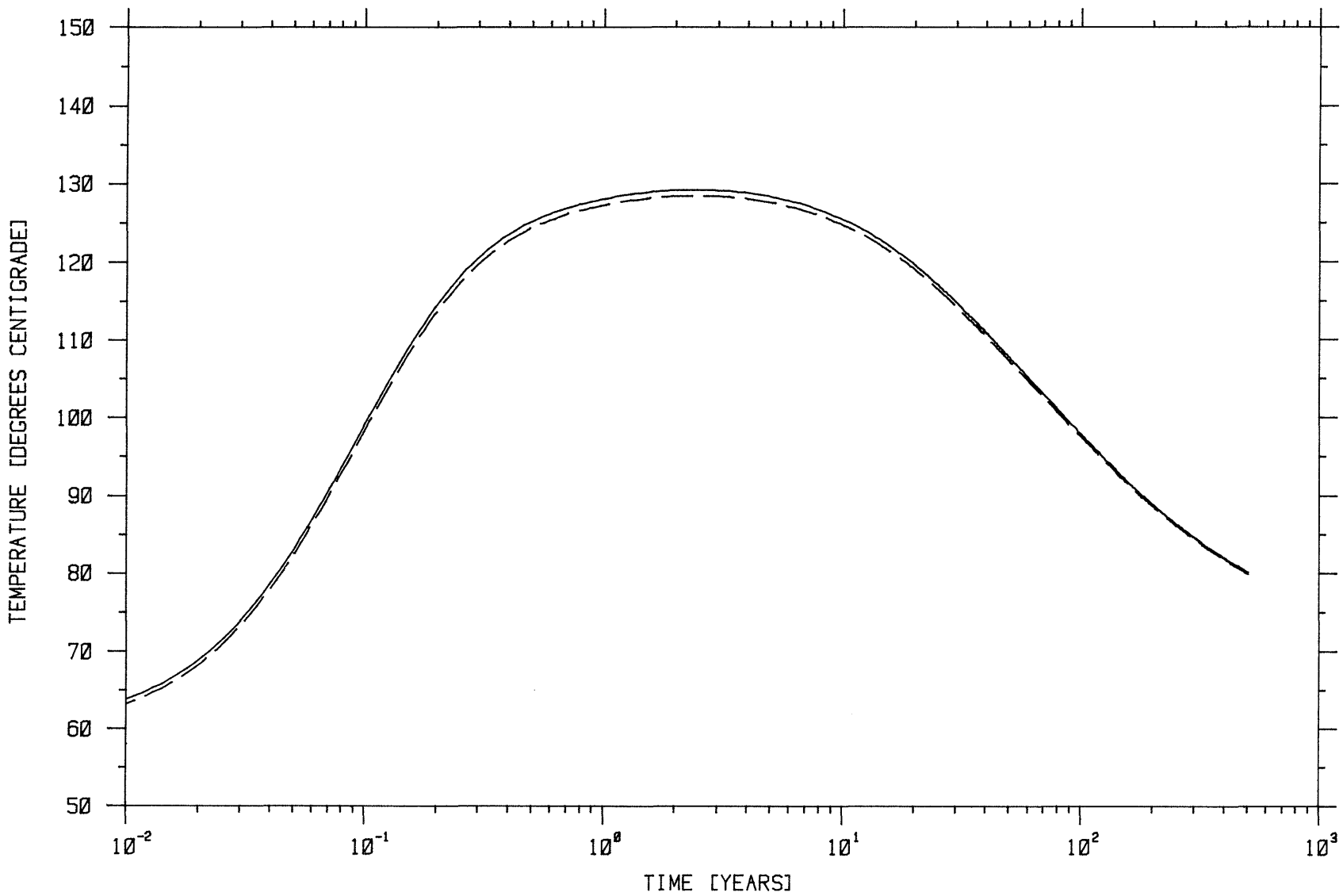

FIGURE 2.14: TEMPERATURE TIME HISTORIES: HOTTEST AND COLDEST POINTS IN THE COPPER OVERPACK FOR 10M AXIAL STORAGE SITE PITCH

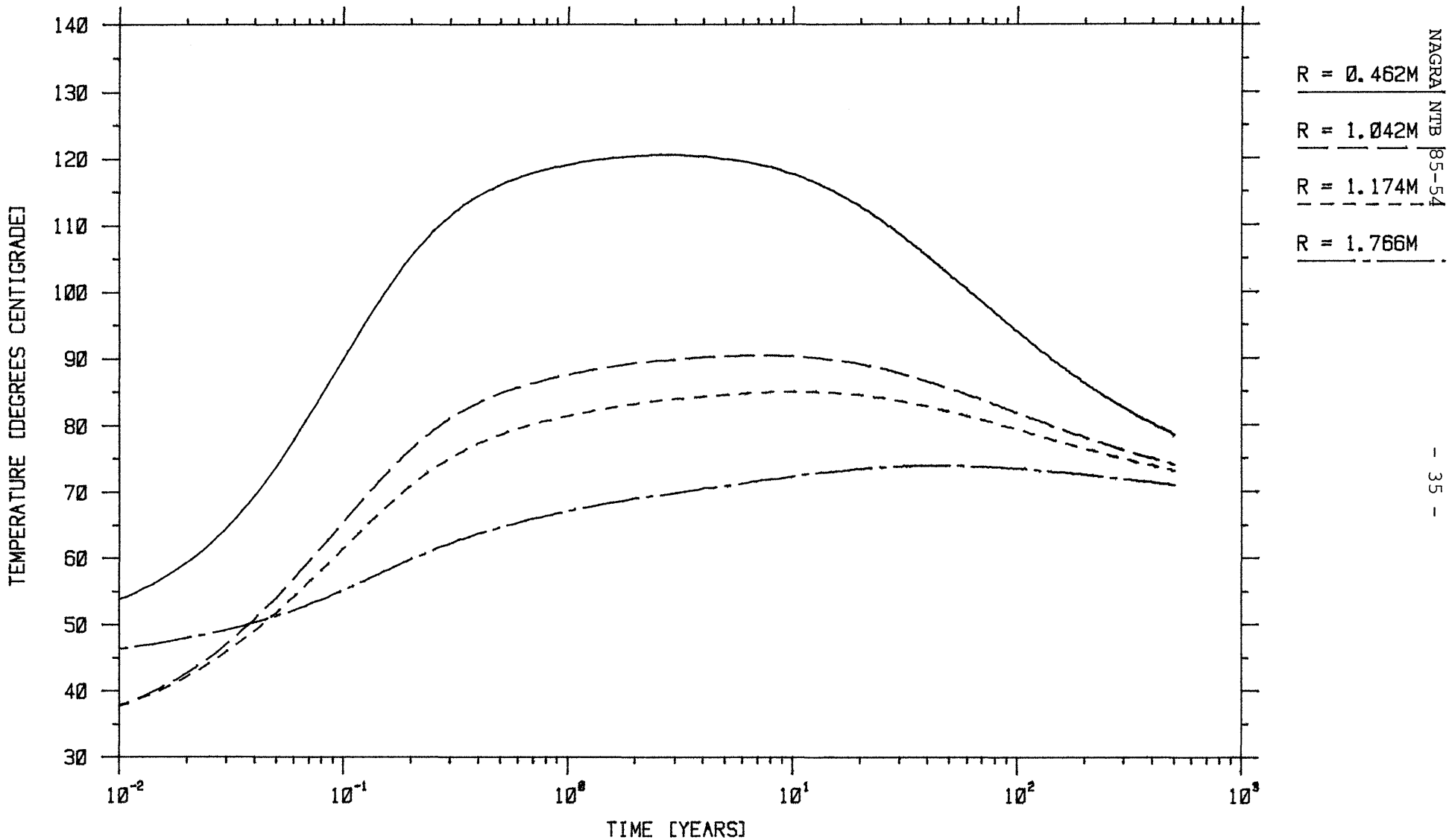

FIGURE 2.15: TEMPERATURE TIME HISTORIES: AT VARIOUS RADII IN THE BACKFILL ON A TRANSVERSE PLANE THROUGH THE CENTRE OF A SPENT FUEL PACKAGE - 10M AXIAL STORAGE PITCH

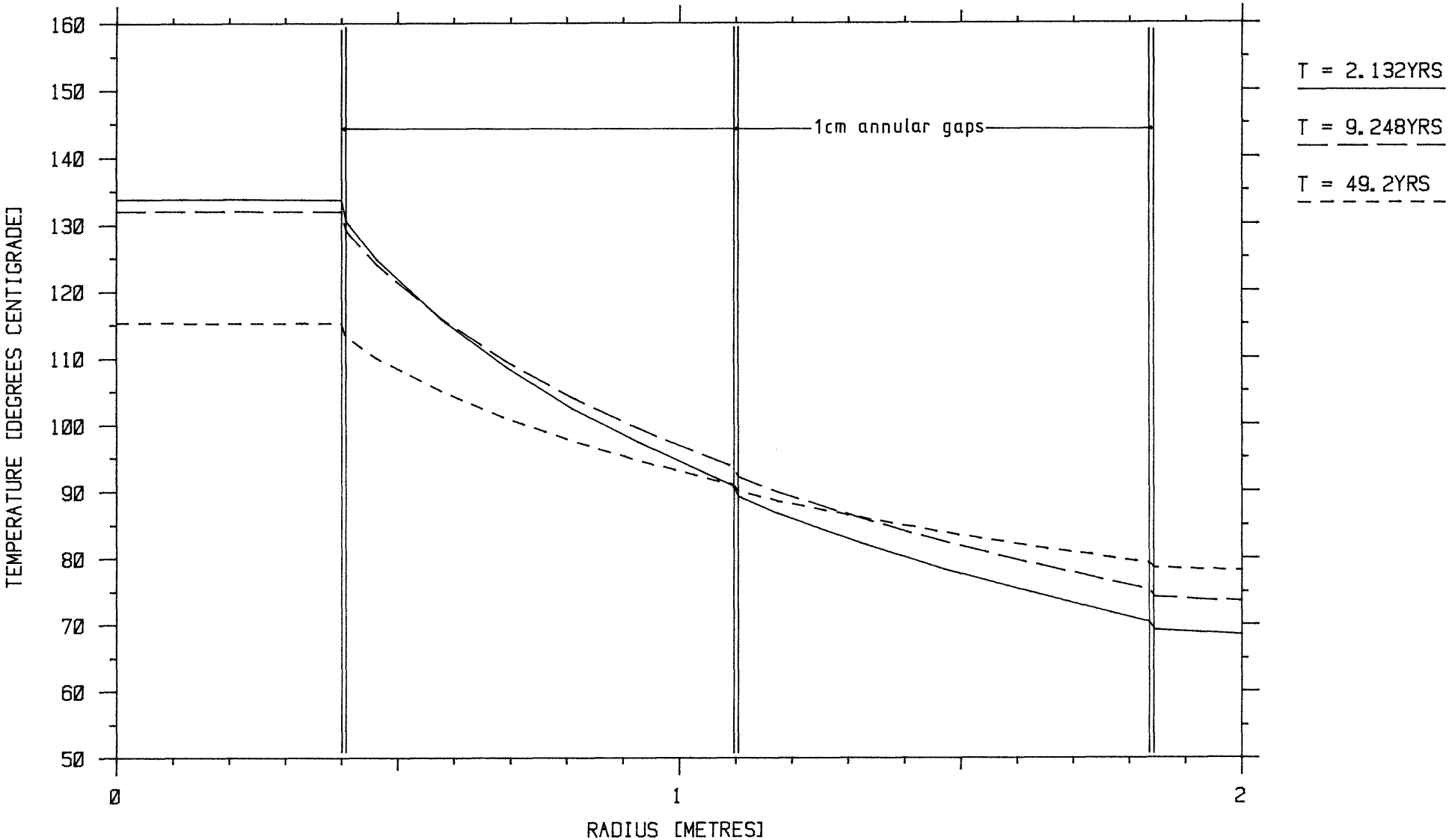

FIGURE 2.16: RADIAL TEMPERATURE PROFILES ON A TRANSVERSE PLANE THROUGH THE CENTRE OF A PACKAGE OF SPENT FUEL ELEMENTS - 7M AXIAL STORAGE PITCH

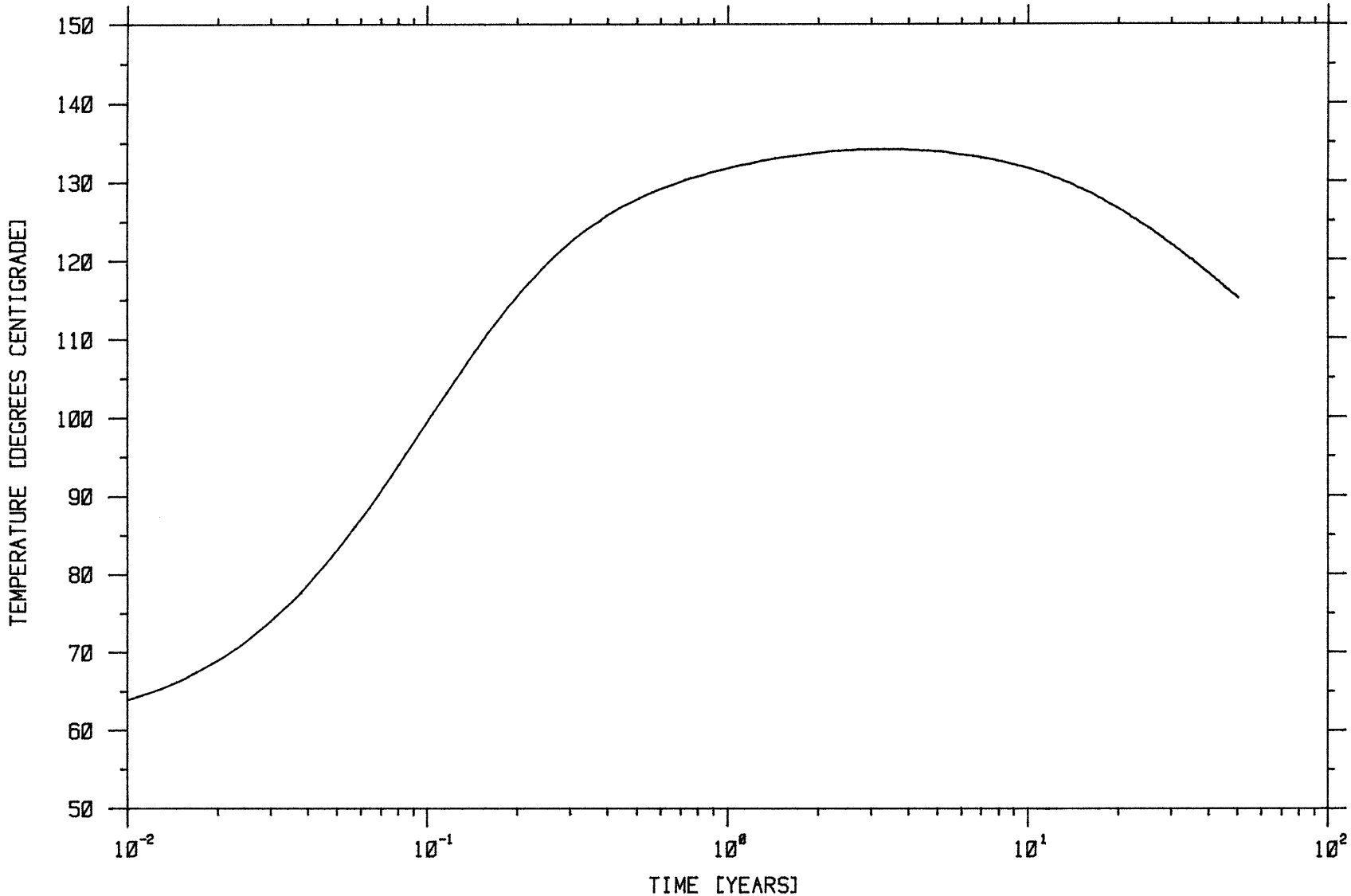

FIGURE 2.17: TEMPERATURE TIME HISTORY: CENTRE OF SPENT FUEL ELEMENT PACKAGE AT 7M AXIAL STORAGE SITE PITCH

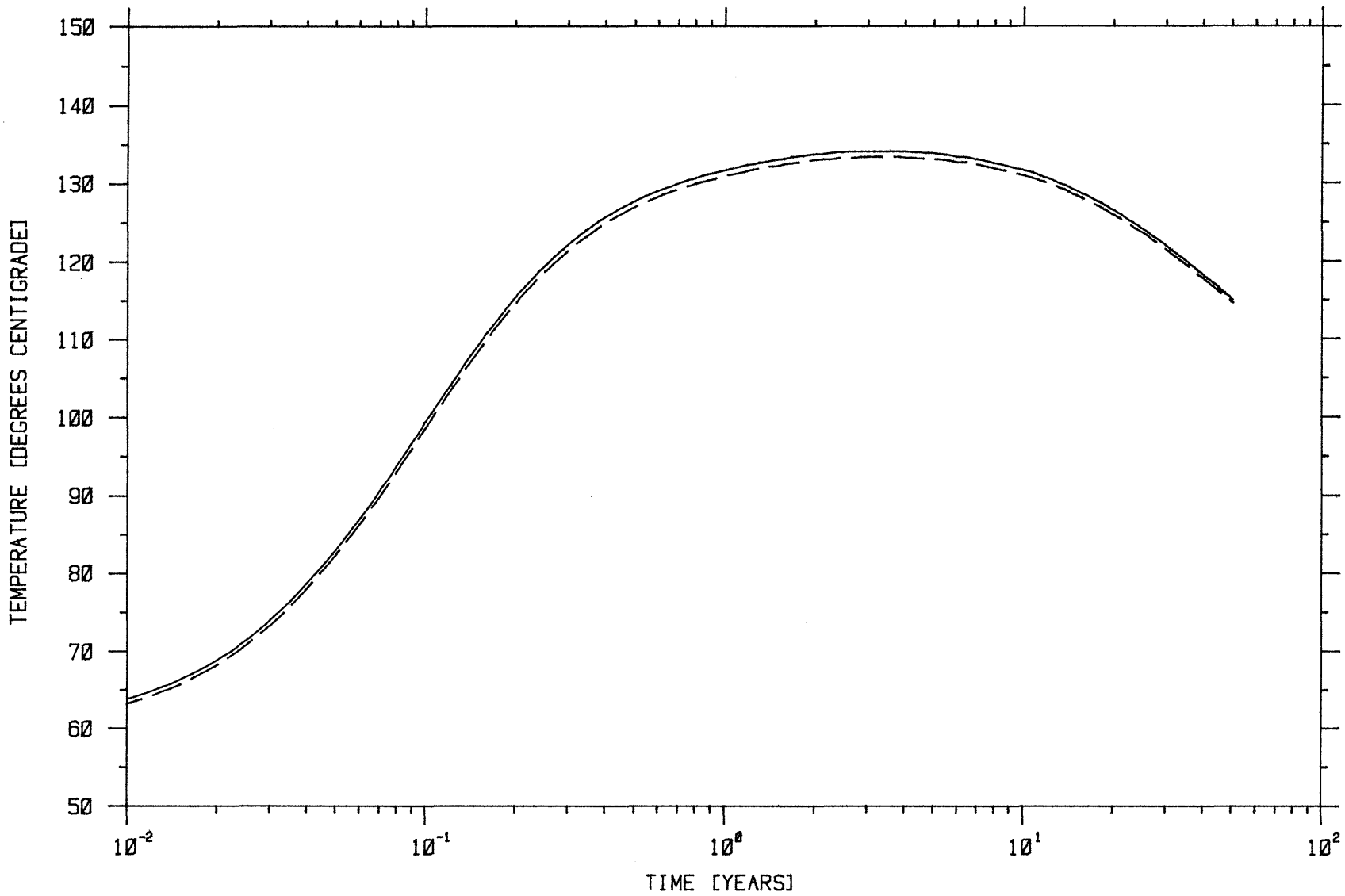

FIGURE 2.18: TEMPERATURE TIME HISTORIES: HOTTEST AND COLDEST POINTS IN THE COPPER OVERPACK FOR 7M AXIAL STORAGE SITE PITCH

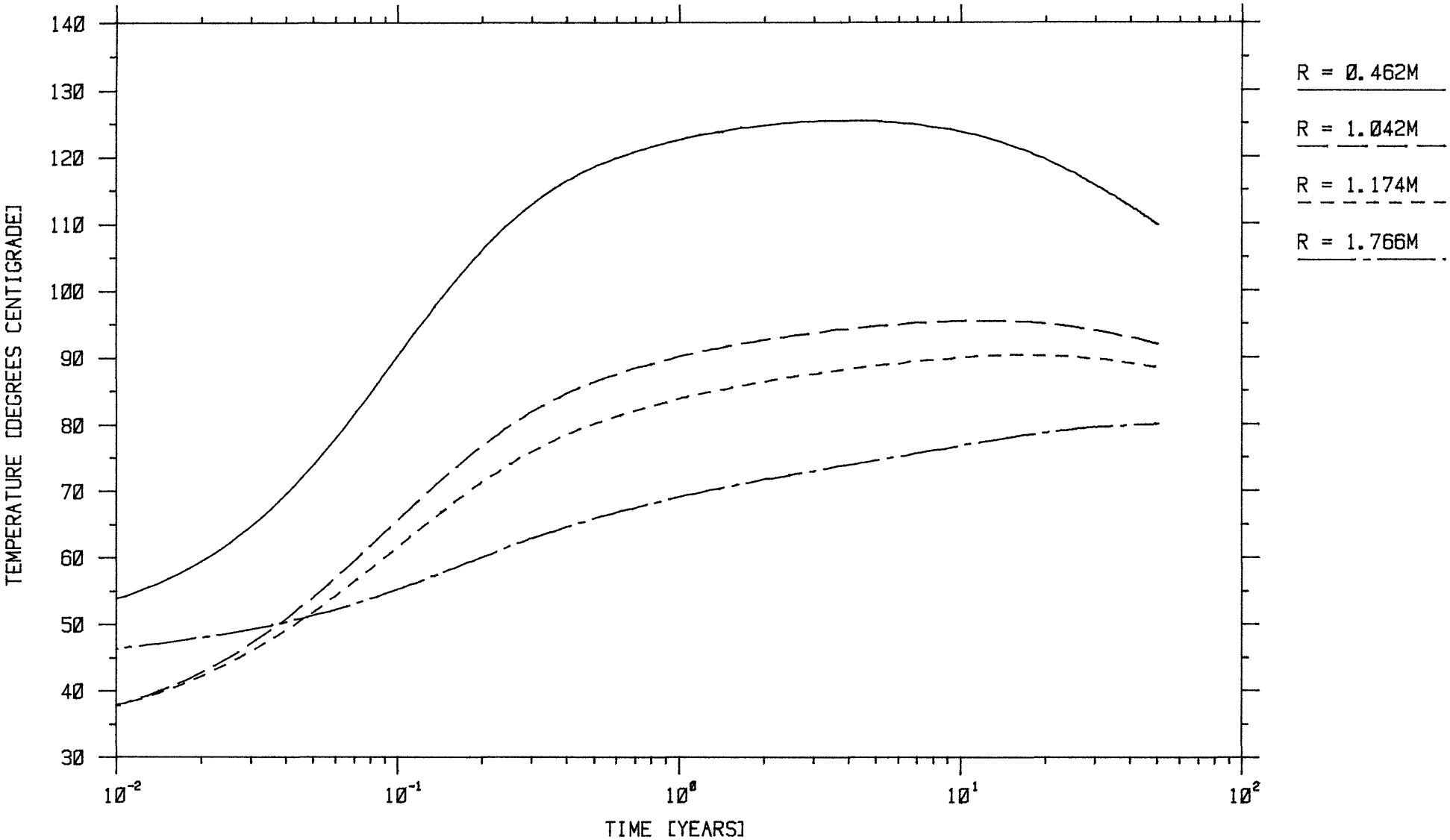

FIGURE 2.19: TEMPERATURE TIME HISTORIES: AT VARIOUS RADII IN THE BACKFILL ON A TRANSVERSE PLANE THROUGH THE CENTRE OF A SPENT FUEL PACKAGE - 7M AXIAL STORAGE PITCH

3. INTERMEDIATE LEVEL WASTE IN TYPE C REPOSITORY

3.1 Geometry of the Storage Silos and Overview of the Problem

Provision is made in the concept of the NAGRA Type C repository for high level waste for the additional accommodation of certain intermediate level wastes [9]. These are to be disposed of in vertical cylindrical silos (see Figure 3.1) accessed by the same transport tunnel network as the high level waste storage tunnels at the design depth of approximately 1200 m [16].

Figure 3.2 is a vertical cross section through a storage silo demonstrating the arrangement with a free-standing, hollow concrete cylinder within the excavated cavern. The inside diameter of the concrete cylinder is 7 m, its wall thickness is 0.8 m and that of the annular gap between its outer surface and the cavern wall is 0.7 m. When a silo (i.e. a concrete cylinder) is completely filled with waste the outer annulus and all air spaces are backfilled with granulated bentonite. For the calculations it has been assumed that the outer annulus has not already been backfilled.

Also shown in Figure 3.2 is the manner of loading the silos. Waste in drums is taken from the arriving transport vehicle by the crane and lowered to fill the silo layer-by-layer. Each complete layer of drums is backfilled with liquid cement before further diposal.

Two types of waste have been examined. These are the hulls and end caps, which are packed in cement in 1100 l drums, and the co-precipitation sludges from the fuel reprocessing operation, mixed with bitumen and packed in 200 l drums. The dimensions of both drum types are given in Figure 3.3

The disposal of the bituminised waste has been considered as taking place at the earliest possible moment, which is estimated to be three years after removal of the fuel from its reactor. This was believed to

be a reasonable timescale on account of the low thermal loading of the 200 l drums, so the purpose of the analysis is to check the acceptability of the resulting temperatures.

The thermal loading of the 1100 l drums containing fuel hulls and end caps is such that a cooling period prior to disposal had to be assumed. The initial assumption was for a 40 year period (identical to that for the high level waste). The purpose of the analysis in this case was twofold: first to confirm the acceptability of the conservatively selected 40 year cooling time and secondly to examine whether indeed a shorter period would be feasible.

3.2 Additional Repository Construction Materials

Whereas for the storage tunnels for high level waste the only material to be introduced was (see Chapter 2) the bentonite backfill, the silos involve both the inner concrete structure and the special backfill cement. The properties used for these materials are listed in Table 3-1 below.

Table 3-1: Material properties used in the analysis of the intermediate waste in the storage silos [13, 14]

Material	Conductivity [$W\ m^{-1}\ K^{-1}$]	Volumetric heat capacity [$J\ m^{-3}\ K^{-1}$]
Concrete	1.0	2.6×10^6
Cement	1.0	2.2×10^6

3.3 Waste Packages

3.3.1 Hulls and End Caps (NAGRA Waste Type WA-4)

Liquid cement is used for stabilisation of the fuel hulls and end caps in the 1100 l drums shown in Figure 3.3. The drums are to be deposited in the silo, 24 to a layer. When a layer is completed it will be back-filled with cement.

Heat production in these drums as a function of time has been represented by a fifth order log-log polynomial fitted to heat release data derived from [17] and listed in Table 3-2 below.

Table 3-2: Residual heat production of the drums containing hulls and end caps (Waste Type WA-4)

Time from unloading [years]	Heat production / 1100 l drum [W]
20	18.2
25	10.2
30	6.14
40	2.82
50	1.81
100	0.84

The fitted function and the point data are compared in Figure 3.4. The material properties of the waste/cement mixture in the drums are (derived from [13, 14 and 17]):

Thermal conductivity: $1.45\ W\ m^{-1}\ K^{-1}$

Volumetric heat capacity: $2.19 \times 10^{6}\ J\ m^{-3}\ K^{-1}$

The simple geometry of the layers in the cylindrical silos has led to the use of a simple model and a one-dimensional computer code. This

implies the use of bulk properties for the highly inhomogeneous mix of backfill and waste drums within the silo. For the hulls and end caps the conservative decision has been taken to use for the bulk properties the lower values of the individual component materials for both conductivity ($1.00\ W\ m^{-1}\ K^{-1}$) and for volumetric thermal capacity ($2.19 \times 10^6\ J\ m^{-3}\ K^{-1}$).

3.3.2 Bituminised Co-Precipitation Sludges (NAGRA Waste Type WA-2)

These are filled into the 200 l drums shown in Figure 3.3. Only 3 years after the unloading of the fuel, the bituminised waste sludges in these smaller drums are scheduled to be deposited in an underground repository. The silos represent one possible solution for their disposal. The smaller 200 l drums are to be stored 92 to a layer. As in the case of the WA-4 drums (hulls and end caps), a completed layer will be backfilled with cement before any further disposal is undertaken.

Heat production as a function of time has been represented by a log-log polynomial of fourth order fitted to heat release data derived from [17]. The point data are listed in Table 3-3 below and are compared with the fitted function in Figure 3.5.

Table 3-3: Residual heat production of the drums of bituminised co-precipitation sludges (Waste Type WA-2).

Time from unloading [years]	Heat production / 200 l drum [W]
3	0.79
4	0.47
6	0.22
10	0.13
15	0.108
20	0.098
25	0.091

The bitumen/waste mixture in the drums has the following properties (see 19):

Thermal conductivity:	$0.26\ W\ m^{-1}\ K^{-1}$
Volumetric heat capacity:	$2.2 \times 10^{6}\ J\ m^{-3}\ K^{-1}$

Although on the scale of the silo diameter the inhomogeneity is smaller in this case than in that of the hulls and end caps because of the smaller drum size and heat release rates, a similar type of conservatism in material properties has been first considered here. This comprises the assumption of bulk thermal material properties as the lower of the individual material conductivities ($0.26\ W\ m^{-1}\ K^{-1}$). Data for the volumetric heat capacity are identical for both backfill and waste.

In order to treat an alternative situation, a higher conductivity value based upon the wellknown relationship:

$$k_{ave} = k_1^{\varepsilon_1}\ k_2^{\varepsilon_2} \qquad (3.1)$$

(see [15] for example) for homogeneously mixed materials of different thermal conductivities k and volume fractions ε in the mixture has been used. This offers a lower degree of conservatism, but is felt to be justifiable on account of the large number of drums of the 200 l size which are accommodated per layer in the silo. The packing density of 92 drums per layer gives in this case:

$$k_{ave} = 0.42\ W\ m^{-1}\ K^{-1}$$

3.4 Method of Analysis

3.4.1 Problem Domain, Initial and Boundary Conditions

The layerwise filling of the cylindrical silos and the requirement for a conservative model has led to calculations being made for a one-dimen-

sional radial (cylindrical) domain representing one layer of waste drums. A one radian sector of such a layer is modelled with the help of the TRAD-1D code, which is a version of the MC.TRAD-2D code [20]. Figure 3.6 is a sketch of this model domain. The upper and lower surfaces of the disc sector are zero flux boundaries as a result of assuming axial invariance. This assumption is not only simplifying in that it reduces the problem to that of a single layer of drums, it is also conservative in that the net loss of heat in the axial direction from the central (hottest) region is inhibited. In reality, natural convection cells can be expected to be formed in the hollow cylindrical air space above the deposited drums. Additionally, heat will be transferred by radiation.

The outer boundary of the model domain at a radius of 50 m, which remains unperturbed during the period of transient under study and is assigned the fixed temperature of 55 °C. This temperature level conforms to the assumption of host rock temperature at Type C repository depth used in Chapter 2. Any interaction between neighbouring silos is neglected. This is a reasonable assumption because of the total energy release possible (see Figures 3.4 and 3.5) and the short duration of the temperature peak (Figures 3.7 and 3.8).

The initial condition within the silo is assumed to be 35 °C, that is to say, slightly above the air temperature allowed as a working environment.

3.4.2 Processes Treated

Heat is transferred by conduction in all solid materials shown in Figure 3.6. However, in the air gap between the outer wall of the concrete silo and the rock wall of the cavern both natural convection and radiation have to be considered during the period prior to backfilling. Because of the aspect ratio of this gap (axial length over 40 m, radial aperture 0.7 m) and the fact that end effects at top and bottom of the cavity are ignored, these processes may be represented well by simple relationships.

The natural convection has been modelled by use of the effective thermal conductivity k_{eff} of the air in the gap, derived from the relationships first developed by Kraussold [21] and discussed by Eckert and Drake [13]. The effective conductivity (an augmented value) is expressed as a function of the Rayleigh Number based upon the gap's width and upon the surface temperature difference across it:

For $Ra \leqq 1841$:

$$k_{eff} = k \qquad \text{(pure molecular thermal conduction)} \qquad (3.2a)$$

For $1841 < Ra \leqq 10^6$:

$$k_{eff} = k \left(\frac{Ra}{1841}\right)^{0.285} \qquad \text{(laminar convection)} \qquad (3.2b)$$

For $Ra > 10^6$;

$$k_{eff} = k \left(\frac{Ra}{100}\right)^{0.2} \qquad \text{(turbulent convection)} \qquad (3.2c)$$

The nomenclature of the Rayleigh Number is explained in Section 4.4.1 in connection with the repository for low and medium level waste. Because of the wide variation in temperature differences during the transient the Rayleigh Number varies over a very broad range.

Radiation transfer across the air gap has been calculated for unit axial length of silo and for the 1 radian sector of the domain shown in Figure 3.6 by the approximate relationship:

$$\dot{q}'_{i \to o} \cong r_i \, \eta \, \sigma \, (T_i^4 - T_o^4) \qquad (3.3)$$

which is effectively a simplified version of equation (2.6).

where:

η Net effective emissivity of the silo outer wall [-]

r Radius [m]

σ Stefan-Boltzmann constant [W m^{-2} K^{-4}]

T Surface temperature [K]

i Inner surface of gap (concrete)

o Outer surface of gap (rock)

In the present case the nature of the surface of the rock walls cannot be specified precisely. Thus, the use of a more refined radiation exchange expression is not justified. The insensitivity of the central temperature to the surface properties of the materials adjacent to an air gap is demonstrated in Appendix 2. The net emissivity η, which may be thought of as the product of emissivity and absorptivity, has been given a value of 0.5 for the silo calculations. This is based upon values for the emissivity of concrete of around 0.7. It will be noted that use of equation 3.3 as compared with 2.6 for the particular geometry and properties of the concrete silo results in a slightly lower radiative transmission coefficient (89.9 %) and therefore represents a conservative approach.

3.5 Results

3.5.1 Hulls and End Caps

The temperature at the centre of a deposited layer has been calculated over 10 years for a number of alternative pre-cooling periods prior to disposal. Temperature time histories on the vertical axis of the waste corresponding to each of the cooling periods considered are plotted in Figure 3.7. In addition, Table 3-4 lists the maximum temperatures reached in each case.

Table 3-4: Maximum temperatures and their times of occurrence at the centre of a silo loaded with hulls and end caps (NAGRA Waste Type WA-4, 1100 l drums)

Intermediate storage time [yrs]	Max. temp. at silo centre [°C]	Time of maximum after disposal [yrs]
20	91.0	2.34
25	75.4	2.70
30	67.3	3.24
40	61.1	5.80

It may be concluded from the table that the intermediate storage period for the hulls and end caps may be reduced from the originally proposed period of 40 years to 20 years without any portion of the waste reaching a temperature of 100 °C. This temperature level is frequently used as a design limit in concrete constructions in order to avoid damage by excess pore water pressures.

3.5.2 Bituminised Co-Precipitation Sludges

The results of the calculations of temperatures at the centre of the silo for the NAGRA WA-2 waste drums are presented in Figure 3.8 with the two alternative assumed values of the bulk average thermal conductivity of the waste/backfill layer discussed in Section 3.3.2. The effect of the conductivity is seen quite clearly here. A conductivity of 0.42 $W\ m^{-1}\ K^{-1}$ leads to a temperature peak of 64.8 °C against 67.9 °C with conductivity of 0.26 $W\ m^{-1}\ K^{-1}$. The bituminised waste starts to soften (see [19]) at around 90 °C. Thus, in neither of the two assured conductivity cases would there be any danger of softening.

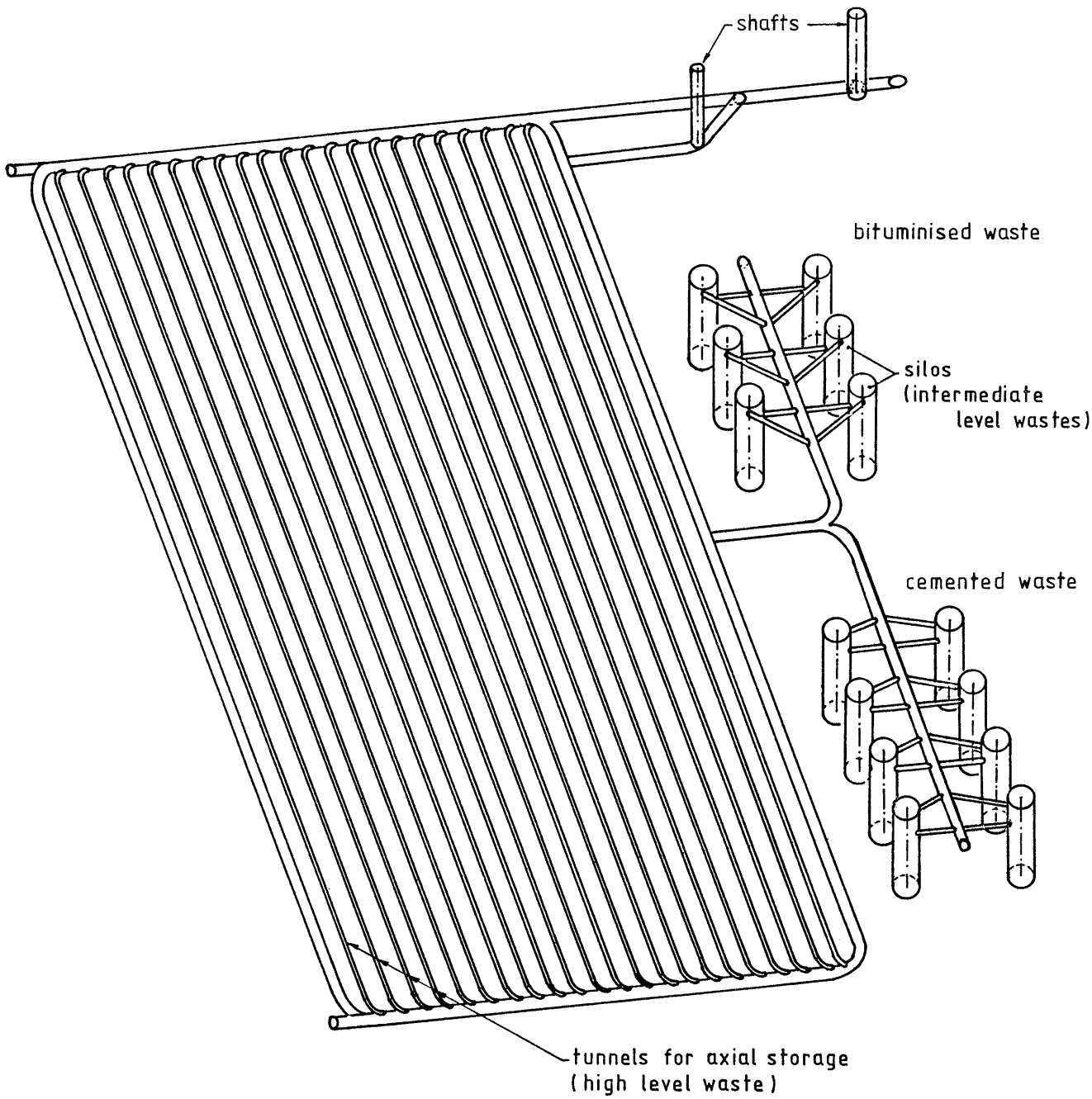

FIGURE 3.1: POSSIBLE ARRANGEMENT OF THE EXCAVATIONS FOR A REPOSITORY FOR HIGH LEVEL WASTE SHOWING TUNNEL AND SILO STORAGE REGIONS

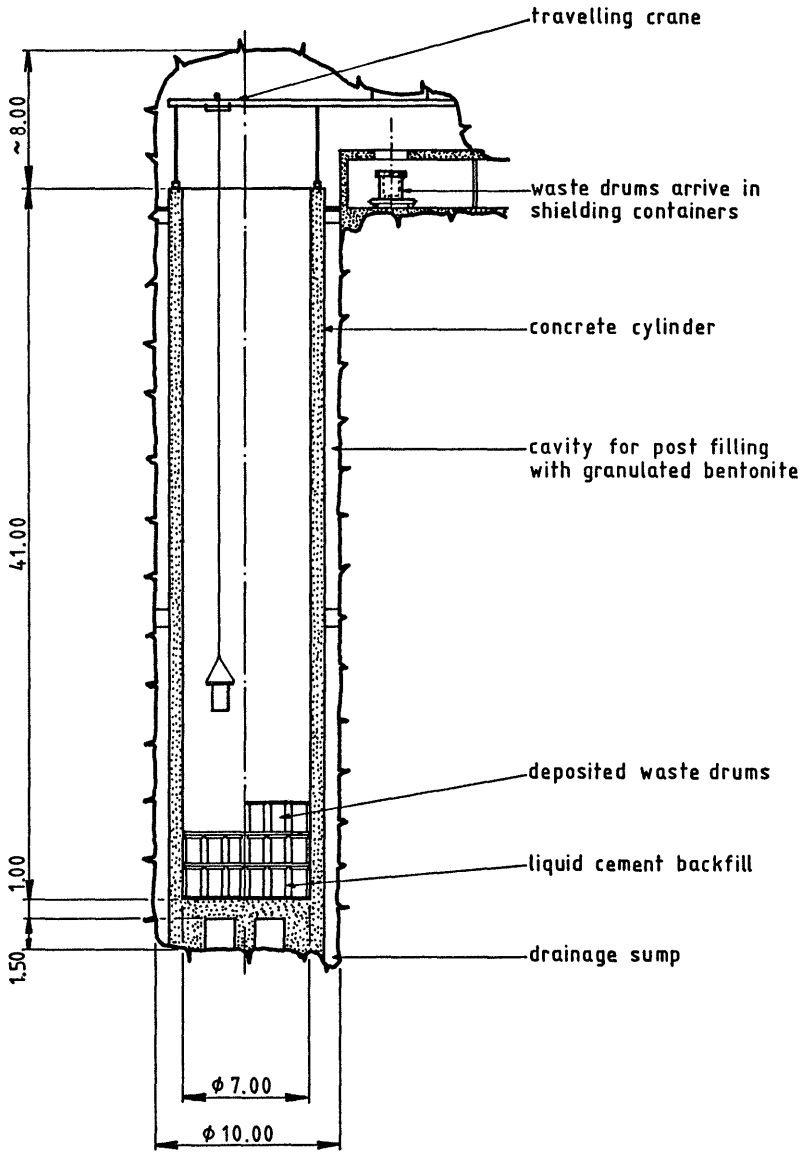

FIGURE 3.2: CROSS - SECTION OF AN INTERMEDIATE LEVEL WASTE STORAGE SILO IN THE TYPE C REPOSITORY

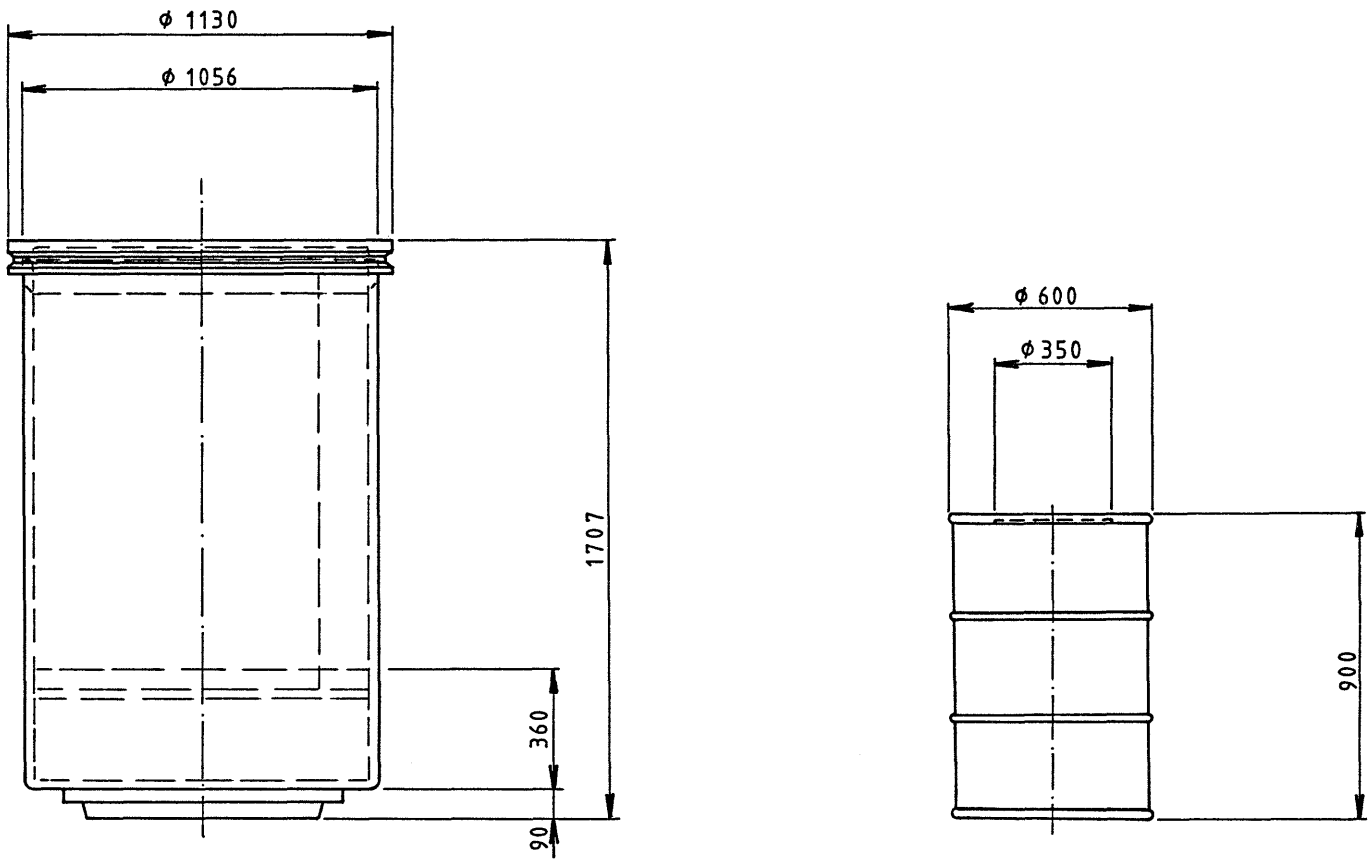

1100 l drum for hulls and end caps

200 l drum for bituminised waste sludges

FIGURE 3.3: DIMENSIONS OF THE DRUMS FOR INTERMEDIATE LEVEL WASTES

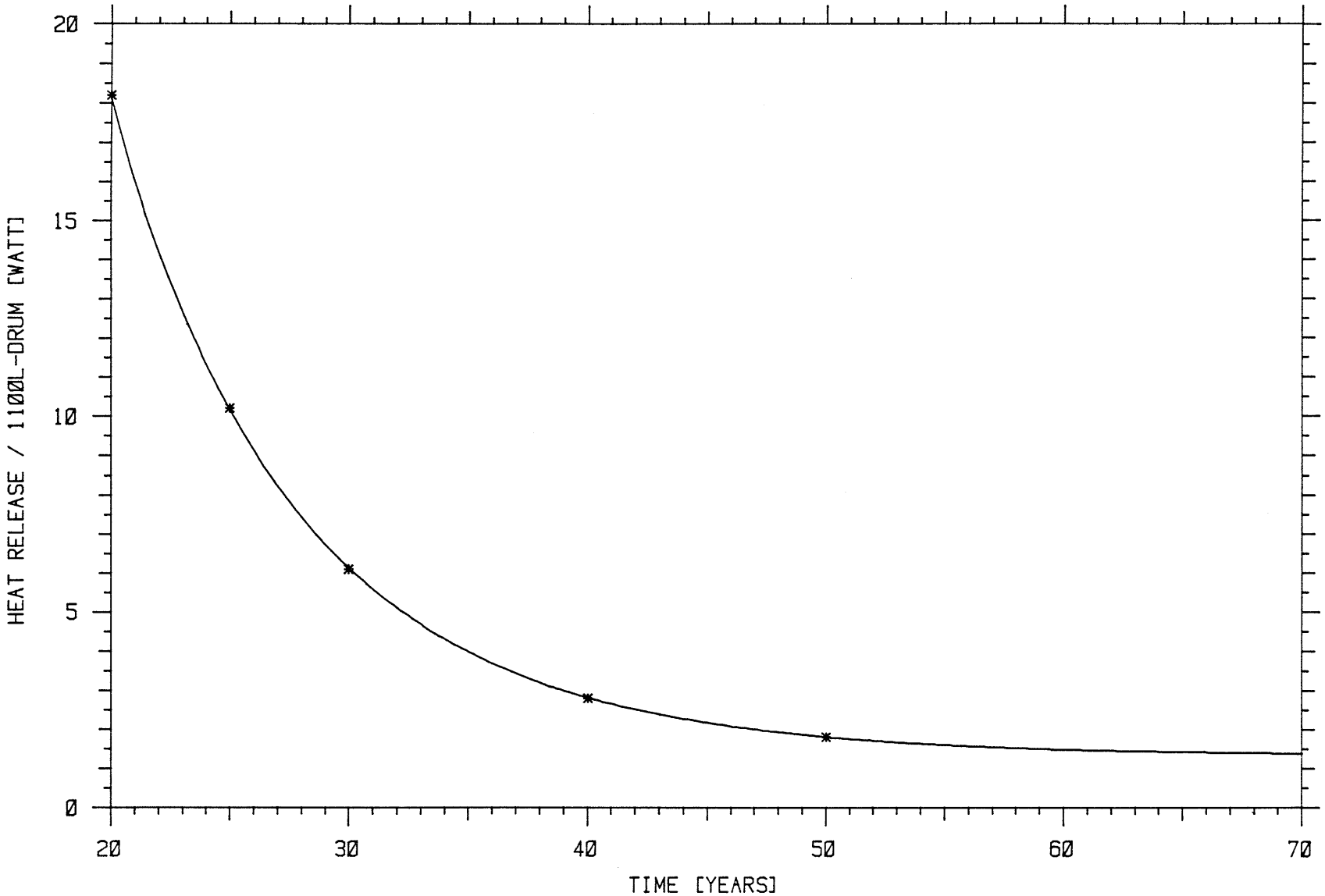

FIGURE 3.4: HEAT RELEASE RATES FROM 1100L DRUMS OF CEMENT STABILISED FUEL HULLS AND END CAPS AT DISCRETE TIMES AFTER UNLOADING FROM THE REACTOR COMPARED WITH THE FITTED FUNCTION USED IN THE ANALYSIS

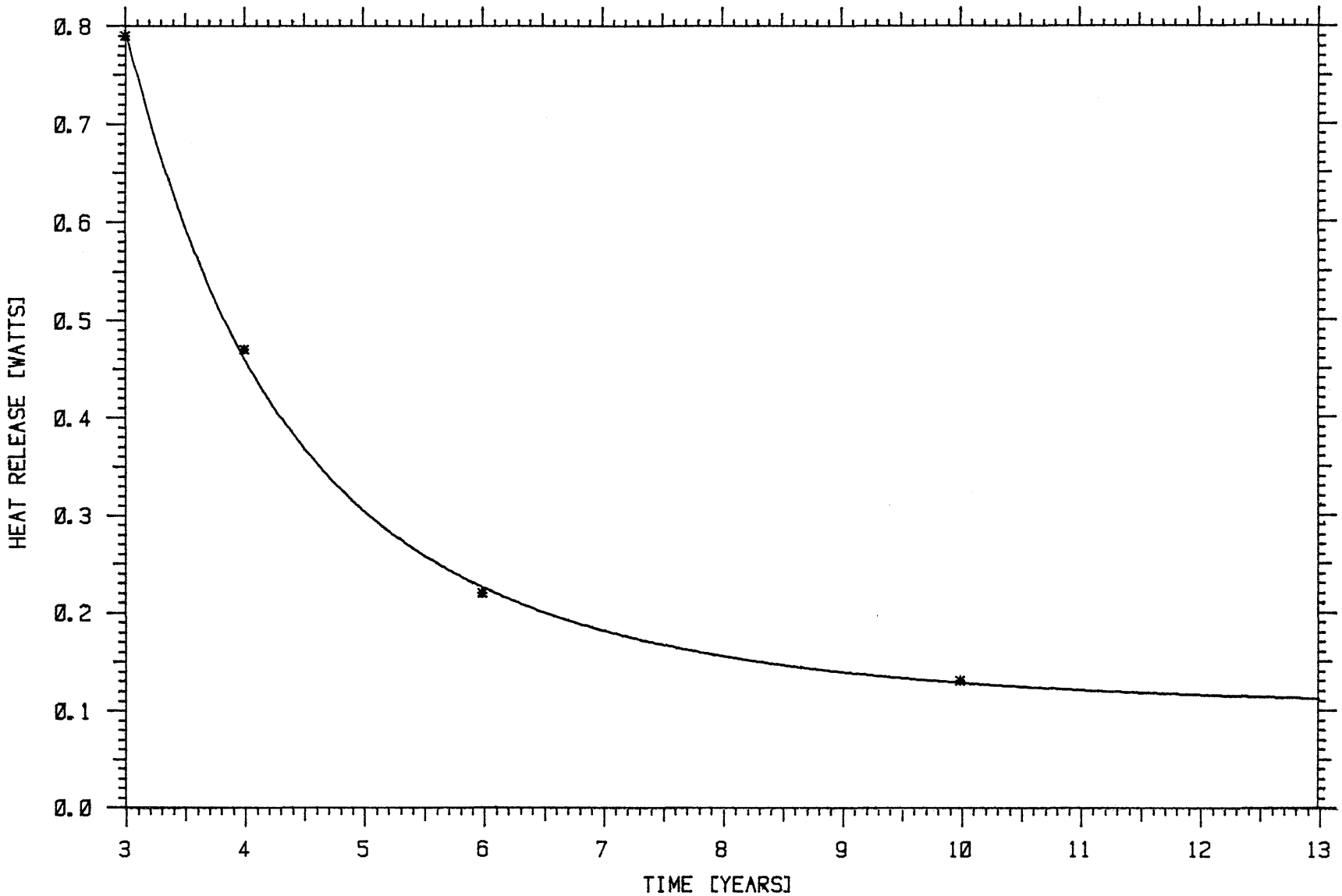

FIGURE 3.5: HEAT RELEASE RATES FROM 200L DRUMS OF BITUMINISED COPRECIPITATION SLUDGES AT DISCRETE TIMES AFTER UNLOADING FROM THE REACTOR COMPARED WITH THE FITTED FUNCTION USED IN THE ANALYSIS

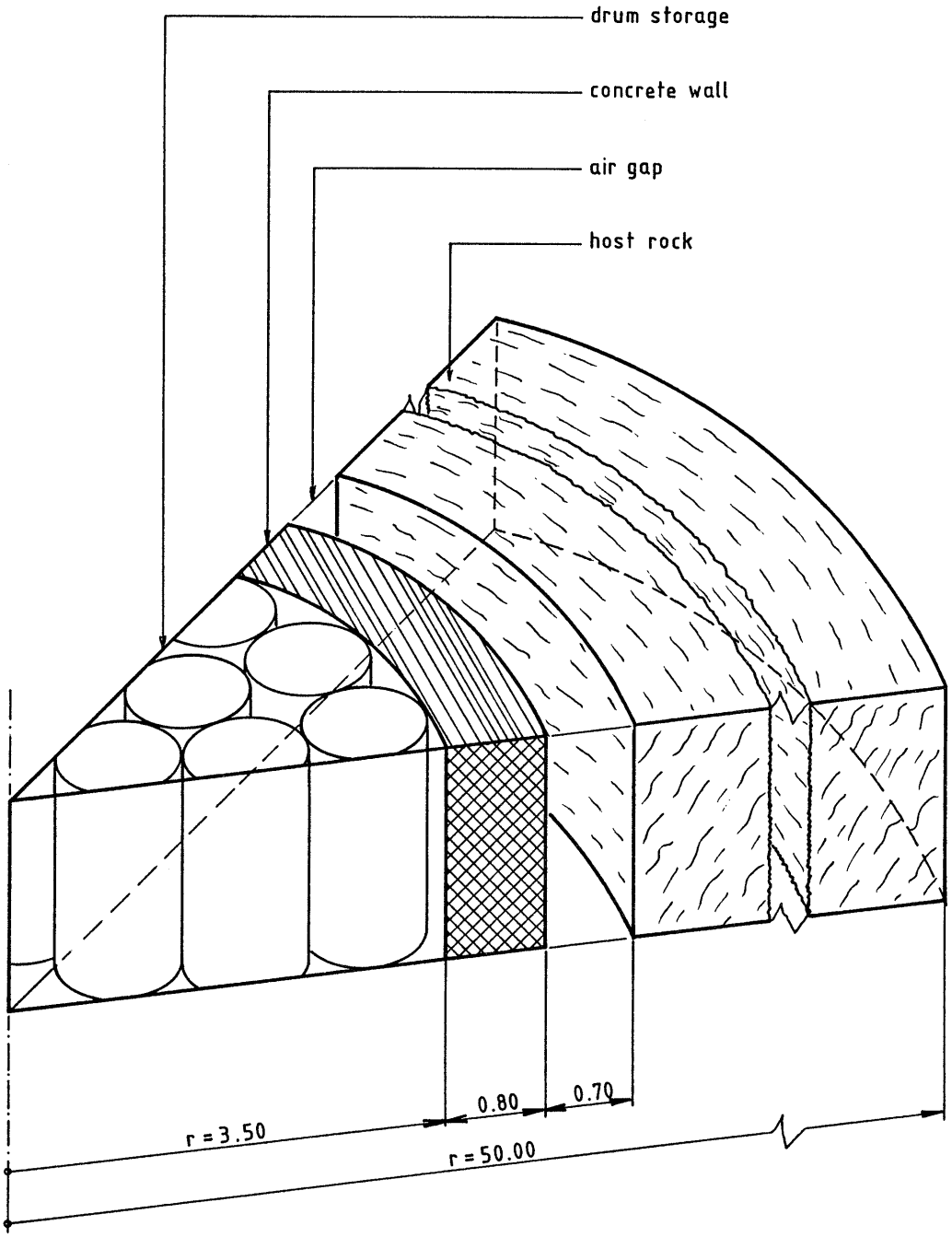

FIGURE 3.6: MODEL DOMAIN FOR THE STUDY OF DRUM STORAGE IN SILOS

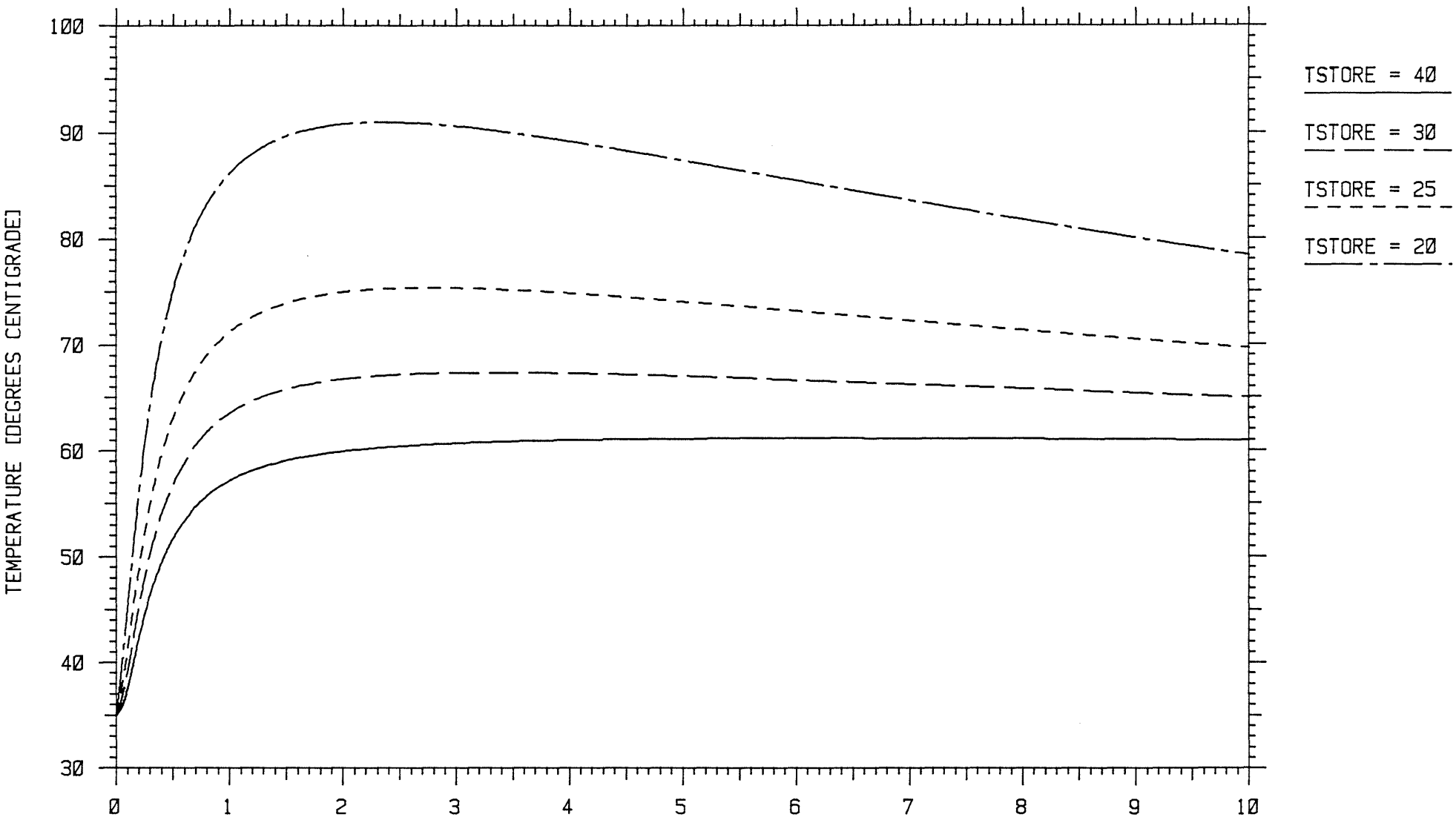

FIGURE 3.7: TEMPERATURE DEVELOPMENT AT THE CENTRE OF A SILO LOADED WITH 1100L DRUMS CONTAINING FUEL HULLS AND END CAPS - EFFECT OF DIFFERENT COOLING PERIODS (TSTORE [YR])

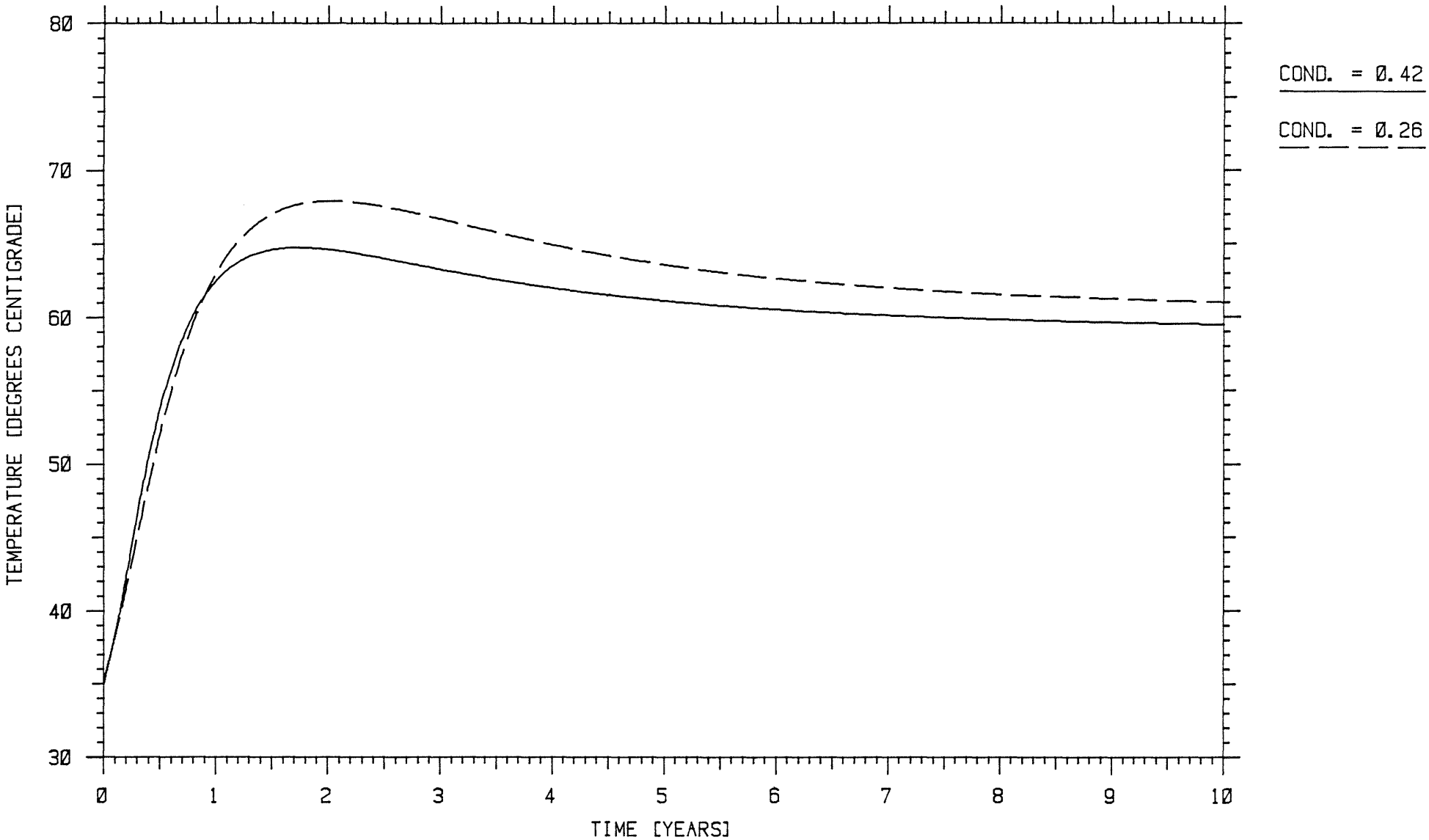

FIGURE 3.8: TEMPERATURE DEVELOPMENT AT THE CENTRE OF A SILO LOADED WITH 200L DRUMS CONTAINING BITUMINISED COPRECIPITATION SLUDGES - EFFECT OF THE AVERAGE BULK THERMAL CONDUCTIVITY, COND. [W/MK], ASSUMED WITHIN THE SILO

4. HEAT PRODUCING WASTE IN THE TYPE B REPOSITORY

4.1 Geometry of the Storage Caverns and Overview of the Problem

The design of the repository for low and intermediate level waste comprises a central access gallery, from both sides of which storage caverns of cross-sections similar to that shown in Figure 4.1 are excavated. These caverns are to be exploited for storage in discrete stages. During each such stage a length of approximately 50 metres of cavern is filled with standard waste containers, walled off and backfilled with liquid cement. Figure 4.2 shows a vertical axial section through such a cavern interval, showing the filling sequence (see also [18]).

All waste types are packed into the standard rectangular concrete containers for disposal. (Figures 4.1 and 4.2). Two types in particular have been considered in the present study:

- Co-precipitation sludges, stabilized in bitumen in 200 l steel drums, which are packed into the standard containers, 42 to a container, in a liquid cement backfill.

- Power plant decommissioning waste, cut up and mixed directly with concrete for stabilisation in the standard containers.

Figure 4.3 shows one of these containers. The steel drums, nominally of 200 l capacity, are identical to those described in Chapter 3.

At present a detailed filling schedule for this repository is not available, although the sequence of operations follows that shown in Figure 4.2. For the calculations presented in this chapter a tunnel interval has been assumed to be filled with only one waste type. A specification of the thermal loading of the bituminised co-precipitation sludge drums is available [9], [17]. For this waste type the acceptability from a thermal standpoint of storage in the type B repository has been examined as a possible alternative to disposal in the silos in the deeper

high level waste repository (Chapter 3). The aim of the study for the decommissioning waste is to establish an acceptable volumetric thermal loading density, which does not put the integrity of the waste packages at risk.

4.2 Repository Materials

Final selection of a site for NAGRA's proposed Type B repository can only be made after extensive investigations in a variety of geologic formations. For the present calculations, therefore, no specific host rock has been selected, but rather a set of slightly unfavourable thermal properties chosen. As apparent from Figures 4.1 and 4.7 the storage cavern is lined with concrete. Backfill material is a special liquid cement. The thermal properties used for these three materials are listed below.

Table 4-1: Materials considered for the repository for low and intermediate level waste (see also Chapter 3).

Material	Conductivity [W m^{-1} K^{-1}]	Volumetric heat capacity [J m^{-3} K^{-1}]
Host Rock	2.0	3.0×10^6
Concrete	1.0	2.6×10^6
Cement	1.0	2.2×10^6

4.3 Waste Packages

4.3.1 Bituminised Co-Precipitation Sludges (NAGRA Waste Type WA-2)

Co-precipitation sludges are mixed with bitumen and filled into 200 l drums of 0.57 m diameter and 0.9 m height (see Chapter 3, Figure 3.3).

Three years after fuel unloading, these are placed in the standard concrete containers of 4.78 m x 2.18 m x 2.08 m in two layers, each consisting of 21 drums in a 3 x 7 array. The container is then backfilled with liquid cement.

Heat production as a function of time for the individual drums has been presented already in Chapter 3, Section 3.3.2. The heat release time history is repeated here for convenience in identical form to that of Chapter 3 in Table 4-2 below and in Figure 4.4.

Table 4-2: Residual heat production of the drums of bituminised co-precipitation sludges (Waste Type WA-2) [17].

Time from unloading [years]	Heat production / 200 l drum [W]
3	0.79
4	0.47
6	0.22
10	0.13
15	0.108
20	0.098
25	0.091

The bitumen/waste mixture in the drums has the following properties [19]:

Thermal conductivity: $0.26\ W\ m^{-1}\ K^{-1}$
Volumetric heat capacity: $2.2 \times 10^{6}\ J\ m^{-3}\ K^{-1}$

The discrepancy in thermal conductivity between this material and the cement backfill, coupled with the close packing of the cylindrical drums (see Figure 4.3), implies that the packed waste containers will exhibit anisotropic bulk conductivity. In the vertical direction, heat conduction is by parallel paths of lower and higher conductivity, whereas in the horizontal direction the drums, nearly touching each other, form low conductivity barriers. Heat is produced within the drums only.

This fact together with the anisotropic bulk conductivity, accentuates the inhomogeneity of the temperature field.

Precalculations have been carried out to determine the effects of the inhomogeneity and anisotropic geometry within the concrete containers. These have been made with the MC.TRAD-2D computer code [20] used for all 2-dimensional calculations described in the present report. It was found that the approximately 10 cm thick container walls were sufficient to equalise temperature on the outside surfaces, so that bulk conductivities could be used for the subsequent thermal load analyses. The thermal properties yielded by the prestudy are:

- Vertical thermal conductivity: $0.531\ W\ m^{-1}\ K^{-1}$
- Horizontal thermal conductivity: $0.469\ W\ m^{-1}\ K^{-1}$
- Volumetric heat capacity: $2.285 \times 10^{6}\ J\ m^{-3}\ K^{-1}$

4.3.2 Decommissioning Waste

Decommissioning waste is stabilised in concrete in the standard concrete containers of 4.78 m x 2.18 m x 2.08 m. The heat release per cubic metre of concrete/waste mixture depends on the type and proportion of waste included. Mixtures with initial heat loads of 10 W/m^3 and 6 W/m^3, respectively, were considered. Because of this variation in the absolute level of heat production, the logarithm of the heat release rate as a function of time has been represented by a third order polynomial in time fitted to residual heat data derived from [17] and normalised with respect to the initial level.

Table 4-3 shows data points for the first ten-year-period. In Figure 4.5 they are compared with the fitted function. The shape of the heat production curve follows very closely the decay curve of Co-60, the dominant heat producing isotope in power plant decommissioning wastes.

Table 4-3: Normalised heat production rates of typical decommissioning waste.

Time [years]	Heat load/Initial heat load
0	1
0.1	0.98
0.2	0.96
0.5	0.93
1.0	0.87
2.0	0.76
5.0	0.48
10.0	0.24

Material parameters of the concrete and waste mixture were conservatively assumed to be those of concrete (see also Table 3-1):

Thermal conductivity: $1.0\ W\ m^{-1}\ K^{-1}$

Volumetric heat capacity: $2.6 \times 10^{6}\ J\ m^{-3}\ K^{-1}$

4.4 Method of Analysis

4.4.1 Problem Domain, Initial and Boundary Conditions

The sequence of filling the caverns determines the model domain to be studied. The filling procedure has been described in Section 4.1 and has been simplified for modelling.

The domain studied makes use of the symmetry of the storage cavern profile and is shown in Figure 4.6. The model represents a section through a cavern in the course of filling. The cavern is shown enlarged in Figure 4.7. The lowest layer of containers (layer 1) is assumed to be deposited and backfilled and then the next 3 layers stacked on top of it, all at time zero. This assumption ensures the maximum possible initial thermal loading. At a later time (up to 3 years delay has been

considered) the top layer (5) of containers is placed transversely on top of the stack and the whole cavern interval will be backfilled with liquid cement.

Implicit in the use of this two-dimensional model is the assumption of translational invariance perpendicular to the model plane. Physically, this implies that at least several of the four layer stacks of identical containers are deposited simultaneously. Such a situation is clearly rather unfavourable from the point of view of thermal loading. The treatment of a transversal slice only is also conservative in the restrictions it places upon the radiative and convective modes of heat exchange from the face, which dominates until the time of backfilling.

Further conservatisms have been introduced in the choice of initial conditions. These are:

Air, Host Rock, Backfill Cement:	35.0 °C
Filled Waste Containers:	38.5 °C

It is estimated that only at more than 600 m below ground surface will the temperature of the undisturbed host rock exceed 35 °C. This then provides a high value for the initial condition of the rock. As for the high level waste repository, ventilation of the repository excavations during construction and operation is assumed to leave the rock in the neighbourhood of the exposed tunnel and cavern walls thermally unperturbed. The air in the storage cavern is considered unventilated and thus having the rock temperature. The same temperature is assumed to apply also for the backfill cement.

The initial temperature for the filled waste containers (38.5 °C) is derived from a pre-examination of the temperatures experienced by the containers following filling.

The examination took the form of calculations with MC.TRAD-2D of vertical cross-sections through a container, employing convective/radiative

boundary conditions to represent heat exchange with the 35 °C ambient background conditions.

In the present study the highest initial thermal loading examined is 10 $W\ m^{-3}$ (for decommissioning waste). The temperature perturbation above the surrounding environment was found to be less than 2.25 °C on the faces of the concrete and less than 3.5 °C in the centre (at the hottest point) for a container with this thermal loading, situated on a horizontal surface awaiting disposal. Thus, a uniform concrete/waste temperature 3.5 °C above the ambient air in the cavern has been assumed, giving the slightly conservative initial condition of 38.5 °C for the repository thermal loading analysis.

For the pre-calculations an empirical expression developed by Churchill and Chu [22] relating average Nusselt Number with Rayleigh and Prandtl Numbers has been used for the vertical faces:

$$\overline{Nu}_H^{1/2} = 0.825 + \frac{0.387\ Ra_H^{1/6}}{\left(1 + \left(\frac{0.492}{Pr}\right)^{9/16}\right)^{8/27}} \qquad (4.1)$$

and a further expression from Al-Arabi and El-Riedy [23] for the horizontal upper surface:

$$\overline{Nu}_Z = 0.145\ Ra_Z^{1/3} \qquad (4.2)$$

where:

$\overline{Nu}_L$	Nusselt Number = $\overline{h}\ L/k$
Pr	Prandtl Number = $C_p\ \mu/k$
Ra_L	Rayleigh Number = $\rho^2\ C_p \beta\ g\ L^3\ \Delta T/\mu k$
ρ	Air density [$kg\ m^{-3}$]
C_p	Air specific heat at constant pressure [$J\ kg^{-1}\ K^{-1}$]

μ	Air viscosity [kg m^{-1} s^{-1}]
k	Air thermal conductivity [W m^{-1} K^{-1}]
β	Air coefficient of thermal expansion [K^{-1}]
g	Gravitational acceleration [m s^{-2}]
L	Characteristic length [m]
$\overline{h}$	Average heat transfer coefficient [W m^{-2} K^{-1}]
ΔT	Temperature difference between heat exchanging surface layer and bulk fluid [K]

Here L takes the value H, the height of the waste containing blocks or Z, the half-width of the top surface of the horizontal blocks. In effect, once a boundary layer in a flow field induced by natural convection has undergone the transition to turbulence, the geometrical length scale becomes irrelevant. More important is the correlation length of the turbulence. Thus, in relationships such as (4.1), (4.2) and later (4.3) and (4.4) the characteristic length scale cancels out. However, the length scale reference basis is included here on each occasion for completeness.

The conservative, uniform initial temperature derived above for the decommissioning waste at 10 W m^{-3} loading has also been applied to the lower loading densities: 6 W m^{-3} (decommissioning waste) and 1.53 W m^{-3} (bituminised co-precipitation sludges).

The two-dimensional model domain representing a cross-section through a storage cavern is illustrated in Figure 4.6. In the figure the boundary conditions are also noted. The upper, lower and right-hand boundaries are fixed at 35 °C. The left-hand boundary is formed by a plane of symmetry and is therefore a zero flux boundary. The initial condition of 35 °C is applied throughout the host rock the structural concrete and the air or backfill present at time zero.

The waste containers in the first four layers have their initial heat load at their time of disposal (problem time zero) and hence also the temperatures of 38.5 °C. Those on layer five have the same heat yield

and temperature at their (later) time of disposal. At this time the cement backfill also is injected at its initial temperature of 35 °C.

4.4.2 Processes Treated and Computations

Three mechanisms are available for heat transfer in the storage caverns of the Type B repository: conduction, convection and radiation. Their zones of applicability before the backfilling operation are depicted in Figure 4.8.

It is apparent from this figure that during the filling phase as defined for modelling there is always a conductive path available via the floor of the cavern. However, in the narrow gaps between the sides of the stacks of containers and in the large air space above the fourth layer of containers only convection and radiation can remove heat.

The physical dimensions of the problem guarantee that the Rayleigh Numbers (see [13]) governing the natural convection heat transfer are so large that turbulent air motion is to be expected.

The approach to treating convective heat exchange in a turbulent medium, is to use again empirical correlations of the type already used for the pre-calculations described in Section 2.4.3 and for those in Section 4.4.1. These correlations, the results of experimental work and dimensional analysis considerations are discussed below.

The relationship:

$$\overline{Nu}_B = 0.145\ Ra_B^{1/3} \tag{4.3}$$

(see [23]) is based on the half-width of the stack of containers, B. It has been used for the convective heat exchange between the horizontal upper surface of the stack and the well-mixed air in the space above it.

A similar relationship:

$$\overline{Nu}_S = 0.13\ Ra_S^{1/3} \tag{4.4}$$

derived by Fujii and Imura [24] for plates of arbitrary orientation has been used for the exchange between air and cavern roof lining (here S is an elemental surface length). The geometrical approximation of the cavern roof as a sequence of straight lines allows the direct use of this expression.

Since turbulent motion throughout the air filled cavity may be safely assumed, the rapid mixing of the bulk air in the space above the waste stack has been simulated by means of:

a) a greatly enhanced thermal conductivity of the air (1×10^4 W m^{-1} K^{-1} apparent) representing the transport of heat in a well-mixed turbulent fluid;

b) the natural thermal capacity for the air (C_p for dry air at 1 atmosphere pressure and 400 K = 1.014 J kg^{-1} K^{-1} [13]); and

c) convective exchange only between solid surfaces and air using (4.3) and (4.4).

These three model assumptions ensure that the air acts only as a rapid convecting medium and that the natural convective exchanges in the surface boundary layers provide the principal resistance to heat transfer across the cavity.

In the vertical slots at the side of the waste stack the convective exchange may be simulated more simply by using the principle first suggested by Kraussold [21] and later by Eckert and Drake [13] of effective thermal conductivity of the turbulent fluid. This may be expressed approximately as:

$$k_{eff} = k \left(\frac{Ra_b}{100}\right)^{0.2} \tag{4.5}$$

where b is the gap width.

The expression (4.5) is valid in the region of Rayleigh Numbers above 10^6 and up into the turbulent flow domain.

Superposed on the convective heat exchange via the air is radiative heat exchange.

Because of the fourth power dependence of radiation flux on the surface temperatures it has a controlling effect on peak temperatures and must be included in a geometrical situation of this type. In the present calculations the participation of the air in the radiative exchange has not been accounted for and heat is assumed to be exchanged directly between mutually exposed surfaces.

For this purpose, as well as for representing convective heat transfer from the air at the surface as discussed above, the curved ceiling of the storage cavern has been modelled by a sequence of straight lines. Each of the straight sections interacts with each surface element of the upper surface of the stack, exchanging energy with it according to the formula:

$$\dot{Q}_{1\to 2} = V_{12}\ \sigma(\varepsilon_1\alpha_2 T_1^4 - \varepsilon_2\alpha_1 T_2^4) \tag{4.6}$$

where:

V_{12}	Geometrical view factor between a pair of heat exchanging surface elements [m]*
ε, α	Emissivity and absorptivity respectively of the two surface elements [-]
σ	Stefan-Boltzmann constant = 5.67×10^{-8} W m^{-2} K^{-4}

T_1, T_2 Surface temperatures of emitting and receiving surface elements respectively [K]

* a surface is one-dimensional in a 2-D computation.

In fact, since the entire cavity is concrete, materials 1 and 2 are identical. It was assumed, in addition, that for the temperature ranges expected (see, for example [11]):

$\varepsilon = \alpha = 0.7$

Experimental one-dimensional calculations (see Appendix 2) show that the temperature time histories at points inside the waste stack depend very little on the values of ε and α, provided they are non-zero. Therefore, it is appropriate to introduce a simplified procedure in determining the view factors V_{12} by assuming that radiation fluxes occur only in the plane of the modelled domain and have no component parallel to the tunnel axis. Emissivity and absorptivity were assumed to be independent of the incidence angle as well as of the energy spectrum. Radiation across the vertical air gap was treated as purely horizontal, such that only cells facing each other interacted by radiation. Multiple reflections were disregarded in both cases.

4.5 Results

4.5.1 General Remarks

In all the calculations reported in the next two sections, the period between storage of the initial four layers of concrete containers and the time of backfilling has been varied between 1/2 and 3 years. As will be seen, this parameter of the repository operating mode can have a strong effect upon the temperatures within the waste containers. It is particularly important when the thermal loading is high.

4.5.2 Bituminised Co-Precipitation Sludges

The NAGRA WA-2 waste packages, when loaded into the concrete containers yield an average thermal loading of only 1.53 W m^{-3}. The following temperature maxima are observed:

Table 4-3: Absolute maximum temperatures occurring in the stacks of waste containers when filled with bituminised waste packages (NAGRA WA-2, 200 l drums)

Delay period	Maximum temperature	Time of occurrence of maximum temperature
0.5 yrs	48.7 °C	1.54 yrs
1.0 yrs	47.7 °C	1.58 yrs
2.0 yrs	47.6 °C	1.10 yrs
3.0 yrs	47.6 °C	1.10 yrs

The results of the computations are summarised in terms of time after initial disposal in Figures 4.9 and 4.10. In Figure 4.9 the maximum temperatures for various backfill delay periods are shown as functions of time. Figure 4.10 shows the maximum temperature gradients.

Both temperatures and temperature gradients are very low. It is, therefore, not necessary to model the essentially heterogeneous waste packages in detail.

Two points arise from the figures. From Figure 4.9 the effectiveness of the convective/radiative heat transfer compared with the purely conductive case is apparent. Figure 4.10 contains apparent anomalies in the gradient maxima just after the backfill operation. This is because the gradients become momentarily larger when the cool backfill suddenly contacts the hot waste container surface and because at the same time

the position of occurrence of maximum gradient moves from the upper surface to the lateral gap. Because of the simplified repository filling cycle and its stepwise change of materials the high peaks of the gradient maxima curves must be regarded as artificial.

4.5.3 Decommissioning Waste

Two thermal loading densities were examined for this waste type, 10 W m^{-3} and 6 W m^{-3}.

For the first of these the temperature distributions have been calculated for just one backfill delay period - 3 years. Inspection of the results from the calculations with bituminised co-precipitation sludges in the previous section (4.5.2) reveals that the longer the delay period before backfilling, the lower is the maximum temperature reached thereafter. Three years' delay consequently represents the most favourable situation possible within the range of parameter variations used. In the present case, Figure 4.11 shows that 100 °C is exceeded for the first time at just more than one year after disposal. The maximum temperature within the waste stack remains above that level for at least the five years modelled, passing an intermediate maximum of 106.9 °C after 2.22 years, that is to say, before backfilling, and climbing still further afterwards so that at the end of the modelled timespan it has reached 118.1 °C. The maximum at that time is located approximately near the middle of the waste stack on the central vertical axis of symmetry.

It becomes apparent that this thermal loading may not be acceptable, because of internal vapour pressure in the concrete containers. The computation was therefore repeated with the thermal loading of 6 W m^{-3}. This provided an acceptable maximum temperature even with the shortest delay period treated (6 months) as shown in Table 4-4.

Table 4-4: Temperature maxima in the stacks of decommissioning waste containers at 6 W m^{-3} thermal loading

Delay period [years]	Maximum temperature [°C]	Time of occurrence of maximum temperature [years]
0.5	94.2	3.16
1.0	92.2	3.40
3.0**	82.6	4.90

** a first temperature maximum of 77.9 °C occurs at 2.1 years.

Figures 4.12 and 4.13 respectively show the maximum temperatures and gradients reached with this reduced thermal loading. It will be noticed that a similar pattern appears on Figure 4.13 to that emerging on Figure 4.10 for the bituminised co-precipitation sludges.

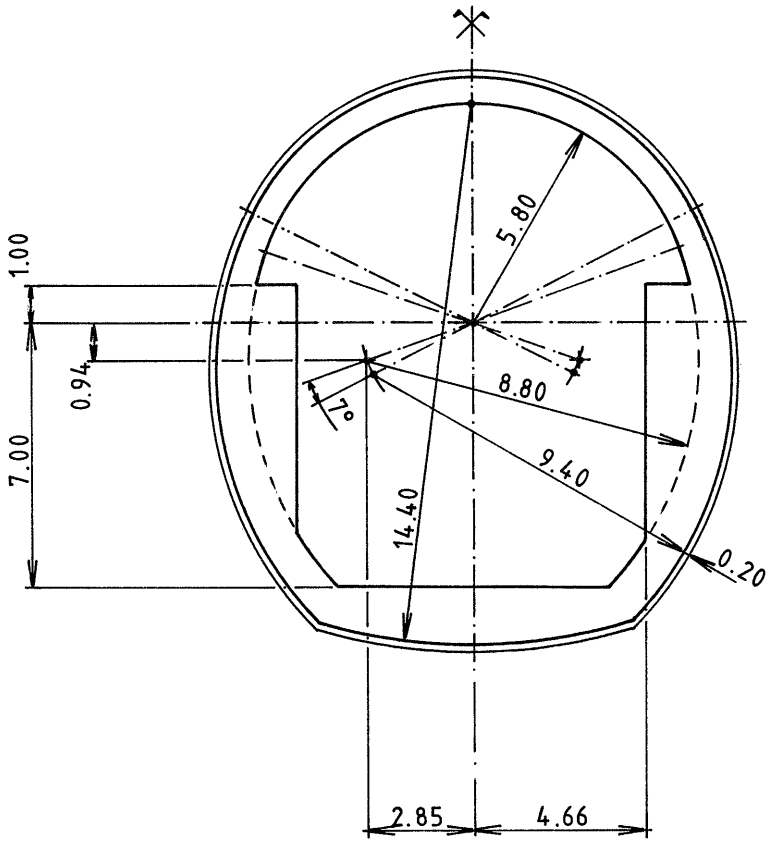

FIGURE 4.1: CROSS SECTION OF A TYPICAL STORAGE CAVERN OF THE NAGRA TYPE B REPOSITORY FOR LOW AND INTERMEDIATE LEVEL WASTE

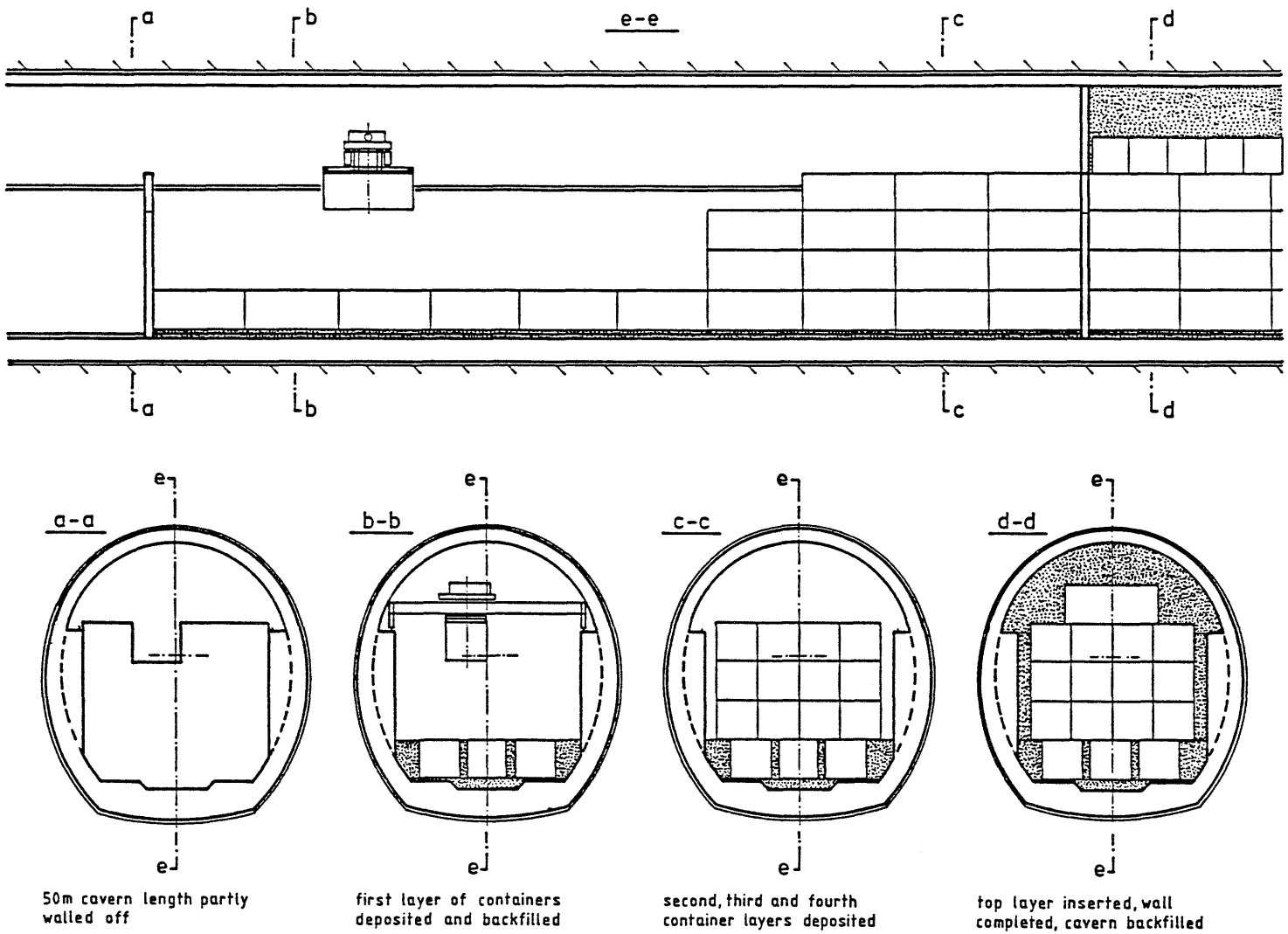

FIGURE 4.2: SECTIONAL VIEWS OF A TYPICAL 50M LENGTH OF STORAGE CAVERN IN THE REPOSITORY FOR LOW AND INTERMEDIATE LEVEL WASTE SHOWING DIFFERENT PHASES OF FILLING

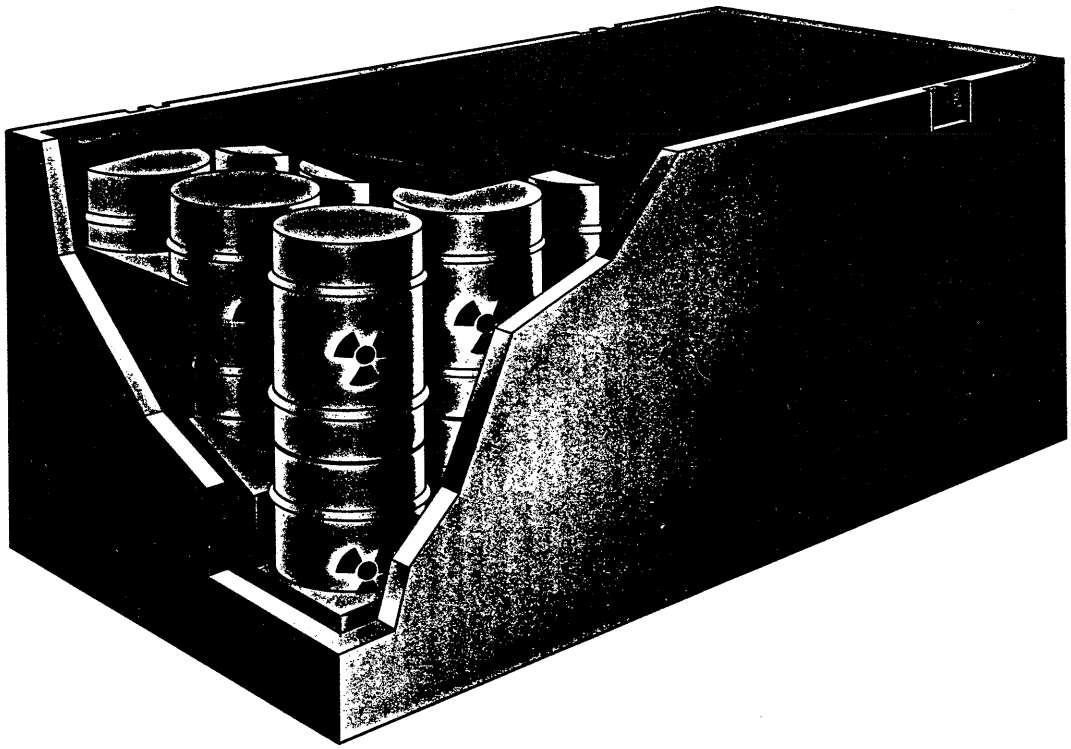

FIGURE 4.3: SKETCH OF A CONCRETE WASTE CONTAINER

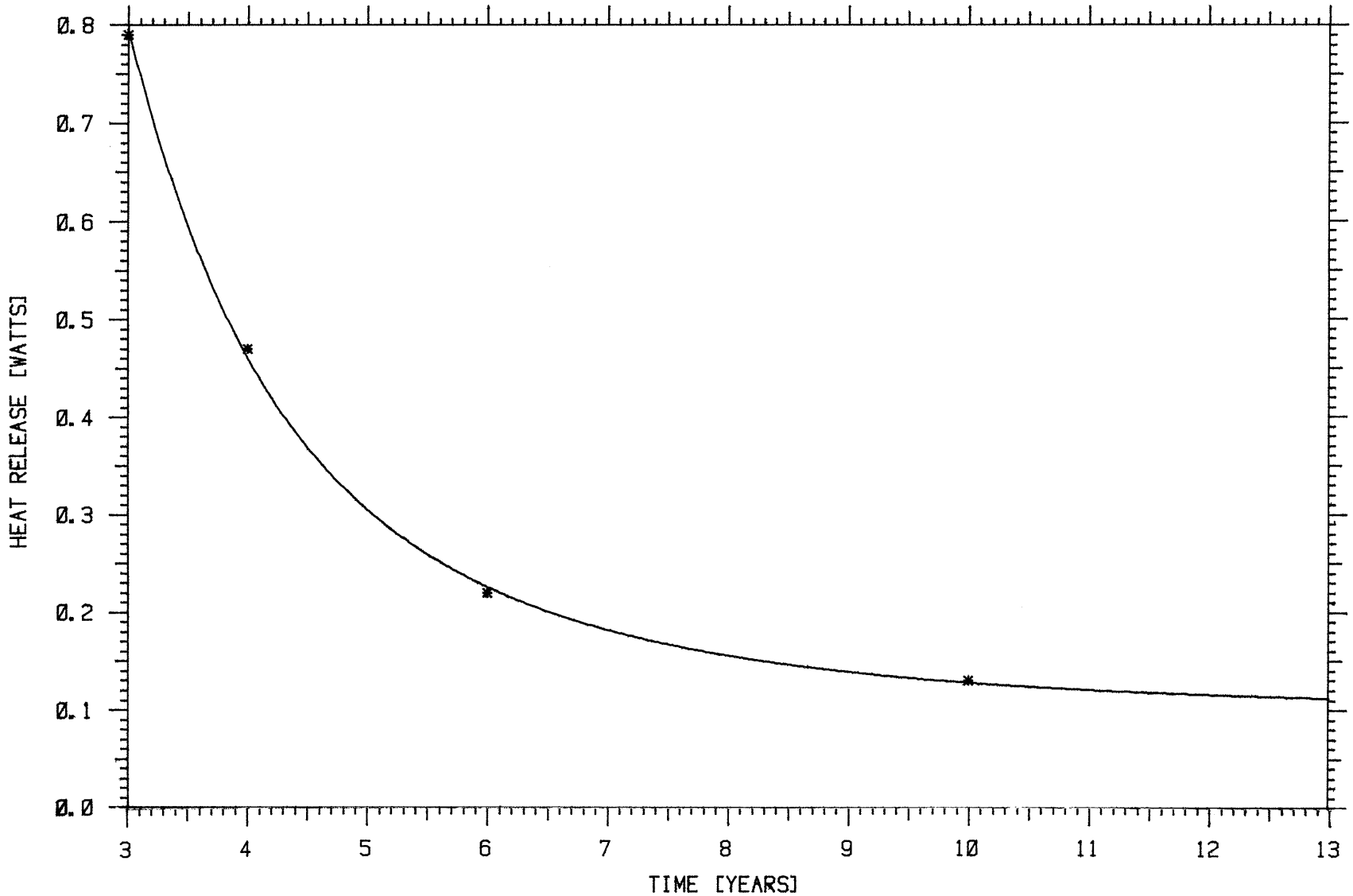

FIGURE 4.4: HEAT RELEASE RATES FROM 200L DRUMS OF BITUMINISED COPRECIPITATION SLUDGES AT DISCRETE TIMES COMPARED WITH THE FITTED FUNCTION USED IN THE ANALYSIS

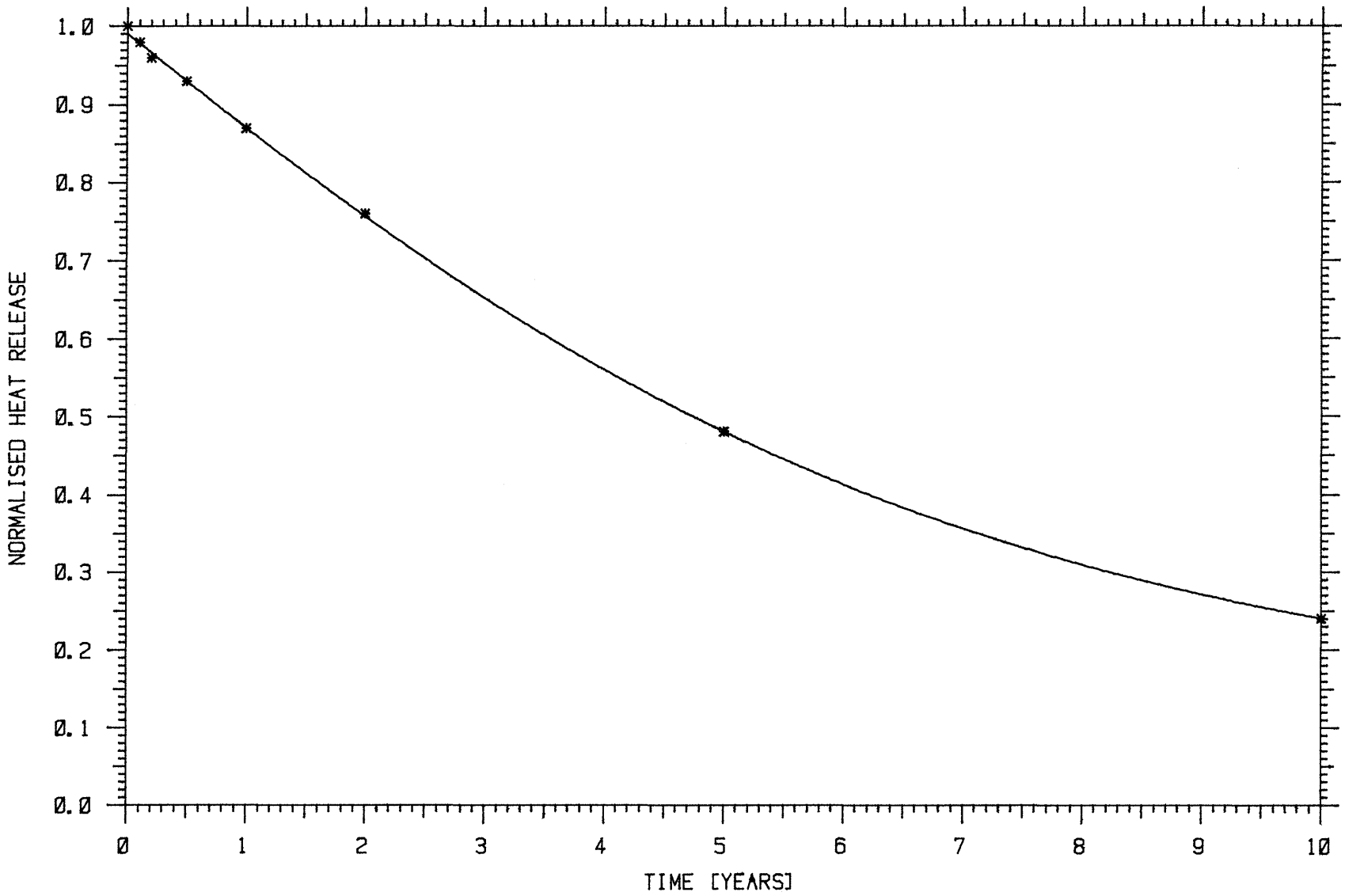

FIGURE 4.5: NORMALISED HEAT RELEASE RATES OF TYPICAL DECOMMISSIONING WASTE AT DISCRETE TIMES COMPARED WITH THE FITTED FUNCTION USED IN THE ANALYSIS

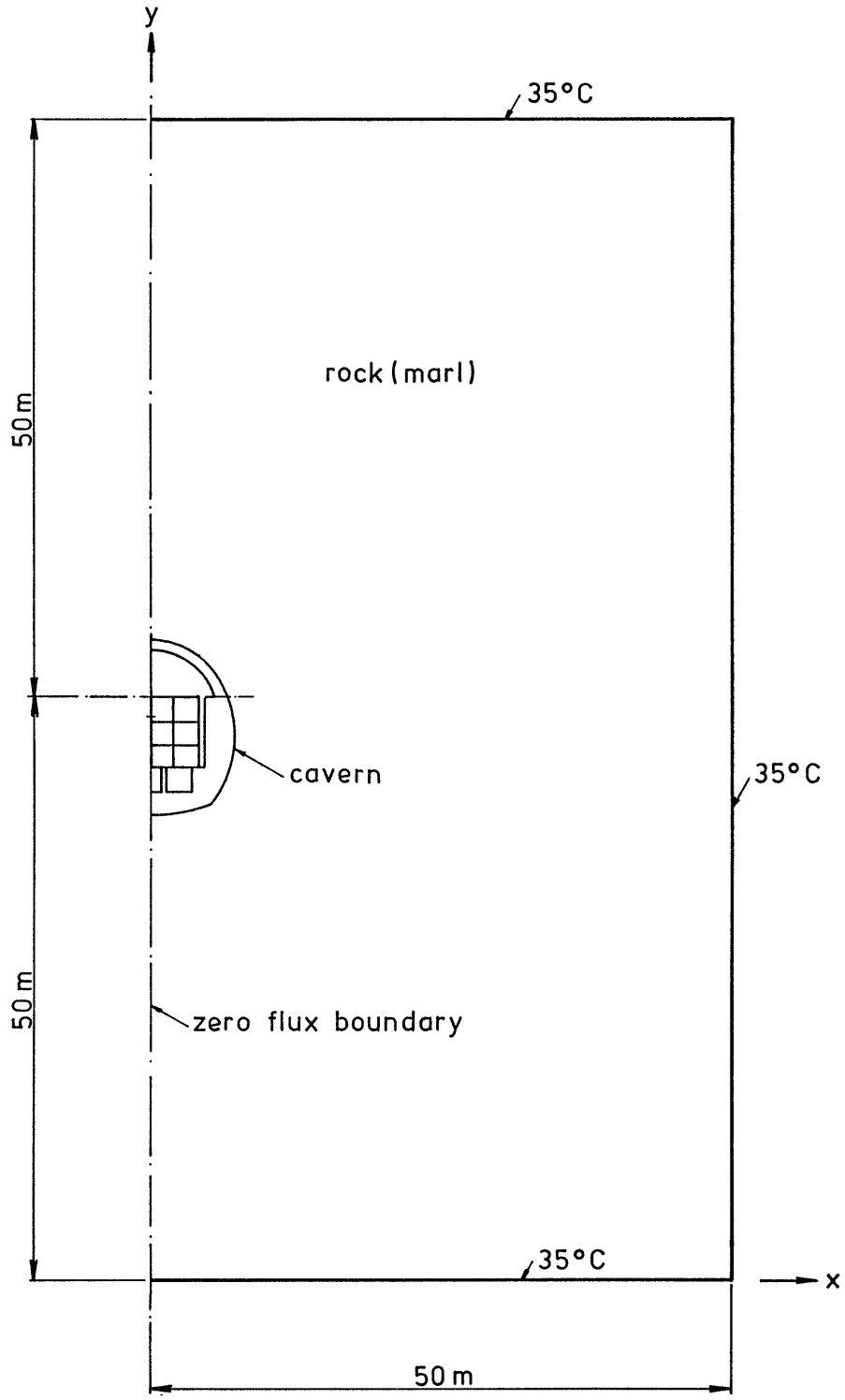

FIGURE 4.6: MODEL DOMAIN - TRANSVERSE SECTION THROUGH A STORAGE CAVERN

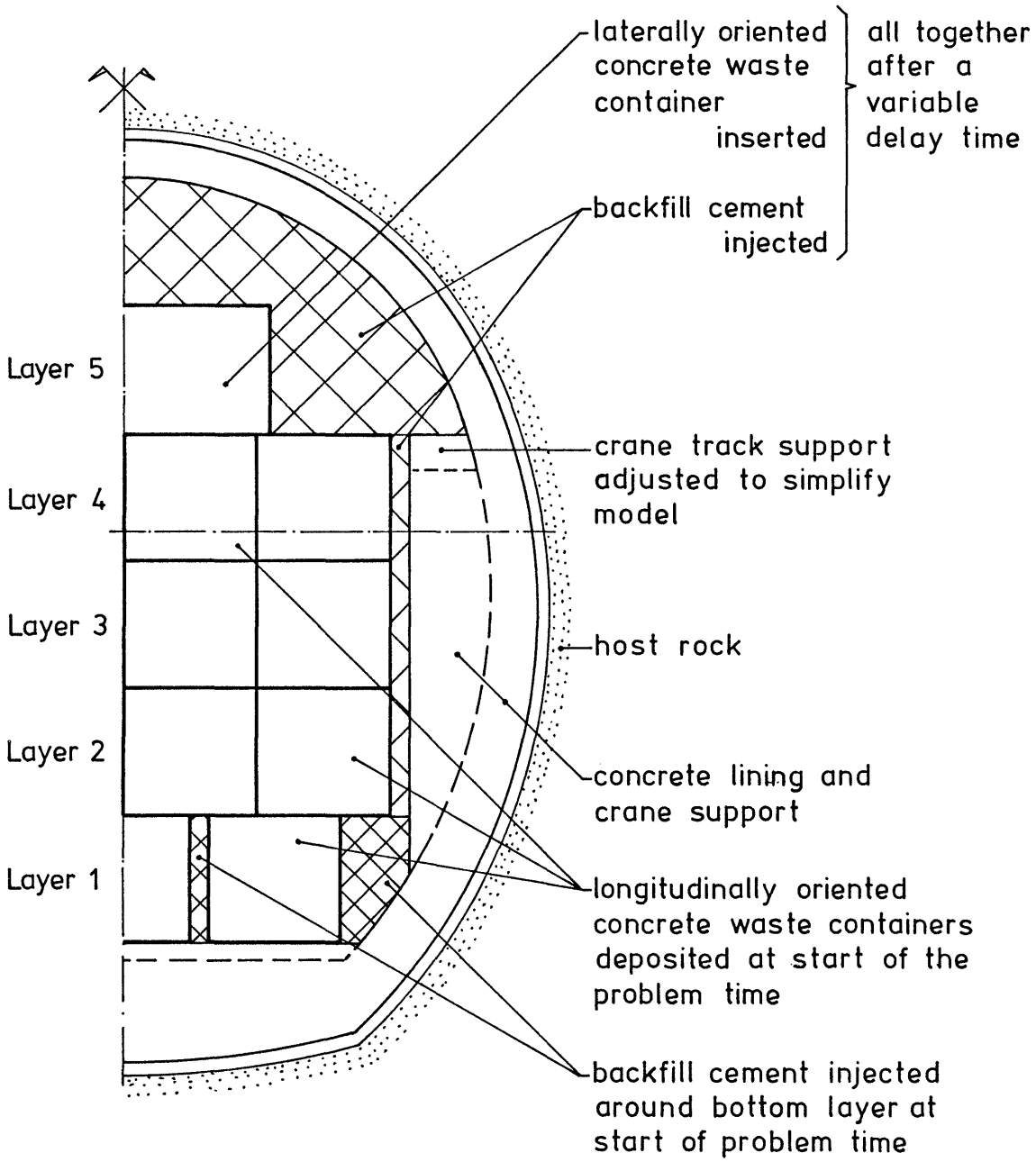

FIGURE 4.7: ENLARGED SECTIONAL VIEW OF A FILLED STORAGE CAVERN SHOWING THE MATERIAL VARIATIONS

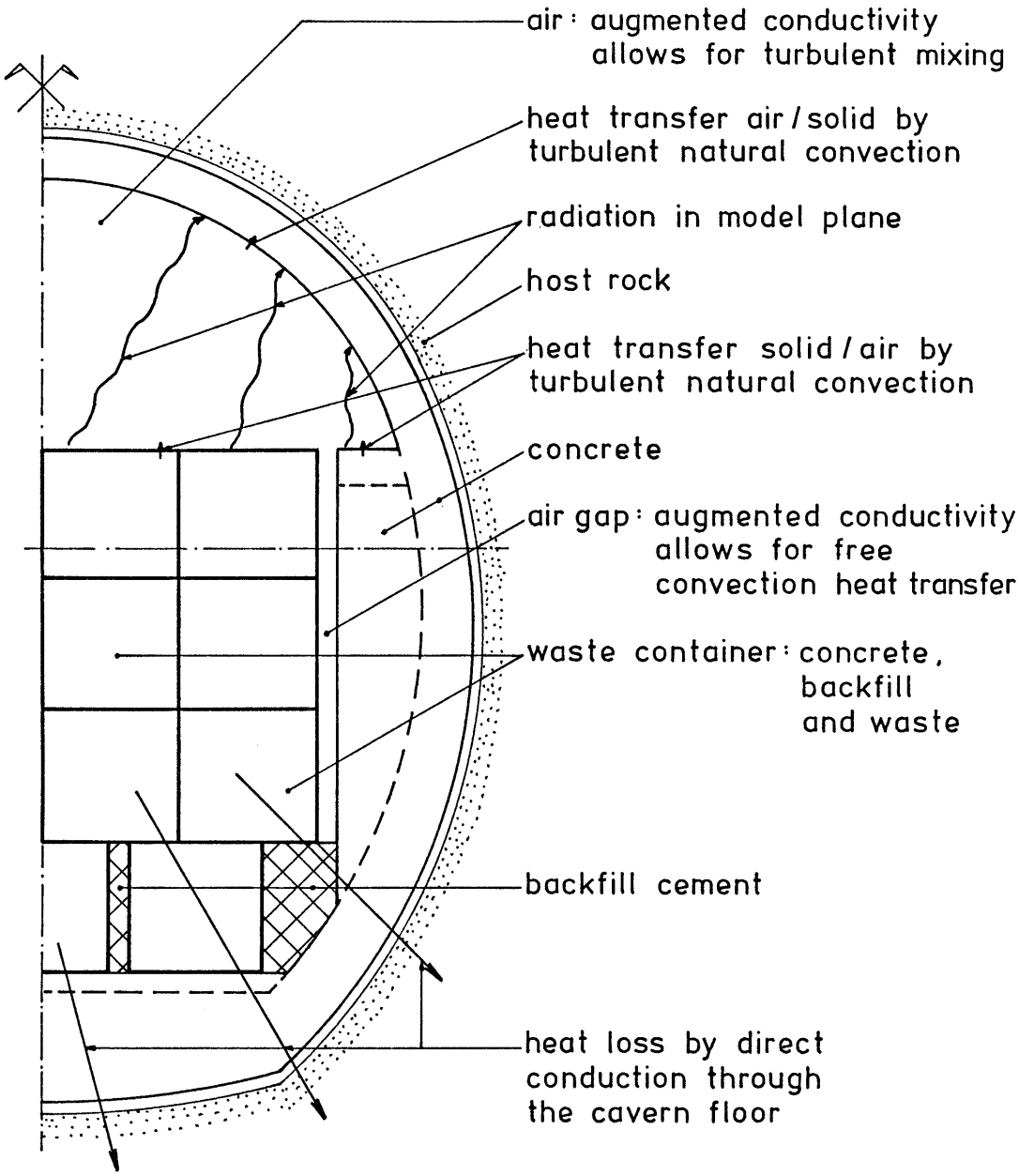

FIGURE 4.8: ENLARGED SECTIONAL VIEW OF A PARTIALLY FILLED STORAGE CAVERN SHOWING THE LOCATIONS AT WHICH THE VARIOUS HEAT TRANSFER MECHANISMS ARE CONSIDERED

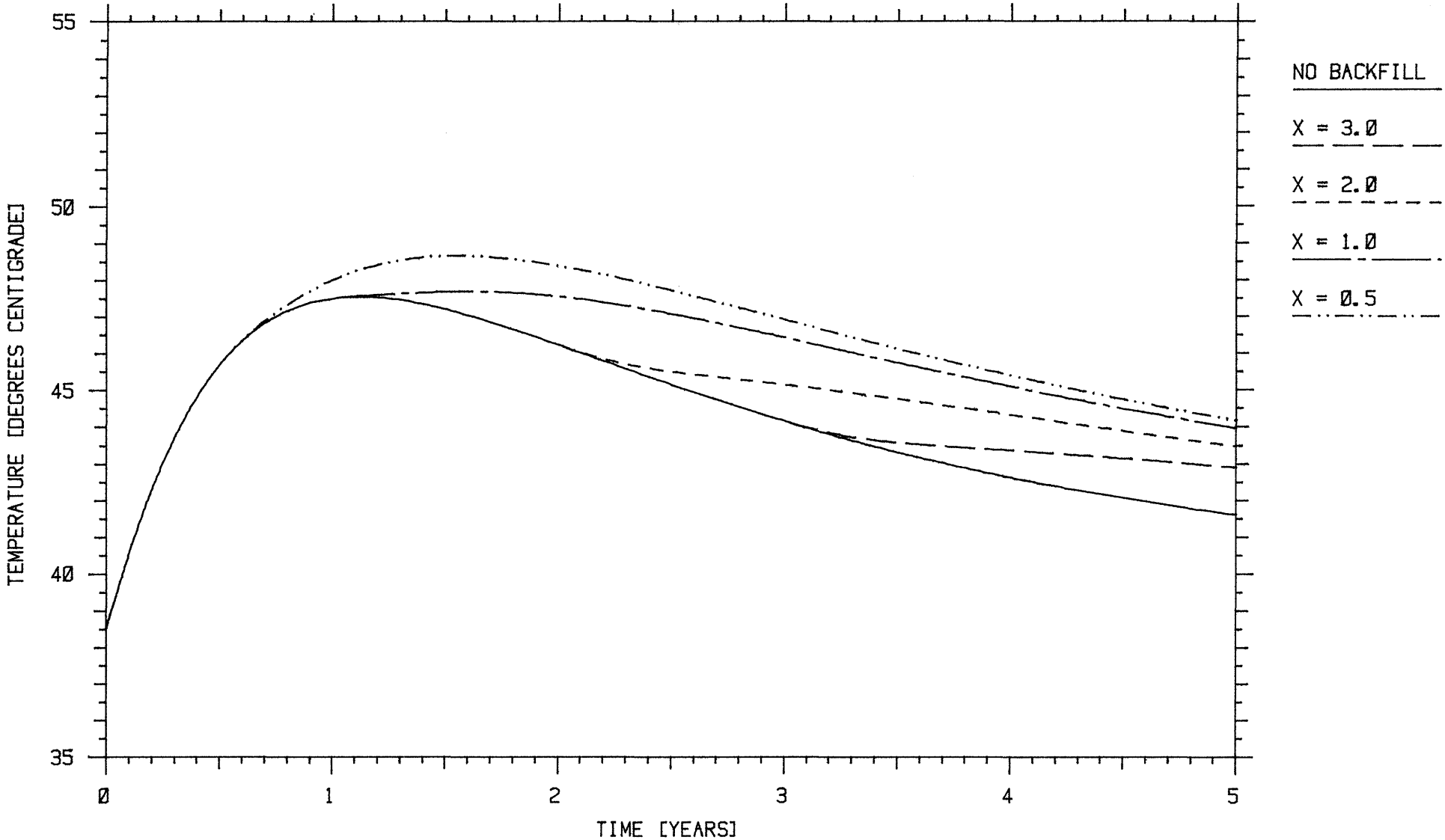

FIGURE 4.9: MAXIMUM TEMPERATURES OF BITUMINISED WASTE IN A TYPE B REPOSITORY WITHOUT BACKFILL AND BACKFILLED WITH CEMENT AFTER X YEARS

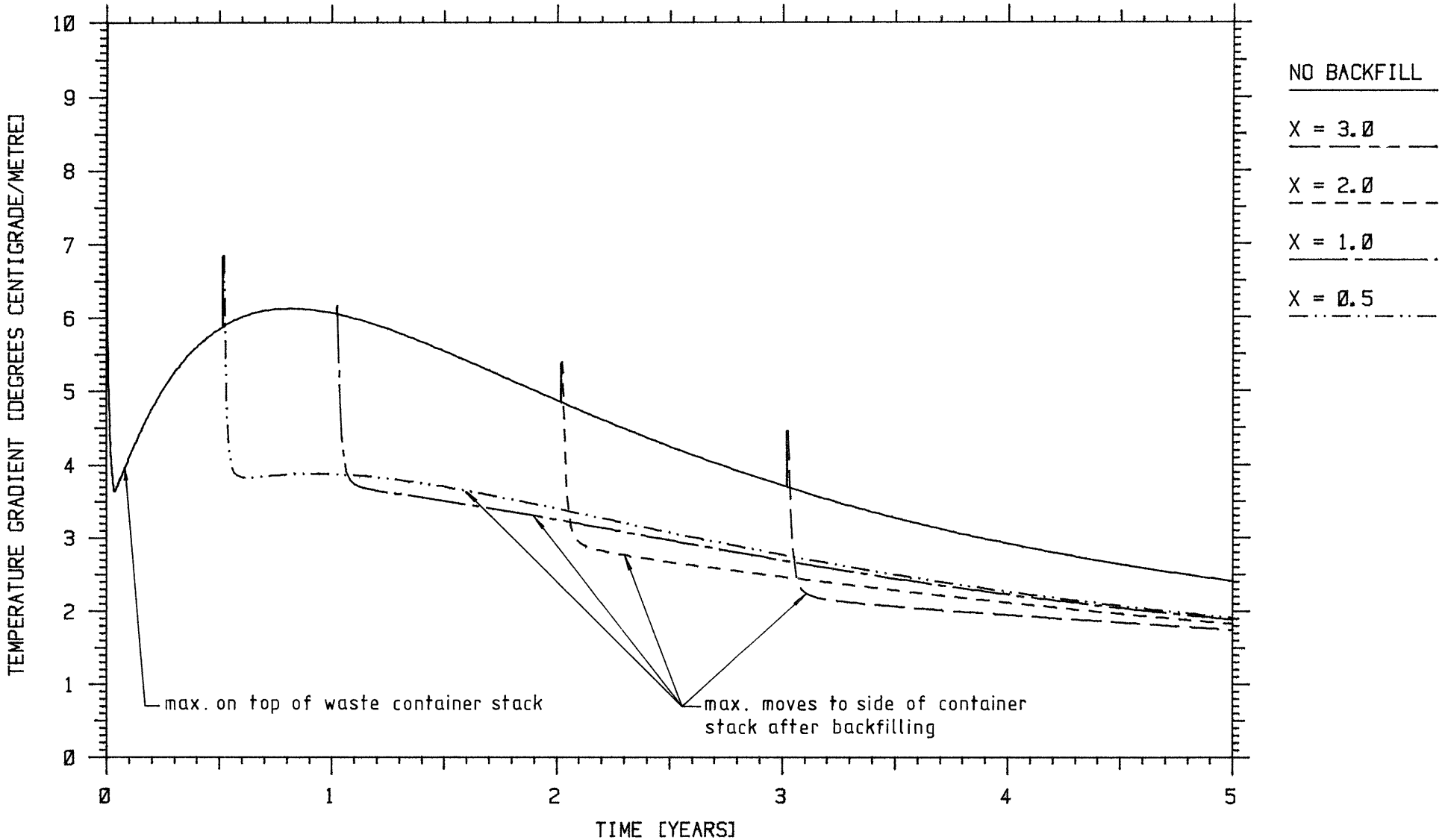

FIGURE 4.10: MAXIMUM TEMPERATURE GRADIENTS IN THE BITUMINISED WASTE IN A TYPE B REPOSITORY WITHOUT BACKFILL AND BACKFILLED WITH CEMENT AFTER A DELAY TIME OF X YEARS

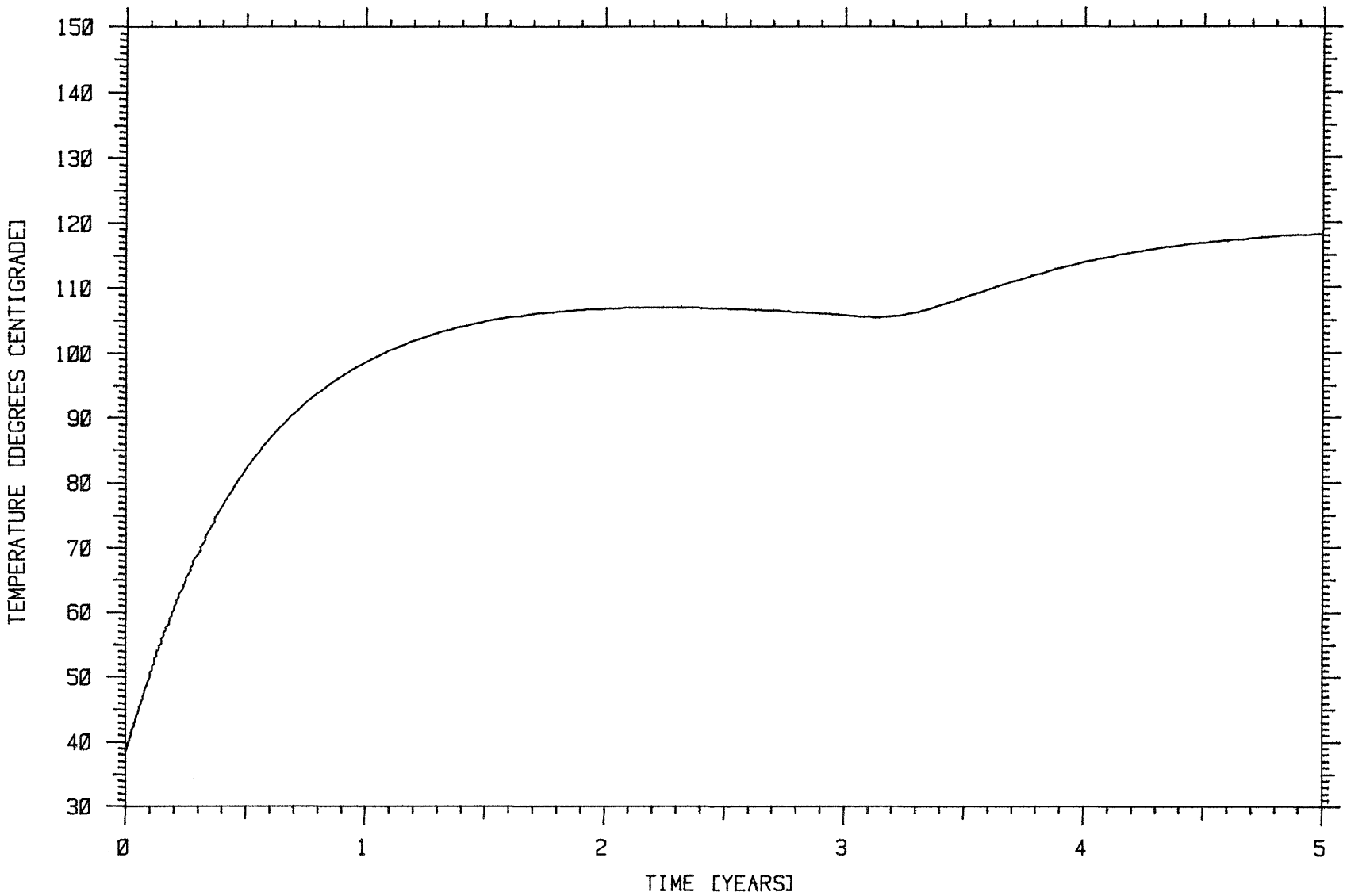

FIGURE 4.11: MAXIMUM TEMPERATURE IN THE DECOMMISSIONING WASTE IN A TYPE B REPOSITORY BACKFILLED WITH CEMENT AFTER 3.0 YEARS. HEAT LOAD 10 W/M^3

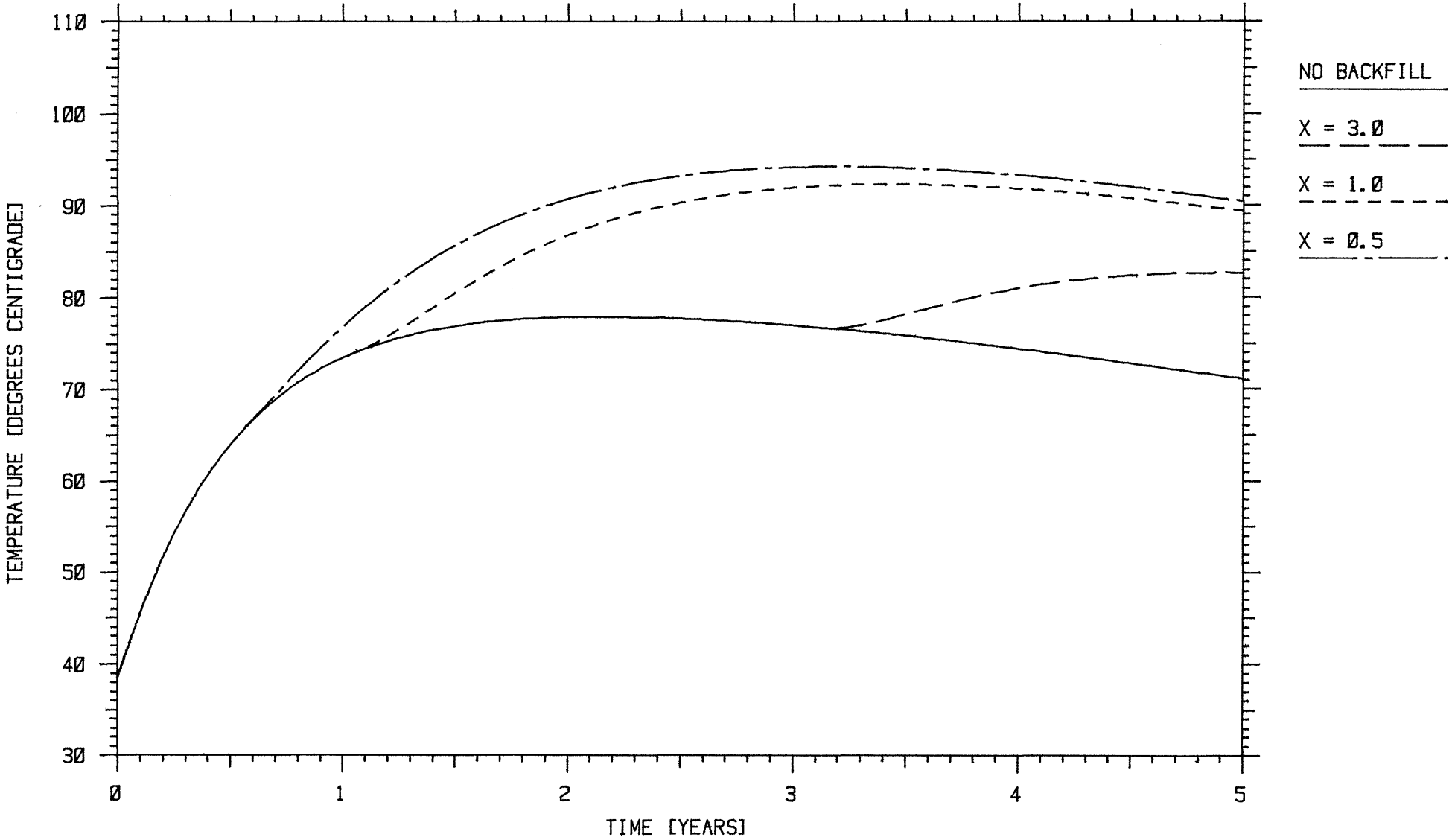

FIGURE 4.12: MAXIMUM TEMPERATURES IN THE DECOMMISSIONING WASTE IN A TYPE B REPOSITORY WITHOUT BACKFILL AND BACKFILLED WITH CEMENT AFTER A DELAY TIME OF X YEARS. HEAT LOAD 6 W/M^3

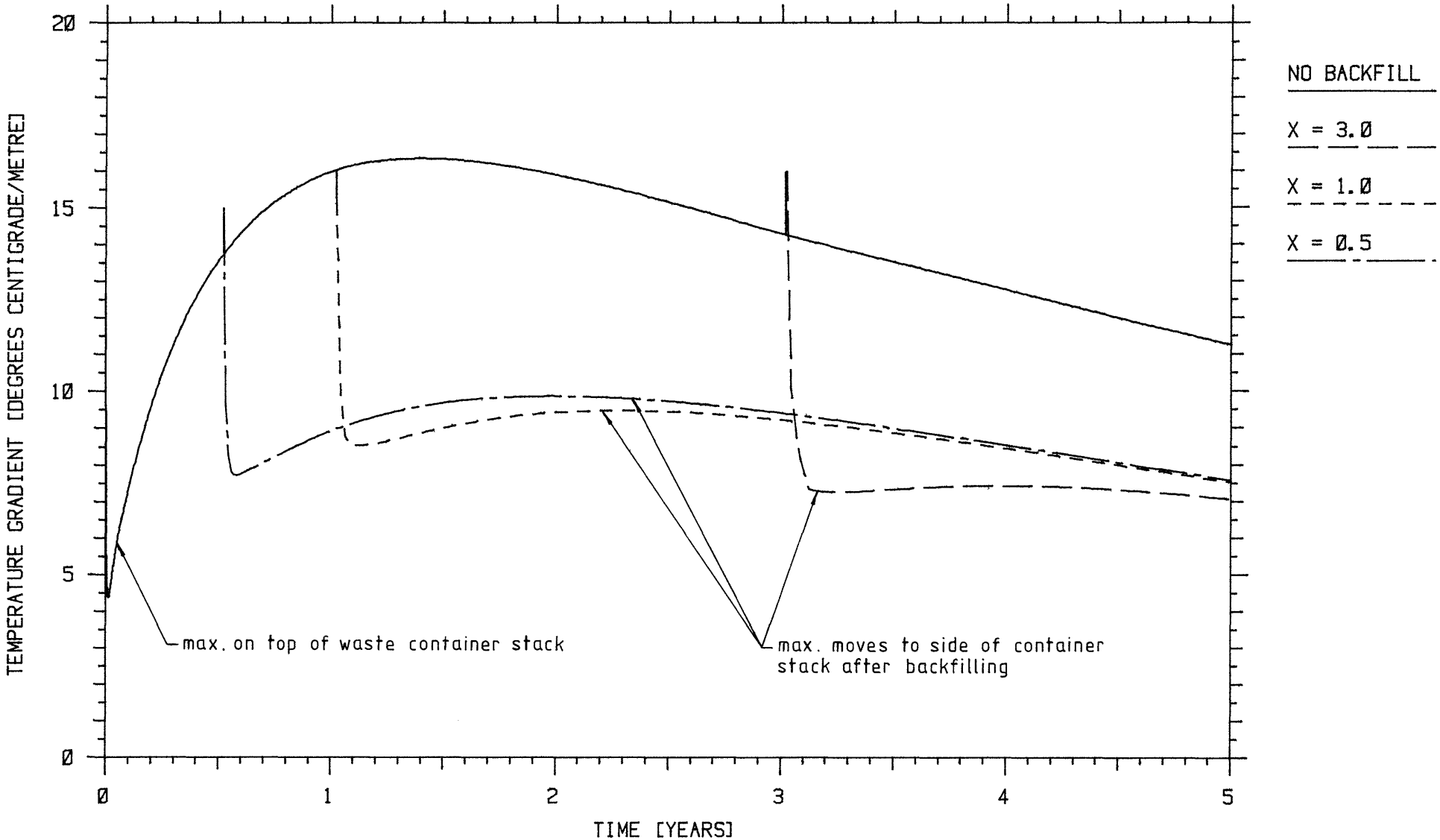

FIGURE 4.13: MAXIMUM TEMPERATURE GRADIENTS IN THE DECOMMISSIONING WASTE IN A TYPE B REPOSITORY WITHOUT BACKFILL AND BACKFILLED WITH CEMENT AFTER A DELAY TIME OF X YEARS. HEAT LOADS 6 W/M^3

5. GENERAL SUMMARY

Near field thermal loading calculations have been performed for all types of heat producing waste at present foreseen for disposal in the NAGRA nuclear waste repositories. At present, some of the data ideally necessary for such calculations, in particular concerning material properties and repository operating schedules, are not yet defined. In these cases conservative assumptions have been made.

The 40 years cooling period proposed for the vitrified reprocessing waste is sufficient to maintain temperatures in the waste below 200 °C and to leave an approximately 80 cm thick annulus of bentonite backfill in which the temperature does not exceed 100 °C. The same cooling period extended to the unreprocessed spent fuel packages gives lower temperatures in the centre of the waste. Even at 7 m axial storage pitch, an annulus of almost 1 m thickness of backfill remains always below 100 °C.

For the project GEWAEHR disposal of co-precipitation sludges has been analysed for both Type B and Type C repositories. Calculations on the bituminised co-precipitation sludges show that only very small temperature rises are to be expected in either the caverns of a Type B repository (low and intermediate level waste) or in the silos of the Type C (high level waste) repository. In both situations the maximum temperature rise is less than 15 °C, the peak being passed in the course of the second year of storage. No extra cooling period beyond the 3 years allowed for reprocessing is necessary for this waste type.

The silos of the Type C repository may also be used for storage of the fuel hulls and end caps from reprocessing. For these a cooling period of 40 years has been proposed. It is apparent from the results in Chapter 3 that this period may be reduced to 20 years without temperatures in the concrete filling or cement backfill exceeding 90 °C.

For disposal of the decommissioning waste the type B repository has been proposed. The objective of the computational study was to determine

an approximate thermal loading density, which will enable concrete/ cement temperatures to be held below 100 °C. An acceptable performance is readily obtained at 6 W m^{-3} loading.

It may be concluded that, although the still undefined data have been replaced by assumptions which must ultimately be confirmed, the present design of the NAGRA waste repositories offer acceptable near-field thermal environments for the waste packages and that equally acceptable solutions for decommissioning waste disposal are available.

Not considered in the calculations reported here was the heat production by the cement introduced both in the Type B and Type C repository and in the standardised containers for low and intermediate level waste.

6. NOMENCLATURE

Parameters

α	Surface radiation absorptivity [-]
α	Thermal diffusivity (= $k/\rho C$) [$m^2\ s^{-1}$]
β	Thermal expansion coefficient [T^{-1}]
C	Specific heat capacity [$J\ kg^{-1}\ K^{-1}$]
C_p	Specific heat at constant pressure [$J\ kg^{-1}\ K^{-1}$]
C_v	Volumetric specific heat capacity [$J\ m^{-3}\ K^{-1}$]
ε	Surface radiation emissivity [-]
ε	Volume fraction in a mixture of materials [-]
η	Net surface radiation emissivity [-]
g	Acceleration due to gravity [$m\ s^{-2}$]
$\overline{h}$	Average surface heat transfer coefficient [$W\ m^{-2}\ K^{-1}$]
k	Thermal conductivity [$W\ m^{-1}\ K^{-1}$]
K_{ii}	Diagonal tensorial component of thermal conductivity [$W\ m^{-1}\ K^{-1}$]
L	Characteristic (reference) length [m]
μ	Molecular fluid viscosity [$kg\ m^{-1}\ s^{-1}$]
ν	Kinematic viscosity [$m^{-2}\ s^{-1}$]
r, R	Radial distance [m]
ρ	Density [$kg\ m^{-3}$]
S	Source strength [$W\ m^{-3}$]
σ	Stefan-Boltzmann constant [$W\ m^{-2}\ K^{-4}$]
T	Temperature (except where stated to be in °C) [K]
ΔT	Temperature difference [K]
ϕ	Water content of compressed bentonite [weight %]
$V_{1\to2}$	Geometric view factor between surfaces 1 and 2 [m^2] in 3-D
$V_{1\to2}$	Geometric view factor between lines 1 and 2 [m] in 2-D
x,y	Linear distances in cartesian coordinates [m]
z	Axial distance in cylindrical coordinates [m]

Non-Dimensional Groups Used in Convective Heat Transfer Calculations

$\overline{Nu}$	Average Nusselt number ($= \overline{h}L/k$)
Pr	Prandtl number ($= \nu/\alpha$)
Ra	Rayleigh number ($= \frac{\beta g}{\nu\alpha} L^3 \Delta T$)

Suffices

ave.	Average value
b	Bulk property
d	Of dry bentonite
eff.	Effective value
i	At the inner radius
o	At the outer radius
r	Of the host rock
w	Of the pore water

7. BIBLIOGRAPHY

[1] NAGRA: "Projekt Gewähr 1985 - Endlager für hochaktive Abfälle: das System der Sicherheitsbarrieren", NAGRA NGB 85-04, NAGRA, Baden, 1985.

[2] R. Pusch: "Swelling pressure of highly compacted bentonite", KBS TR 80-13, SKBF, Stockholm, 1980.

[3] R. Pusch: "Use of clays as buffers in radioactive repositories", KBS TR 83-46, SKBF, Stockholm, 1983.

[4] F. Bucher, U. Spiegel: "Quelldruck von hochverdichteten Bentoniten", NAGRA NTB 84-18, NAGRA, Baden, 1985.

[5] R.J. Hopkirk, D.J. Gilby, I. Schwanner: "Preliminary calculations of the temperature distributions around a Type C (highly active) nuclear waste repository", NAGRA NTB 83-20, NAGRA, Baden, 1983.

[6] G. Kahr, M. Müller-Vonmoos: "Wärmeleitfähigkeit von Bentonit MX80 und von Montigel nach der Heizdrahtmethode", NAGRA NTB 82-06, NAGRA, Baden, 1982.

[7] R. Pusch, L. Börjesson, S. Knutsson: "Buffer Mass Test - Improved Models for Water Uptake and Redistribution in the Heater Holes and Tunnel Backfill", Stripa Project, Internal Report, SKBF, Stockholm, October 1983.

[8] SKBF-KBS: "STRIPA Project - Quarterly Report", for each quarter in 1983, 1984, SKBF, Stockholm, 1983, 1984, 1985.

[9] NAGRA: "Projekt Gewähr 1985 - Radioaktive Abfälle: Eigenschaften und Zuteilung auf die Endlager-Typen", NAGRA NGB 85-02, NAGRA, Baden, 1985.

[10] NAGRA: "Projekt Gewähr 1985 - Endlager für hochaktive Abfälle: Sicherheitsbericht", NAGRA NGB 85-05, NAGRA, Baden, 1985.

[11] H.C. Hottel, A.F. Sarofim: "Radiative Transfer", Mc Graw Hill, 1967.

[12] S.W. Churchill, H.H.S. Chu: "Correlating equations for laminar and turbulent free convection from a horizontal cylinder", Int. J. Heat Mass Transfer, Vol. 18 (1975), pp. 1049-1053.

[13] E.R.G. Eckert, R.M. Drake, jr.: "Analysis of Heat and Mass Transfer", Mc Graw Hill, 1982.

[14] G.W. Kaye & T.H. Laby: "Tables of Physical and Chemical Constants"; Longmans, London 1968.

[15] Ph. Bodmer and & L. Rybach: "Processing and representation of heat flow density maps. Part I: Subsurface temperatures and thermal conductivities"; Zbl. Geol. Paläont. Teil 1, 1983, H 1/2, pp. 80-86, Stuttgart, May 1983.

[16] NAGRA: "Projekt Gewähr 1985 - Endlager für hochaktive Abfälle: Bautechnik und Betriebsphase", NAGRA NGB 85-03, NAGRA, Baden, 1985.

[17] NAGRA: "Inventar und Charakterisierung der radioaktiven Abfälle in der Schweiz", NAGRA NTB 84-47, NAGRA, Baden, 1984.

[18] NAGRA: "Projekt Gewähr 1985 - Endlager für schwach- und mittelaktive Abfälle: Bautechnik und Betriebsphase", NAGRA NGB 85-06, NAGRA, Baden, 1985.

[19] NAGRA: "Projekt Gewähr 1985 - Endlager für schwach- und mittelaktive Abfälle: das System der Sicherheitsbarrieren"; NAGRA, NGB 85-07, NAGRA, Baden, 1985.

[20] D.J. Gilby, R.J. Hopkirk: "MC.TRAD-2D - a multiple coordinate computer code for calculation of transport by diffusion in two dimensions", NAGRA NTB 85-37, NAGRA, Baden, 1985.

[21] H. Kraussold: "Wärmeabgabe von zylindrischen Flüssigkeitsschichten bei natürlicher Konvektion", Forschung a.d. Gebiet des Ingenieurwesens, 5, Heft 4, pp. 186-191, 1934.

[22] S.W. Churchill, H.H.S. Chu: "Correlating equations for laminar and turbulent free convection from a vertical plate", Int. J. Heat Mass Transfer, Vol. 18 (1975), pp. 1323-1329.

[23] M. Al Arabi, M.K. El-Riedy: "Natural convection heat transfer from isothermal horizontal plates of different shapes", Int. J. Heat Mass Transfer, Vol. 19 (1975), pp. 1399-1404.

[24] T. Fujii, H. Imura: "Natural convection heat transfer from a plate with arbitrary inclination", Int. J. Heat Mass Transfer, Vol. 15 (1972), pp. 755-767.

APPENDIX 1

Verification of the Two-Stage, Two-Dimensional Calculation Technique Used for the High Level Waste

In order to verify the basic assumption of axial invariance outside the immediate surroundings of the tunnels a verification study has been carried out using the r-z model with high level waste packages whose centres are separated by an axial pitch of 5 m, but with a fixed temperature boundary at a distance of 50 m from the tunnel axis. The time history of the temperature calculation was calculated up to 50.2 years.

The results are presented in Figures A1.1 to A1.6. Figures A1.1 to A1.5 each show three radial temperature profiles on planes perpendicular to the tunnel axis, the first of them intersecting the package centre, second a symmetry plane at mid-distance between two adjacent packages and a third plane halfway between the first two. The profiles correspond to times varying from 1.31 years (Figure A1.1) to 50.2 years (Figure A1.5). From the profiles it is obvious that at a radial distance of about 3 m the temperature is already practically independent of axial position during the first 50 years. By this time the temperatures have reached or passed through their peak values nearly everywhere in the tunnel. Rates of temperature change tend consequently to slow down and it may be safely assumed that the situation with respect to axial invariance will rather improve during the further evolution of the temperature field.

Figure A1.6 shows axial temperature profiles at a radius of 4.682 m, the interface radius chosen for the calculations and at times corresponding to those chosen for Figures A1-1 to A1-5. The axial temperature variation is seen to be 0.1 °C at worst, a deviation which is insignificant.

This result is complemented by checks of rotational invariance in the context of the large scale model calculations. In Figures A1.7 to A1.10 horizontal and vertical radial temperature profiles have been superposed showing that they differ only little (less than 0.2 °C) in the range of interest, i.e. in the neighbourhood of the interface radius of 4.682 m. In order to ensure conservatism even with respect to those very small deviations the horizontal profile temperatures have been used as boundary values for the r-z model calculations.

These calculations have been extended out to 500 years after disposal in order to determine more profoundly the effect of the disparate horizontal and vertical boundary treatments in the x-y domain. Even at these long times the axisymmetry remains unimpaired.

It may be concluded that the simplified two-stage calculational process using only two-dimensional solutions for the temperature field and appropriate choice of small-scale domain size, will result in no significant errors in the calculated temperatures within the repository storage tunnels.

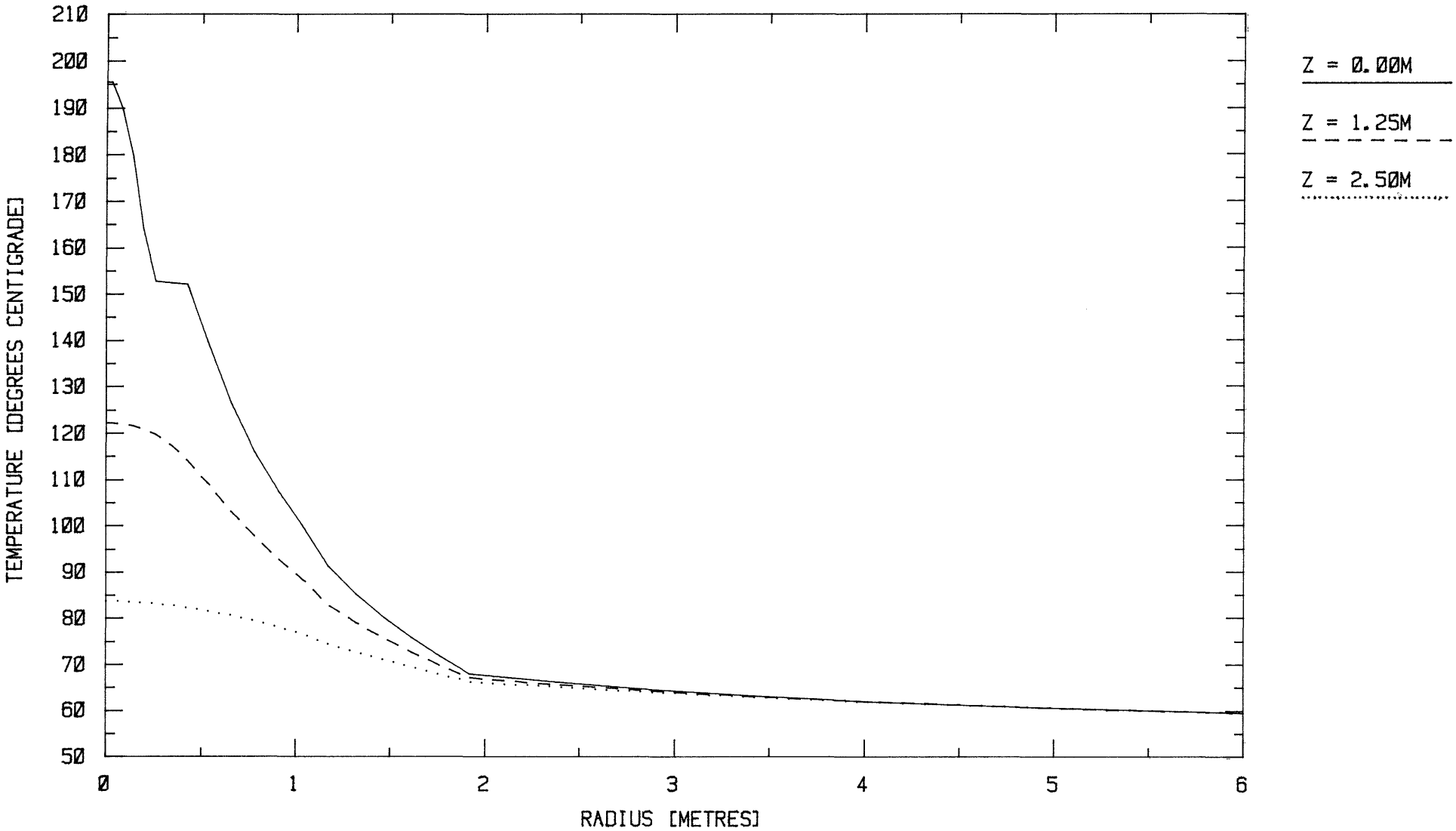

FIGURE A1.1: TEMPERATURE PROFILES AT VARIOUS AXIAL DISTANCES FROM CENTRE. T = 1.31 YEARS

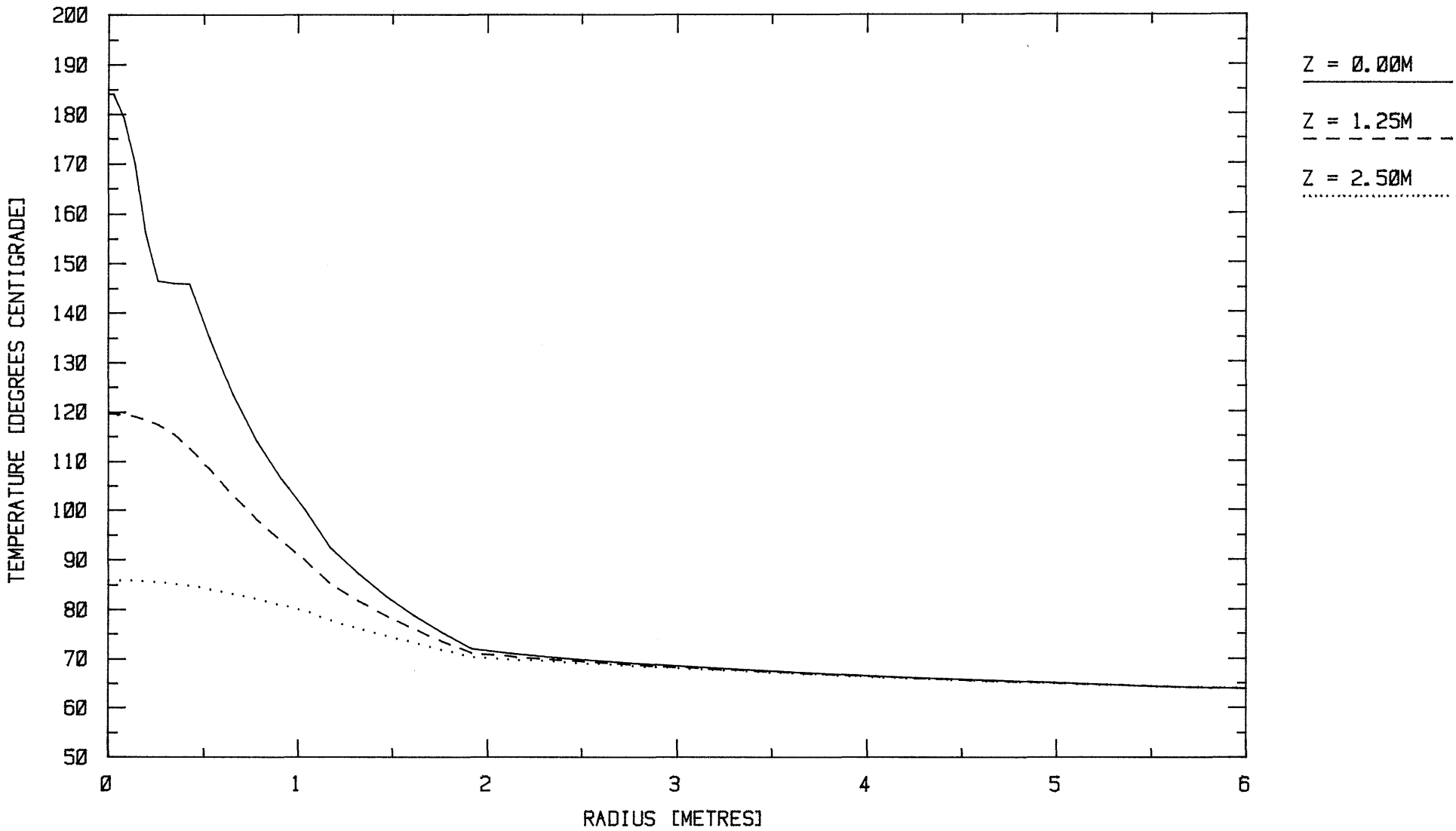

FIGURE A1.2: TEMPERATURE PROFILES AT VARIOUS AXIAL DISTANCES FROM CENTRE, T = 5.67 YEARS

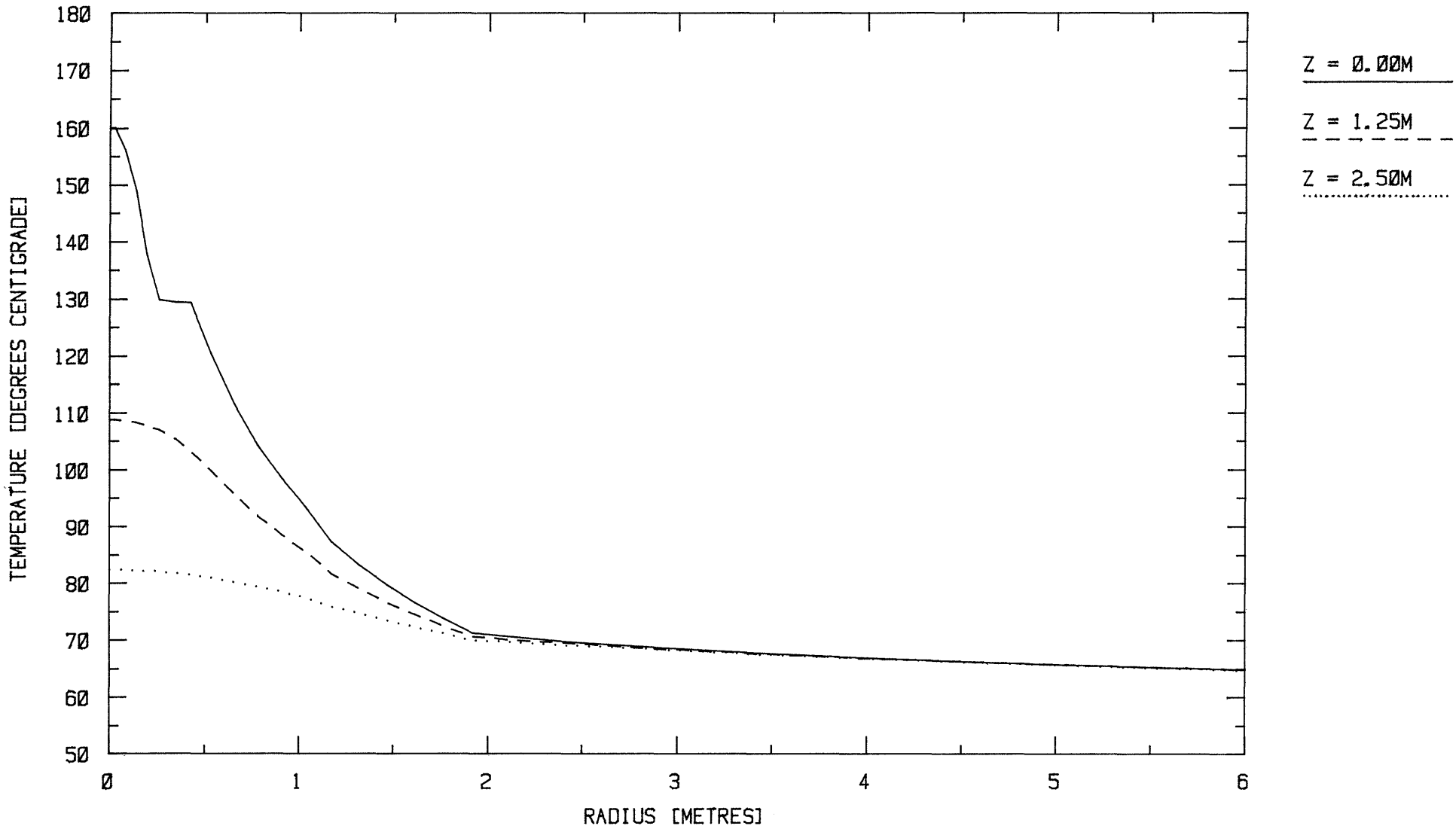

FIGURE A1.3: TEMPERATURE PROFILES AT VARIOUS AXIAL DISTANCES FROM CENTRE. T = 14.2 YEARS

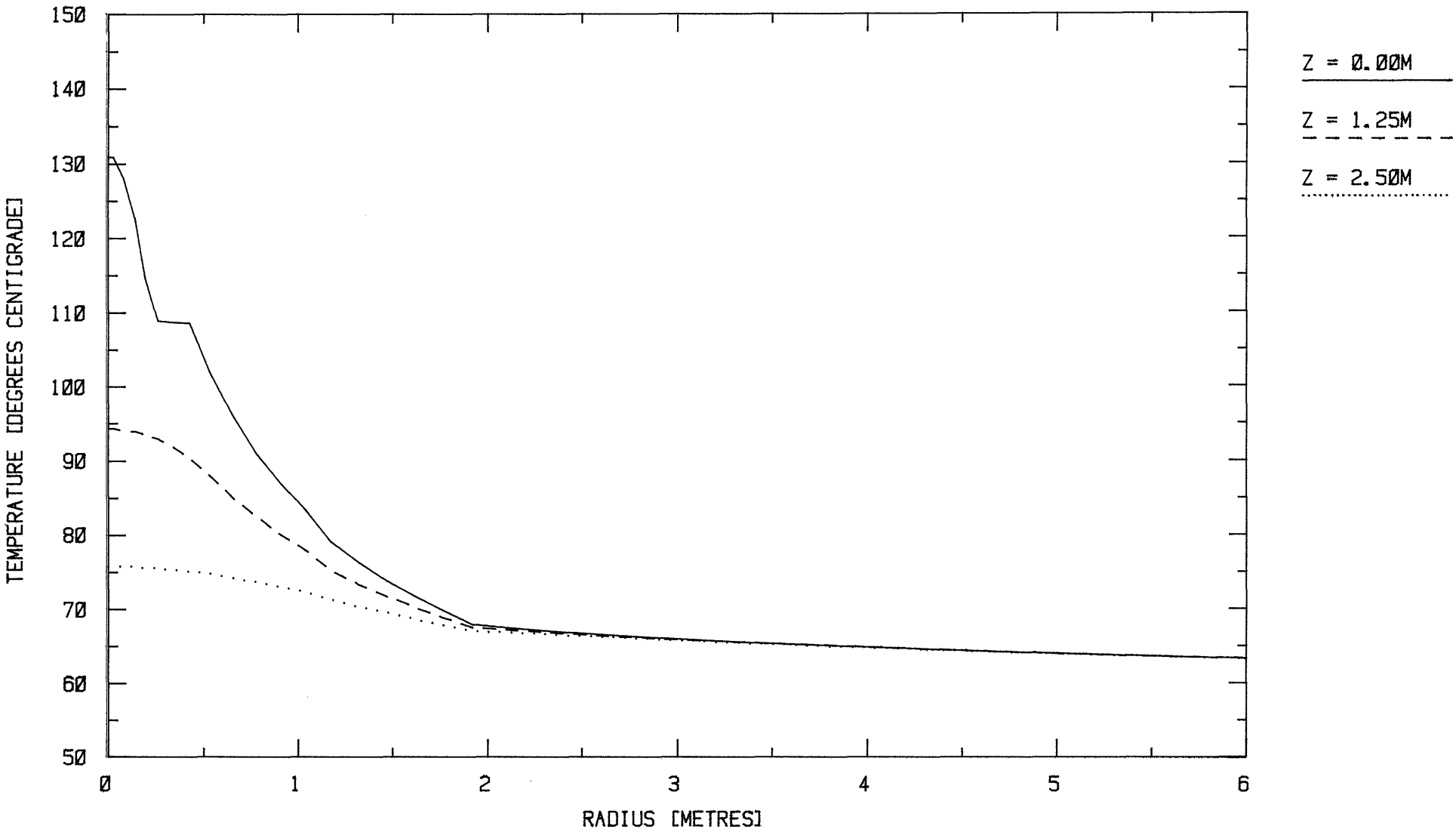

FIGURE A1.4: TEMPERATURE PROFILES AT VARIOUS AXIAL DISTANCES FROM CENTRE, T = 29.2 YEARS

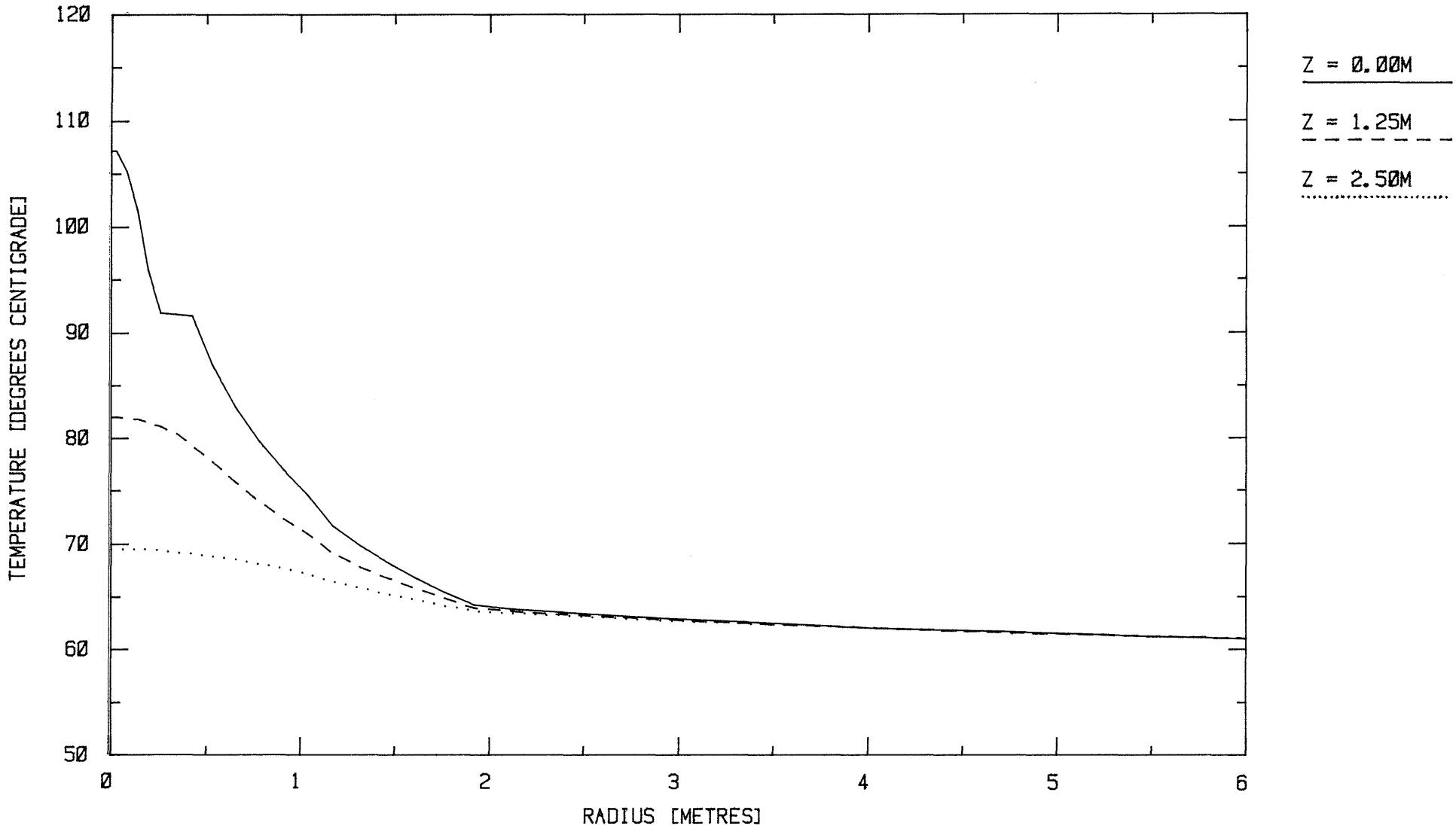

FIGURE A1.5: TEMPERATURE PROFILES AT VARIOUS AXIAL DISTANCES FROM CENTRE, T = 50.2 YEARS

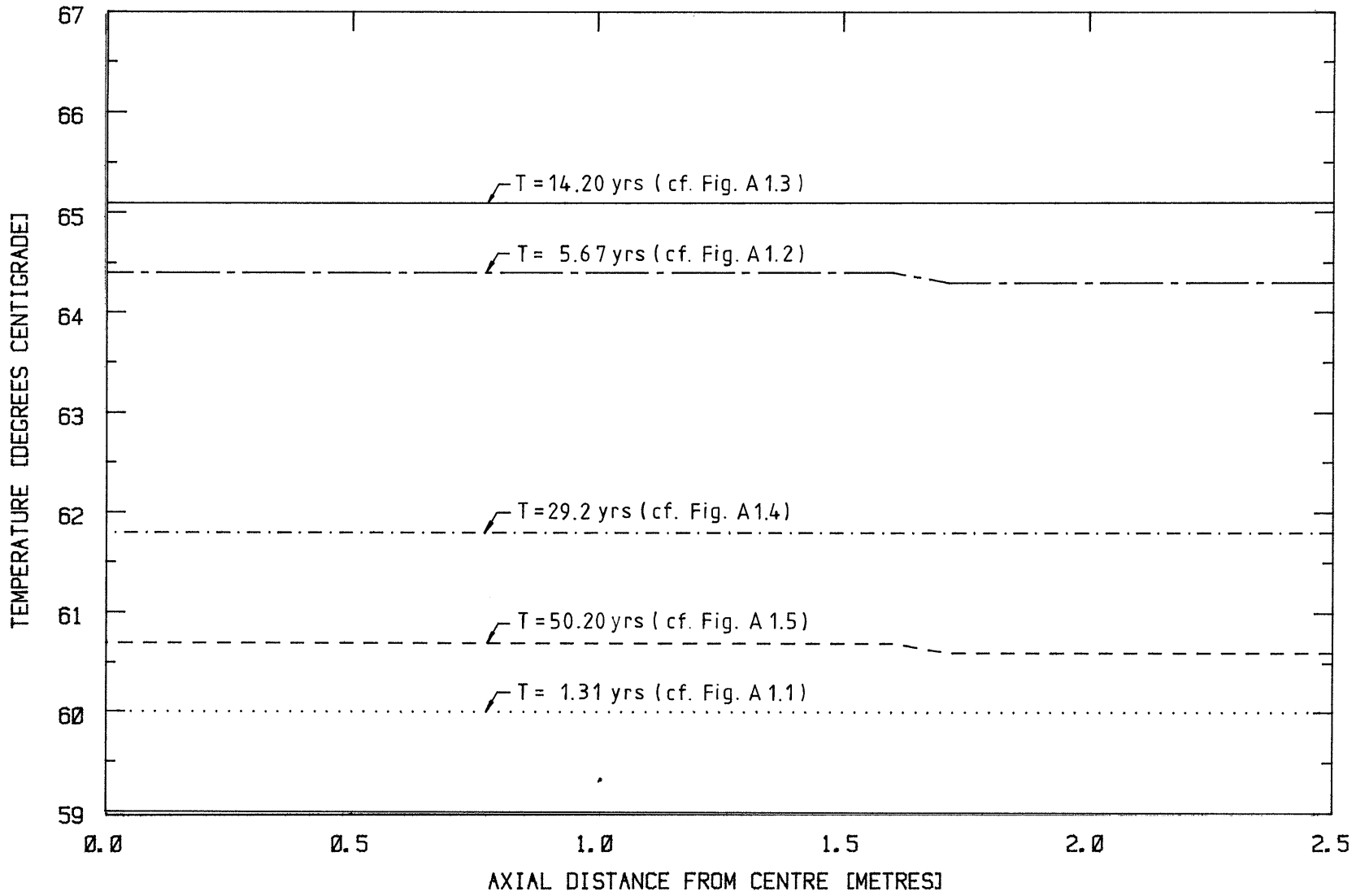

FIGURE A1.6: TEMPERATURE PROFILES AT VARIOUS TIMES, R = 4.682 METRES

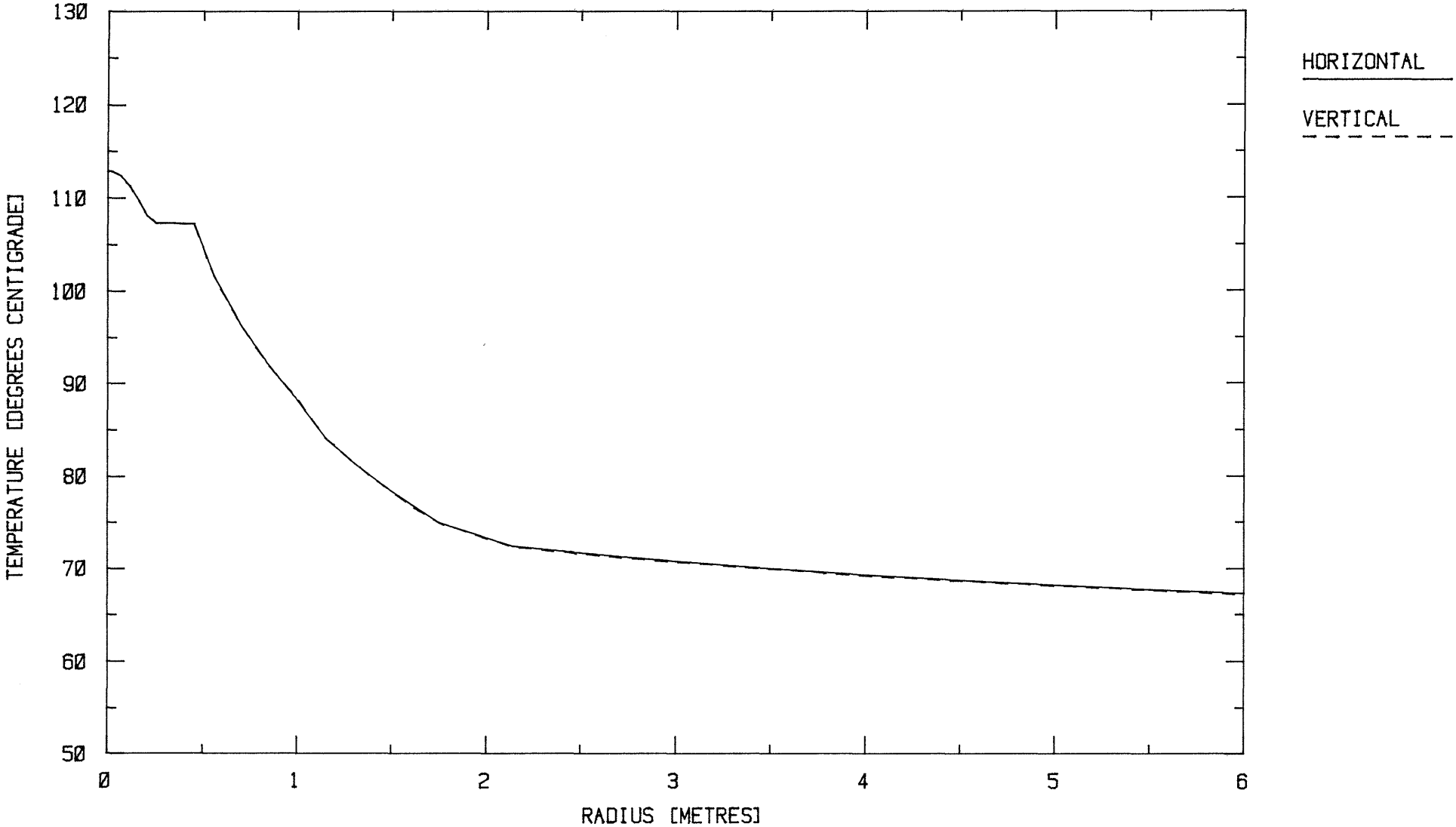

FIGURE A1.7: XY - TEMPERATURE PROFILE COMPARISON, T = 14.2 YEARS

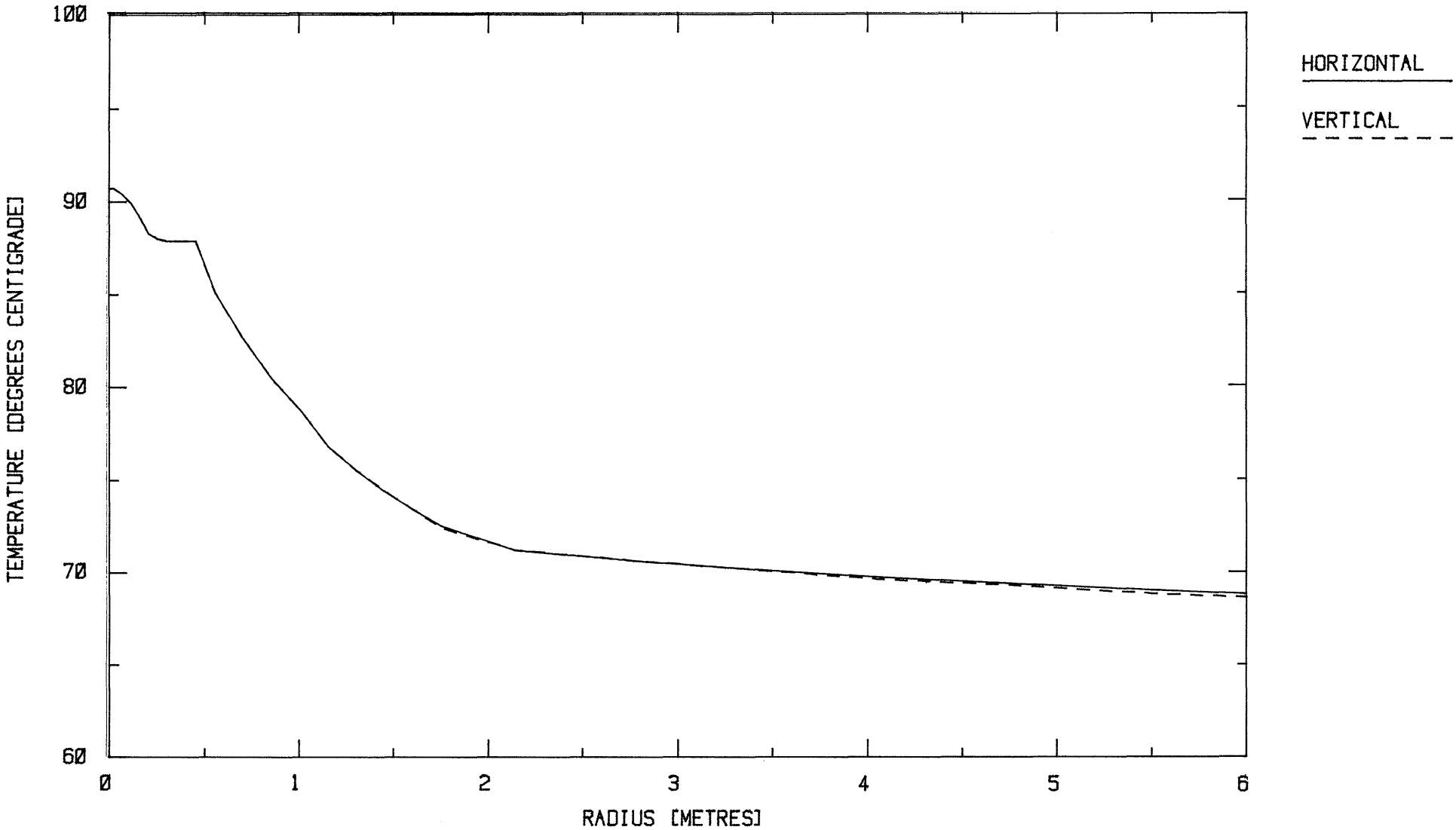

FIGURE A1.8: XY - TEMPERATURE PROFILE COMPARISON, T = 50.2 YEARS

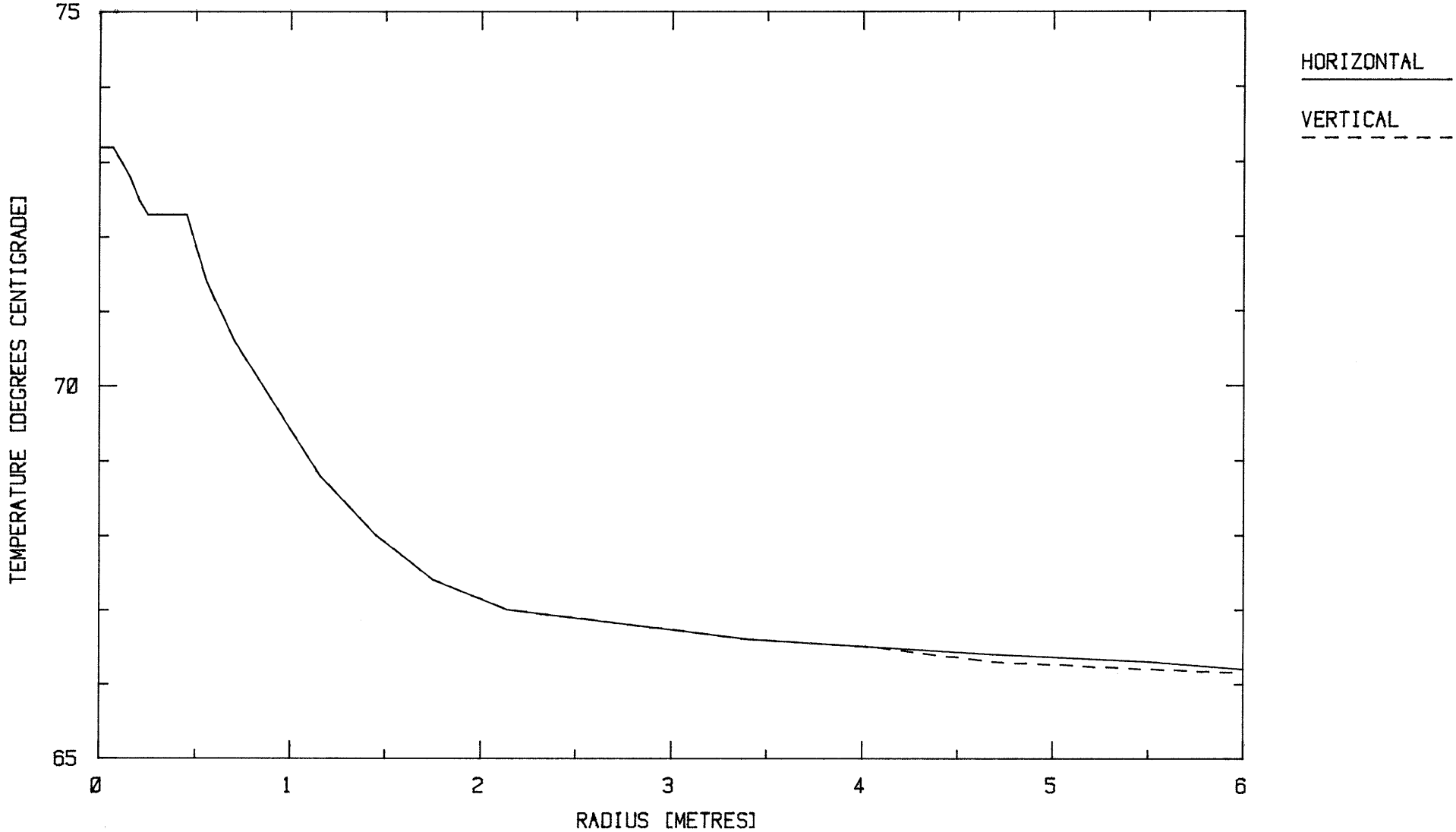

FIGURE A1.9: XY - TEMPERATURE PROFILE COMPARISON, T = 159.4 YEARS

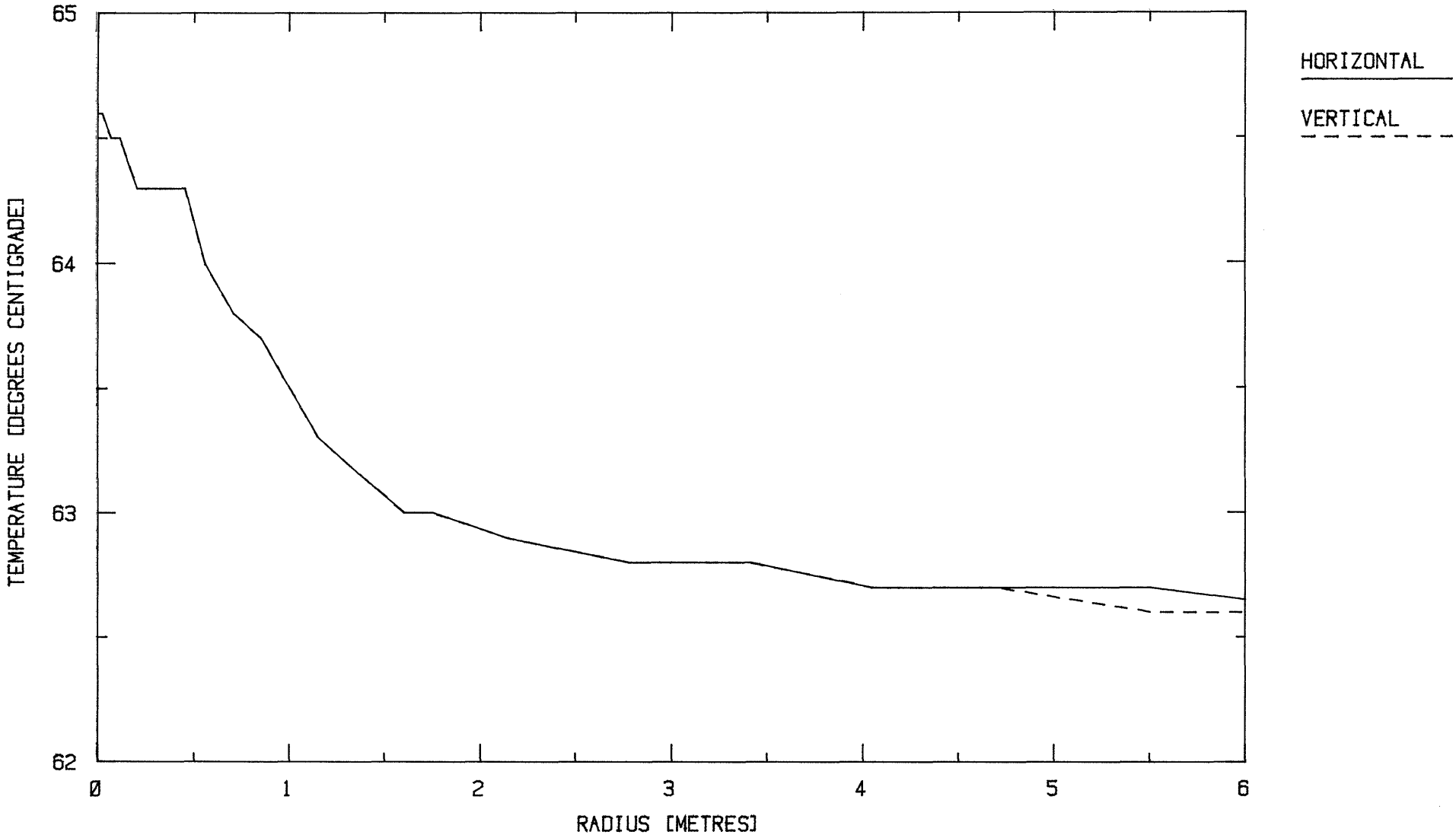

FIGURE A1.10: XY - TEMPERATURE PROFILE COMPARISON, T = 499.4 YEARS

A P P E N D I X 2

Sensitivity of heat fluxes across narrow gaps to surface contact and emissivity

Several of the situations modelled concern radiative heat transfer across cracks, joints or gaps of high aspect ratio. In general, knowledge of the emissivities and absorptivities of the exposed surfaces is vague. In addition, the influence of imperfect contact between the concrete containers in the Type B Repository was not apparent.

Simple heat transfer calculations have been performed in order to reveal the sensitivity of the resulting maximum temperatures to the heat flux variations induced by differing values of these parameters.

In order to check the sensitivity, computations were performed for heat transfer in a one-dimensional cylindrical radial domain. This domain represents in a grossly simplified manner a cross-section through a partially filled storage cavern in the Type B Repository, as shown in Figure 4.8. The dimensions of the 1 radian circular sector occupied by the domain are shown in Figure A2.1.

Initial conditions are defined in a similar way to those for the 2-dimensional calculations described in Chapter 4:

- Tunnel lining and host rock: 35 °C
- Waste containers 38.5 °C

The outer boundary at 50 m radius is maintained constant at 35 °C during each of the calculations. These have been pursued to a time of 10 years.

The first calculations were for an initial heat generation rate within the central "waste" region of 10 W m^{-3}. The heat generation rate reduces with time, following the normalised trend shown in Figure 4.5 for typical decommissioning waste.

All material properties are identical to those used in Chapter 4 for the decommissioning waste studies.

The results of this set of calculations are presented in Figures A2.2 A2.3 and A2.4, which show the temperature time histories of the centre of the cylindrical domain under various conditions.

In Figure A2.2 the 0.3 m wide air gap is assumed to be filled with concrete. The upper curve in Figure A2.3 shows the result of replacing the concrete with air again, whereby natural convection according to the Kraussold relationship [21] is considered, but radiation transfer ignored. The three other curves in this Figure represent three assumptions of emissivity (approx. equal to absorptivity) covering the range of probable variation. The insensitivity of the core temperature to the emissivity at this gap width is clearly seen. It will be observed that the temperatures predicted by these purely one-dimensional calculations are considerably higher than those demonstrated in Chapter 4 for the more realistic geometry. This is simply the result of the cylindrical geometry and the resulting high heat flux densities.

A similar picture is revealed by the two remaining Figures. Of these, Figure A2.4 in particular requires some explanation. Here, in addition to the 30 cm air gap a 1 mm joint is assumed to exist at 2.5 m radius, offering imperfect contact (only a proportion of the total area of the joint faces offer conductive heat transfer paths directly via concrete). Across the rest of the imperfectly mating face areas heat transfer occurs by a combination of conduction and radiation in air (no convection is considered).

In the uppermost curve the emissivity, ε (EPsilon), across both gap and joint is zero - that is to say, heat transfer across the gap in this case is entirely by conduction in the air and across the joint by conduction in air over 99 % of the joint and via concrete over a contact area (C.A.) in only 1 % of the total. Comparing this with the upper curve of Figure A2.3 shows that the resistance of a 1 mm layer consisting almost entirely of air is insignificant. The fourth curve on Figure A2.4 quotes only air conduction across the joint (EP1=0) and a fairly typical emissivity (EP2=0.7) across the wider gap.

It will be seen from all these cases that the degree of imperfection of such a narrow joint region affects the core temperature scarcely at all.

Finally, Figure A2.5 is a repeat of the calculation for Figure A2.3, but with a reduced heat generation rate of only 1 W m^{-3}. It is seen again that if radiation is considered, the core temperature is rather insensitive to the surface emissivity.

A further detailed comparison of Figures A2.2 and A2.3 shows that the resistance to heat transfer offered by the gap, when filled with concrete, is slightly larger than in the cases where radiation and convection across an air gap are considered. The superior efficiency of transfer via the air path is the result of both the convective and radiative transmissivities increasing in a non-linear way with temperature difference, whereas the conductive transmissivity of the filled gap remains at the rather low level determined by the concrete's thermal conductivity. The importance of this effect may be realised by comparing the transmissivity of a gap of width Δx when filled with concrete (conductivity k_c) with that of the same gap in which both convection according to the effective conductivity of moving air k_{eff} (see relationship (4.5)) and radiation according to (3.3). The expressions for the specific heat fluxes (per m^2) across the gap are:

For conduction via the solid filling:

$$\dot{q}'' = k_c \frac{(T_1 - T_2)}{\Delta x}$$

For convection and radiation:

$$\dot{q}'' \sim (k_{eff} + \sigma\eta\Delta x(T_1^2 + T_2^2)(T_1 + T_2))(\frac{T_1 - T_2}{\Delta x})$$

where T_1 is the higher and T_2 the lower surface temperature [K].

It will be seen that the effectiveness of the radiative and convective heat transfer mechanisms are dependent in different ways upon the temperature levels and upon the gap width, and also that the two transfer mechanisms both contribute to the total heat transfer capability.

It must be noted that the relative participation of the two mechanisms in the heat transfer varies with the strength of the heat source feeding the flux in an extremely non-linear fashion.

The above commentary reveals that at the temperatures reached in both repositories, the precise radiation characteristics of surfaces exposed to air gaps are not important, but that the radiation exchange process itself must be considered if air gaps are present which are greater than those formed by construction joints.

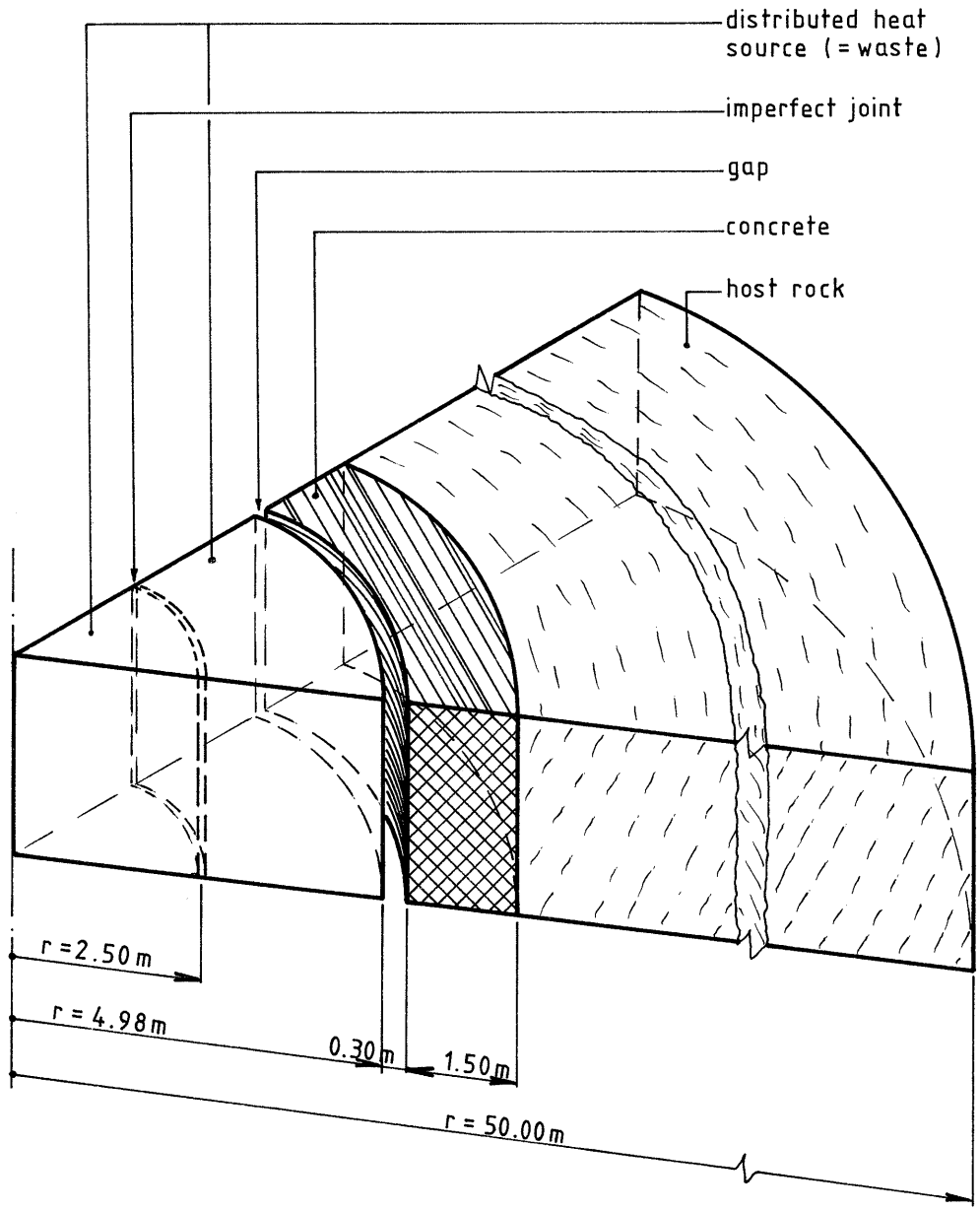

FIGURE A2.1: MODEL DOMAIN. BASED ON TYPE B REPOSITORY STORAGE CAVERN DIMENSIONS. USED FOR TESTING RADIATION AND CONTACT EFFECTS.

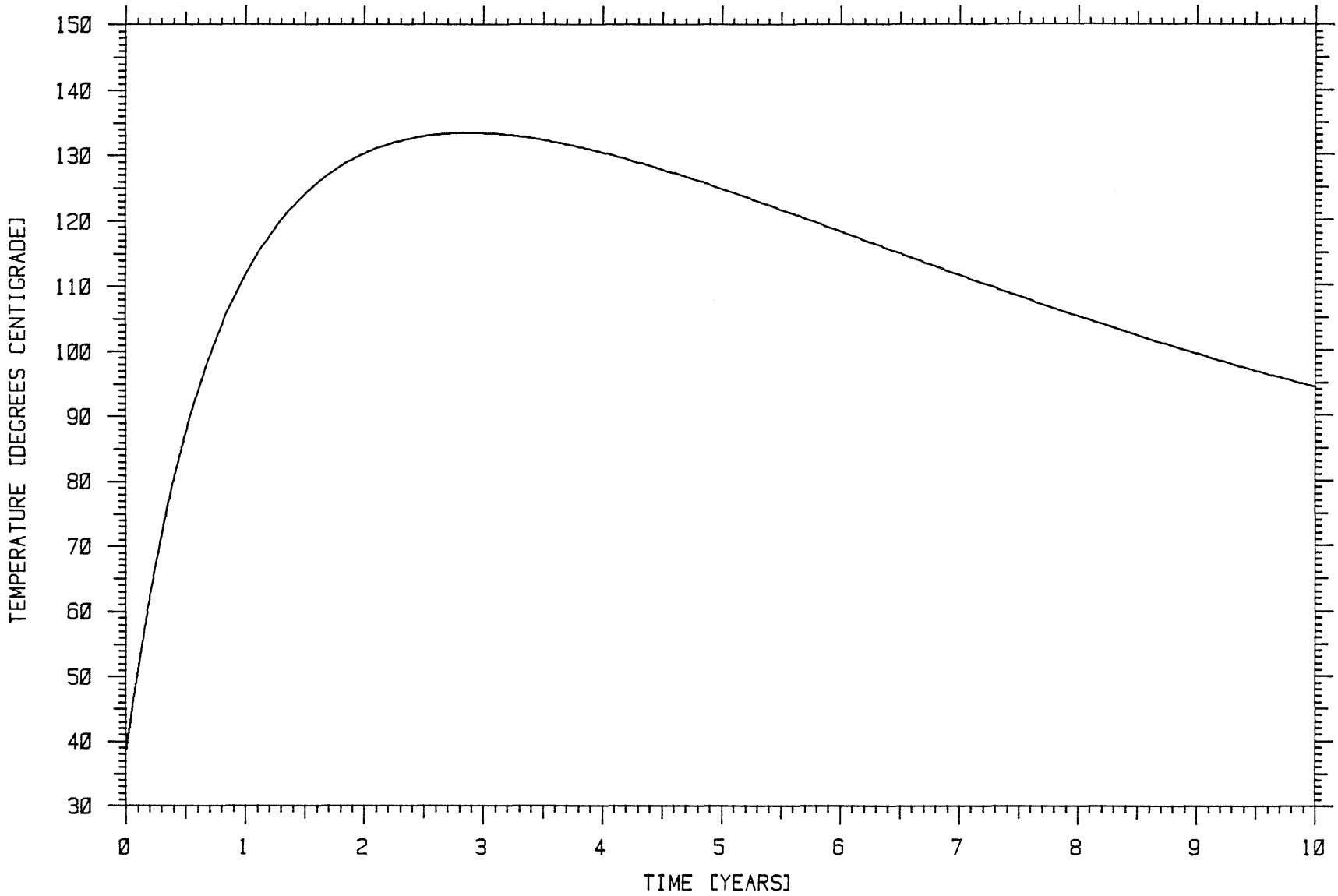

FIGURE A2.2: TEMPERATURE AT CENTRE OF WASTE. 30CM-GAP CONCRETE-FILLED. HEAT LOAD 10 W/M^3

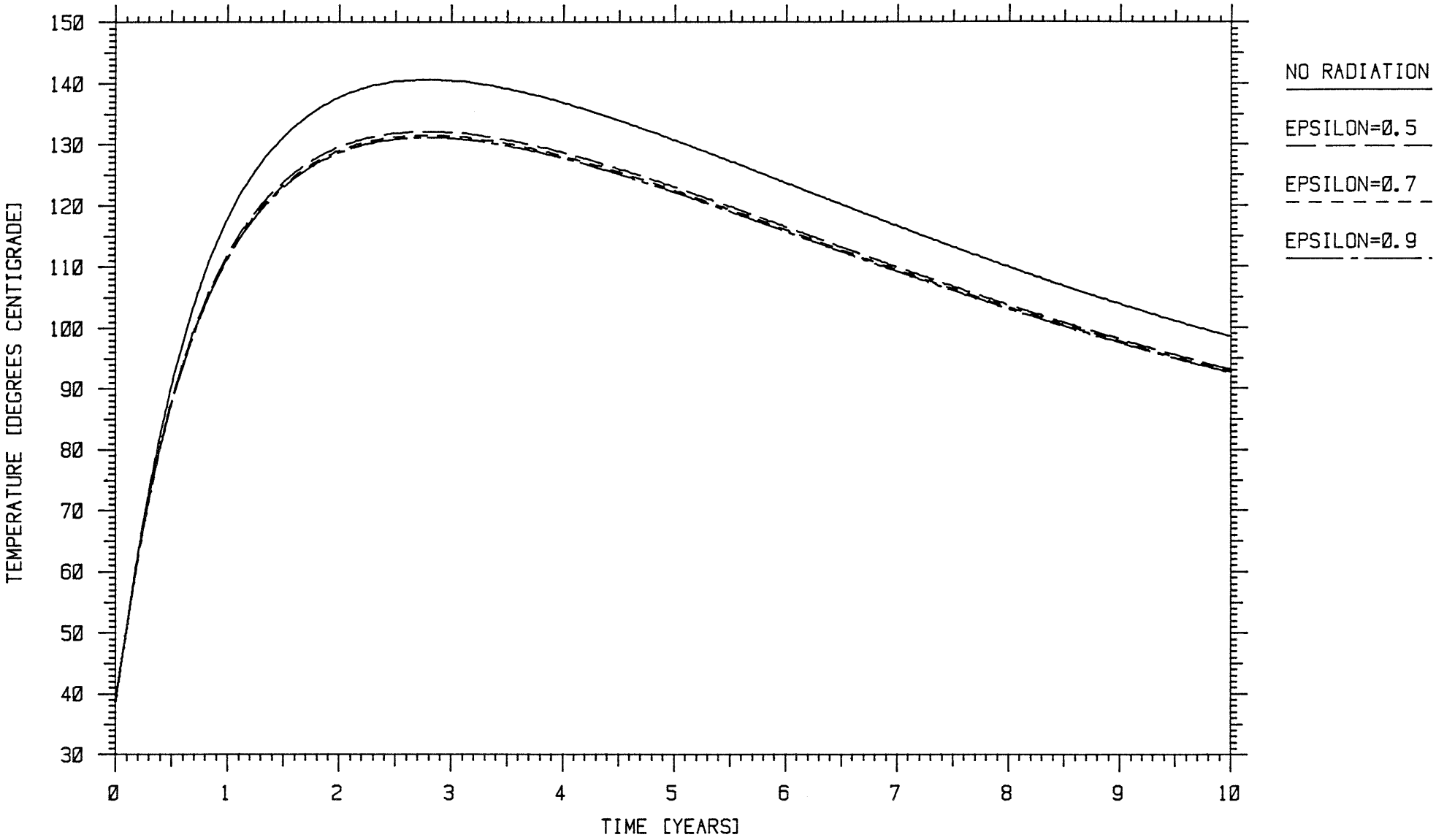

FIGURE A2.3: TEMPERATURE AT CENTRE OF WASTE. 30CM-GAP OPEN. HEAT LOAD 10 W/M^3

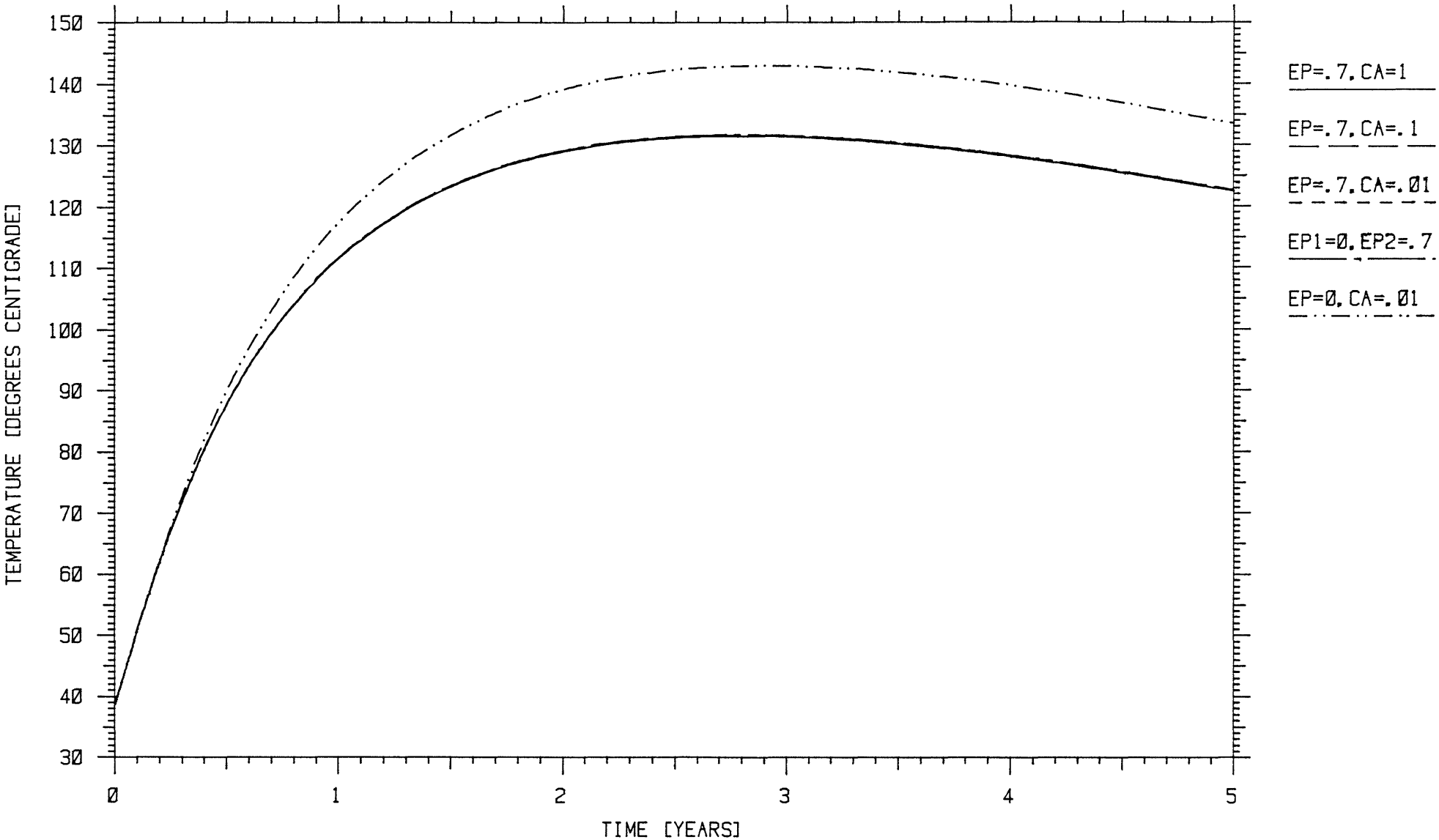

FIGURE A2.4: TEMPERATURE AT CENTRE OF WASTE. 30CM-GAP OPEN. 1MM-FISSURE IN CONCRETE 2.5M FROM CENTRE. HEAT LOAD 10 W/M^3

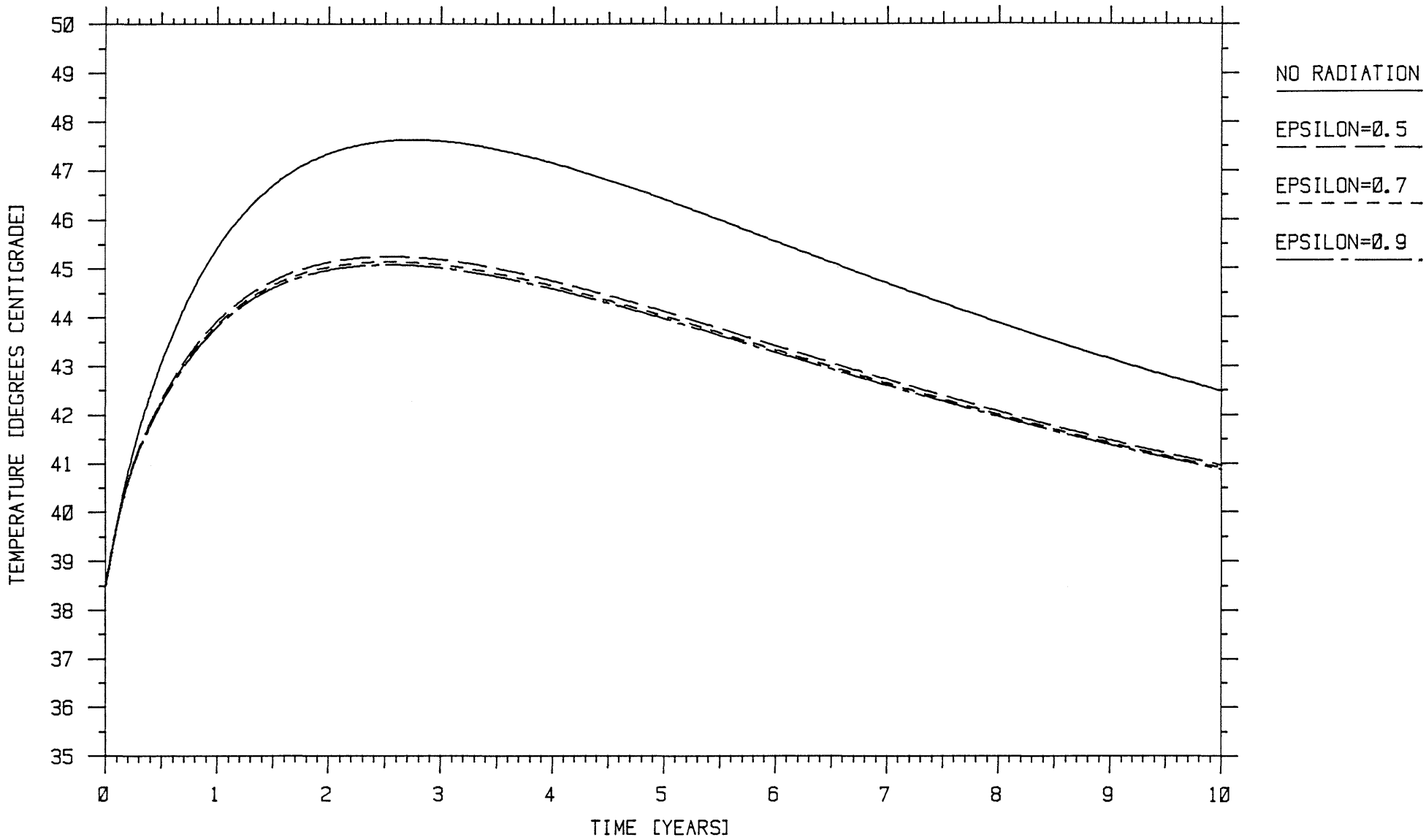

FIGURE A2.5: TEMPERATURE AT CENTRE OF WASTE. 30CM-GAP OPEN. HEAT LOAD 1 W/M^3